JAERI-Data/Code
2000-008

MEASUREMENTS OF ACTIVATION REACTION RATE DISTRIBUTIONS ON A MERCURY TARGET BOMBARDED WITH HIGH-ENERGY PROTONS AT AGS

February 2000

Hiroshi TAKADA, Yoshimi KASUGAI, Hiroshi NAKASHIMA,
Yujiro IKEDA, Takashi INO*, Masayoshi KAWAI*,
Eric JERDE* and David GLASGOW*

日本原子力研究所
Japan Atomic Energy Research Institute

本レポートは、日本原子力研究所が不定期に公刊している研究報告書です。
入手の問合わせは、日本原子力研究所研究情報部研究情報課（〒319-1195　茨城県那珂郡東海村）あて、お申し越し下さい。なお、このほかに財団法人原子力弘済会資料センター（〒319-1195　茨城県那珂郡東海村日本原子力研究所内）で複写による実費頒布を行っております。

This report is issued irregularly.
Inquiries about availability of the reports should be addressed to Research Information Division, Department of Intellectual Resources, Japan Atomic Energy Research Institute, Tokai-mura, Naka-gun, Ibaraki-ken 〒319-1195, Japan.

編集兼発行　日本原子力研究所

JAERI－Data/Code 2000－008

Measurements of Activation Reaction Rate Distributions on a Mercury Target Bombarded with High-Energy Protons at AGS

Hiroshi TAKADA, Yoshimi KASUGAI, Hiroshi NAKASHIMA, Yujiro IKEDA,
Takashi INO[*1], Masayoshi KAWAI[*1], Eric JERDE[*2], and David GLASGOW[*2]

Center for Neutron Science
Tokai Research Establishment
Japan Atomic Energy Research Institute
Tokai-mura, Naka-gun, Ibaraki-ken

(Received January 26, 2000)

A neutronics experiment was carried out using a thick mercury target at the Alternating Gradient Synchrotron (AGS) facility of Brookhaven National Laboratory in a framework of the ASTE (AGS Spallation Target Experiment) collaboration. Reaction rate distributions around the target were measured by the activation technique at incident proton energies of 1.6, 12 and 24 GeV. Various activation detectors such as the ^{115}In(n,n')^{115m}In, ^{93}Nb(n,2n)^{92m}Nb, and ^{209}Bi(n,xn) reactions with threshold energies ranging from 0.3 to 70.5 MeV were employed to obtain the reaction rate data for estimating spallation source neutron characteristics of the mercury target. It was found from the measured ^{115}In(n,n')^{115m}In reaction rate distribution that the number of leakage neutrons becomes maximum at about 11 cm from the top of hemisphere of the mercury target for the 1.6-GeV proton incidence and the peak position moves towards forward direction with increase of the incident proton energy. The similar result was observed in the reaction rate distributions of other activation detectors.

The experimental procedures and a full set of experimental data in numerical form are summarized in this report.

Keywords: ASTE Collaboration, AGS, Mercury, Spallation Target, Reaction Rate, Proton, 1.6, 12 and 24 GeV, Activation Detector

*1: High Energy Accelerator Research Organization
*2: Oak Ridge National Laboratory

JAERI－Data/Code 2000－008

AGS の高エネルギー陽子ビーム照射による水銀ターゲットにおける放射化反応率分布測定

日本原子力研究所東海研究所中性子科学研究センター

高田　弘・春日井　好巳・中島　宏・池田　裕二郎・猪野　隆[*1]・川合　将義[*1]、

Eric JERDE[*2] and David GLASGOW[*2]

（2000年1月26日受理）

ASTE (AGS Spallation Target Experiment) 共同実験の一環として、ブルックヘブン国立研究所の AGS 加速器施設において厚い水銀ターゲットを用いた核破砕ターゲット実験を実施した。実験では 1.6, 12 及び 24 GeV 陽子を入射して、放射化法によって水銀ターゲットにおける反応率分布を測定した。しきい値で 0.3 ～ 70.5 MeV にわたる ^{115}In(n, n')^{115m}In, ^{93}Nb(n, 2n)^{92m}Nb, ^{209}Bi(n, xn) などの反応を放射化検出器として用いて、水銀ターゲットの核破砕中性子源特性を評価するための反応率分布データを得た。^{115}In(n, n')^{115m}In 反応率分布測定結果から、1.6 GeV 陽子入射の場合に、漏洩中性子数は水銀ターゲットの半球状入射面の頂点から 11cm の位置でピークとなり、ピーク位置は入射エネルギーの増加と共にターゲット底面方向に移る特性があることがわかった。同様な結果は他の放射化検出器の反応率分布においても観測された。

本レポートは実験方法及び全ての実験結果を数値データとしてまとめたものである。

東海研究所：〒319-1195　茨城県那珂郡東海村白方白根 2-4

*1: 高エネルギー加速器研究機構

*2: オークリッジ国立研究所

Contents

目　次

1. Introduction

Several projects are under progress [1,2] aiming at the innovation of life and material science with pulsed neutron sources driven by high-energy intense proton accelerators with a power of 1 - 5 MW. The power is higher than ever by one order of magnitude. Liquid heavy metal is more suitable than solid one for the target material of those neutron sources bombarded with intense proton beams by the following reason. With increase of the beam power, solid target contains much more coolant such as light or heavy water composed of light elements so that neutron yield in the solid target becomes lower than in the liquid heavy metal target. Among liquid metals, mercury has been proposed as a promising target material. Due to the lack of experimental data, however, the feasibility of the mercury target as the intense pulsed neutron source has not been verified yet. For evaluating the feasibility, therefore, it is strongly required to study the neutronic, thermal and mechanical characteristics of the mercury target bombarded with high-energy intense pulsed protons through experiments.

In order to solve the problems mentioned above, an international collaboration on a spallation target experiment using protons provided by the Alternating Gradient Synchrotron (AGS) of Brookhaven National Laboratory (BNL) was organized as ASTE (AGS Spallation Target Experiments). The ASTE collaboration was aimed at studying (i) the beam diagnostics and intensity of the beam line as initial condition, (ii) the neutronics characteristics of the mercury target, and (iii) the mechanical properties of the target and its container in terms of pressure wave and induced stress.

The experimental work on the beam diagnostics is described in ref. 3. This report focuses on the neutronics measurement. From the viewpoint of the neutronics performance, the following items were identified to be important and were studied in the present work : (a) total neutron yield, (b) spatial neutron flux distribution and (c) nuclide production yield in the target.

The experiments with activation detectors were carried out using 1.6-, 12- and 24-GeV protons for obtaining the spatial neutron flux distribution on the mercury target. It was expected that the leakage neutrons had broad energy spectrum ranging from keV to GeV region. Thus, a variety of threshold detectors was used as the spectral indices at the cylindrical surface of a mercury target so that the profile of neutron intensity distribution could be studied as precisely as possible as a function of the incident proton energy.

In this experiment, the $^{115}In(n,n')^{115m}In$ reaction was selected as the base-line detector because it had the low threshold energy of 0.34 MeV among available activation detectors and the cross section data were effective to obtain the information about total neutron yield. For detection of the higher energy neutrons, the $^{209}Bi(n,10n)^{200}Bi$ reaction rate with threshold energy of 70.5 MeV was measured. The experimental procedures and measured data are presented in this report.

2. Experimental

2.1 Mercury Target

The top, side and front views of the mercury target are shown in Figs. 1.1, 1.2 and 1.3, respectively. The mercury was contained in a cylindrical target container made of stainless steel, DN-1.4571, which had the dimensions of 200 mm in inner diameter and 1300 mm in inner length with 2.5 mm in thickness. The composition of the DN-1.4571 steel is as follows : Fe (69.5-69.9), Cr (18), Ni (10), Mo (2-2.5), Ti (< 0.8) and C (0.1), where the number in the parentheses indicates the weight fraction in the unit of percent. The target container had a hemispheric beam incident surface on its top end, and also had several flanges to install instruments for pressure wave measurement and thermocouples for temperature measurement. The target container was confined in the secondary container made of DN1.4571 with 3.5 mm in thickness which had a rectangular configuration with a Plexiglas lid. The secondary container was fixed on a movable platform and installed in the blockhouse of the U-line of the AGS facility, as shown in Fig. 2, and then bombarded with 1.6-, 12- and 24-GeV protons. The nominal height of the beam axis was about 1.25 m from the ground level.

2.2 Activation Detector Arrangement

In order to measure the neutron spectrum in a wide energy range, the following high purity metal foils were employed as activation detectors : In, Nb, Al, Bi, Co, Tm, Y, Ni and Ti. The sizes and purities of these foils are summarized in Table 1. Physical properties of activation detectors are listed in Table 2. The threshold energy of detectors ranges from 0.34 MeV to 70.5 MeV. The cross sections of some representative reactions are shown in Figs. 3.1 to 3.3, where the cross section values below 20 MeV were taken from JENDL Dosimetry file [4] and those above 20 MeV were calculated with the ALICE-F code [5].

The details of foil positions on the mercury target are shown in Figs. 4 and 5. The foils were classified into the following three groups : (A) In, (B) Al, Nb, Bi, Co and Ni, (C) Ti, Y and Tm. The foils classified into (B) and (C) were assembled to one foil stack, respectively. These foil stacks were put on an acrylic bar of which size was 22 mm in width, 9 mm in thickness and 1200 mm in length. This bar was indexed as " main" bar. As shown in Figs. 4 and 5, additional three bars were prepared to monitor the effect of the deviation of the beam incident point from the central axis of the mercury target. They were labeled as " sub-1" , " sub-2" and "sub-3", respectively, on which indium and niobium foils were set.

As far as the detector position on the main bar is concerned, indium foils were set on the positions from -1 cm to 100 cm with respect to the top of the hemisphere of the mercury target to

measure the neutron flux profile as precisely as possible, while the other foil stacks were put on 6 to 8 positions. In case which the indium foil was put on the same position as the (B) foil stack, indium was placed on both of the top and the bottom of the (B) stack.

As shown in Fig. 1.3, the acrylic bars with the foil stacks were set on the aluminum support at the four radial positions along the beam axis with an interval of 90° around the target. For 1.6-GeV proton incidence, the main bar was installed on the position of 45° right-hand upward toward the downstream of the beam axis, and the others (sub-1, sub-2 and sub-3) were set in the order of the counter clockwise rotation direction around the target, respectively. For the 12- and 24-GeV cases, on the other hand, the main bar was installed on the position of 45° right-hand downward toward the downstream of the beam axis in order to put the major foils away from the flange structure of the target container.

2.3 Irradiation

The mercury target was irradiated with 1.6-, 12- and 24-GeV protons, respectively, to study the spallation neutron profile as a function of incident energy. The beam profile and the total number of the incident protons were measured to determine the initial conditions of the experiments. The former was obtained by the intensity distribution of the imaging plate placed in front of the secondary target container. It was observed that the center position of the proton beam was 3.6 to 12 cm apart from the center axis of the target with the elliptic profile. The profile decreased with increase of the incident energy. The resultant center positions and beam sizes are summerized in ref. 3.

The total number of the incident protons was obtained by the activation method with the $^{nat}Cu(p, x)^{24}Na$ reaction. The irradiation conditions for the1.6-, 12- and 24-GeV cases were as follows : 630 pulses consisted of 6 bunches with intensity of about $5x10^{11}$ protons per bunch, 32 single bunch pulses with intensity of about $1.3x10^{12}$ protons per bunch and 10 single bunch pulses with intensity of about $5x10^{12}$ protons per bunch. The interval of individual pulse irradiation was about 25 second for all cases. The resultant total number of the incident protons was $(3.7\pm0.3)x10^{13}$, $(4.8\pm0.4)x10^{13}$, $(4.2\pm0.4)10\ x10^{13}$ for 1.6-, 12- and 24-GeV protons, respectively. The details of the beam diagnostics measurements were described in ref. 3.

2.4 γ-ray Measurement

After the irradiation, the four acrylic bars supporting activation detectors were removed from the target and carried to a shed, and then the foil stacks were dismounted. Individual foil was sealed in a plastic bag according to the request from the safety point of view for the handling of radioactive materials, and transported to a counting rooms in the chemistry department building of

BNL. Gamma-rays from activated foils were measured with Ge-detectors. At each proton irradiation, a series of γ-ray measurements for short-lived radioactivities was continued for 10 to 12 hours including the time needed for the foil sorting. Second measurement for modest long half-lived nuclides was performed for a few days after the irradiation. Further measurements for long-lived radioactivities were carried out at ORNL after transmitting the irradiated foils to ORNL.

The reaction rate of a produced nuclide is obtained by the following relation,

$$Y = \frac{\lambda \cdot C}{N_A \cdot \frac{w}{M} \cdot N_P \cdot \varepsilon \cdot a \cdot b \cdot \mu \cdot (1 - e^{-\lambda \cdot Tr}) \cdot e^{-\lambda \cdot Tc} \cdot (1 - e^{-\lambda \cdot Tm})} \quad , \qquad (1)$$

where,

N_A : Avogadro's number [/mol],
w : weight of a foil [g],
M : atomic mass of target element [g/mol],
N_p: number of incident protons [p/sec],
λ : decay constant [1/sec],
C : γ-ray peak counts,
ε : detector efficiency,
a : natural abundance of target element,
b : branching ratio,
μ : absorption rate of a γ-ray in a foil,
Tr : irradiation time [sec],
Tc : cooling time [sec],
Tm : measuring time [sec].

2.5 Physical Data Used in the Data Processing

In order to obtain the reaction rate of activation detectors, the decay data such as decay constant were taken from ref. 6. The half-life, the energy and emission rate of a major γ-ray are listed in Table 2. For the γ-ray emission rate, the uncertainty of the last numerical values of the tabulated data is given in the parentheses.

2.6 Error Estimation

The sources of the error were mainly attributed to the following items :

1) statistical error of peak count,

2) error of weight of foil

3) uncertainty of the number of incident protons,

4) detector efficiency error,

5) decay data, namely, the half-life and γ-ray emission rate.

The errors associated with the present measurements were listed in Table 3. The error of the weight of foil was less than 0.1 %. The detector efficiency error was ±3 % which was estimated from the calibration measurement with standard sources. The uncertainty of the number of incident protons was taken from the results [3] of the activation measurement using the $^{nat}Cu(p, x)^{24}Na$ reaction. This is mainly caused by the uncertainty of the cross section data of the $^{nat}Cu(p, x)^{24}Na$ reaction. The errors of the half-life, γ-ray emission rate were ±6% and ±21% at worst, respectively. The uncertainties concerning to the γ-ray branching ratio, the irradiation time, the measuring time and the cooling time were not taken into account.

The errors of the detector efficiency, the number of incident protons, the half-life and γ-ray emission rate were intrinsic to the γ-ray measurement. They were regarded as the systematic error, and denoted as δ_{sys}. On the other hand, the error of the γ-ray peak count was dependent upon individual foil position. The error of weight of foils also depended upon individual foil. Then, they were regarded as the statistical component of the error and denoted as δ_{sta}.

3. Results and Discussion

Measured reaction rates are summarized in tables and also plotted in Figures. The format of the tables is explained in Table 4. The first column of the table shows the foil position on the cylindrical surface from the top of the hemisphere of the target in the unit of cm. For indium foils, their position on the acrylic bar is indicated as "upward" or "attached" in the next column because the indium foils were put as they sandwiched a foil stack of Al, Nb, Bi, and Co at some positions (see. Figs. 3 and 4). The words " upward" and " attached" represent the position of the In foil with respect to the acrylic bar. The " attached" position means that the In foil was attached on the bar. It is noted that the "upward" position is nearer than "attached" one to the cylindrical surface of the target (see Fig. 1.3). The measured reaction rates, their statistical and total errors are given in the next three columns, respectively.

3.1 The ^{115}In(n,n')^{115m}In Reaction

Measured reaction rates of the ^{115}In(n, n')^{115m}In reaction for the 1.6-, 12- and 24-GeV proton bombardment are summarized in Tables 5.1.1 to 5.1.12. The data on the attached positions are plotted in Figs. 5.1 to 5.3. For the 1.6-GeV case, the reaction rates were measured with a statistical error of ± 3 to ± 4 % except at the positions with distance far from 50 cm or more. Significant difference is observed in the reaction rates among four radial positions. At the peak position of the distribution, the reaction rate at the main bar differs from that at the sub-2 bar by about a factor of two. This indicates that the proton beam was incident on the position shifted to the right-upward with respect to the target center. With increase of the distance from the top of target, the difference among the radial positions becomes smaller. For the 12- and 24-GeV cases, the statistical error lies within ± 3% at almost all positions. The reaction rates on the main bar are almost the same as those on the sub-1 bar. The similar results are observed for the sub-2 and sub-3 bars. This fact suggests that the proton beam was incident on slightly upward position on the vertical direction from the target center. In these cases, almost the same values are obtained among four radial positions at about 80 cm from the top of the mercury target.

It is noted that the slope of the reaction rate distribution becomes abruptly less steep between 80 and 100 cm from the top of target at 1.6 GeV. This may be caused by fluctuation of the neutron field by the flange structure at the bottom end of the mercury target.

As far as the reaction rate for the upward and attached positions is concerned, the former is higher than the latter by 10% or more. One of reasons is that the upward position is nearer to the cylindrical surface than the attached position by about 5.5 mm. In addition, neutron absorption effect by the other foils sandwiched by the indium foils should be included in the difference.

Then, it is necessary to take account of this effect in the analytical studies.

3.2 The ^{93}Nb(n,xn) Reactions

Measured reaction rates of the ^{93}Nb(n, 2n)^{92m}Nb reaction for the 1.6-, 12- and 24-GeV proton bombardment are summarized in Tables 5.2.1 to 5.2.12, and plotted in Figs. 5.4 to 5.6. The statistical errors of the measured data are ±2 to ±4 % for the 1.6-GeV cases, while they are better than ±2% for the 12- and 24-GeV cases. The results among the four bars are different as well as those of the ^{115}In(n, n')^{115m}In reaction rates. The maximum magnitude of the difference is about a factor of two, which is the same level as the case of the ^{115}In(n, n')^{115m}In reaction. The slope of the reaction rate distribution becomes less steep between 80 and 100 cm from the top of target at 1.6 GeV as well as the ^{115}In(n, n')^{115m}In reaction.

The data for the reaction rates of the ^{93}Nb(n, 4n)^{90}Nb reaction for 1.6-, 12- and 24-GeV proton bombardment are summarized in Tables 5.3.1 to 5.3.12, and plotted in Figs. 5.7 to 5.9. The reaction rates were measured with good statistics within ±2% except at the positions of 80 and 100 cm on the main bar. The shape of the reaction rate distribution is the same as the results for the ^{93}Nb(n, 2n)^{92m}Nb reaction at all incident energies. The sensitive neutron energy ranges are 10 to 40 MeV for the ^{93}Nb(n, 2n)^{92m}Nb reaction and 35 to 80 MeV for the ^{93}Nb(n, 4n)^{90}Nb reaction. The results shown in the figures indicate clearly that the high energy neutron production is sensitive to the shift of the beam incident point from the central axis of the mercury target.

3.3 The ^{27}Al(n,x)^{24}Na Reaction

Measured reaction rates of the ^{27}Al(n, x)^{24}Na reaction for the 1.6-, 12- and 24-GeV proton bombardment are summarized in Tables 5.4.1 to 5.4.3 and plotted in Fig. 5.10. The reaction rates have been measured with the statistical error of ±4 to ±5 %. The reaction rate rises up from the front surface to the peak position, and then decreases rapidly as a function of the distance. The peak position moves to forward direction with increase of the incident proton energy. The slope of eyeguide line of the reaction rate for the 24-GeV case is much less steep than that for 1.6 GeV. For the 1.6-GeV case, the slope of the reaction rate distribution changes between 80 and 100 cm from the top of the mercury target as well as the results for the ^{93}Nb(n, xn) reactions.

The reaction rate values for the 24-GeV proton incidence are higher than those for the 1.6-GeV one by about a factor of 3 at the distance of 1 cm. The difference becomes larger with increase of the distance. The peak value for the 24-GeV case is higher than that for the 1.6-GeV one by about a factor of 5. The difference of about a factor of 40 is observed between 1.6- and 24-GeV cases in the tail part of the reaction rate distribution at the distance of 80 cm.

3.4 The ^{209}Bi(n,xn) Reactions

The reaction rates have been obtained for the following reactions at incident proton energies of 1.6, 12 and 24 GeV : ^{209}Bi(n, 4n)^{206}Bi, ^{209}Bi(n, 5n)^{205}Bi, ^{209}Bi(n, 6n)^{204}Bi, ^{209}Bi(n, 7n)^{203}Bi, ^{209}Bi(n, 8n)^{202}Bi and ^{209}Bi(n, 10n)$^{200m+g}$Bi. The results are summarized in Tables 5.5.1 to 5.5.3, 5.6.1 to 5.6.3, 5.7.1 to 5.7.3, 5.8.1 to 5.8.3, 5.9.1 to 5.9.3 and 5.10.1 to 5.10.3, respectively. For the foils placed on the positions from 50 to 100 cm, the γ-ray of the foils was measured in contact with the surface of the Ge detector, while the others were measured with a distace of 5 cm or so. The errors of the caribration factor of the Ge detector for the contact measurement were obtained individually. These errors were shown under the Tables 5.5.1, 5.6.1, 5.7.1, 5.8.1 and 5.9.1, respectively. The resultant reaction rates are plotted in Figs. 5.11 to 5.13.

Smooth change is observed in the reaction rates along the cylindrical surface for these reactions although slight irregular change appears at 50 cm from the top of the mercury for the 1.6 GeV proton incidence. Roughly speaking, the statistical errors of measured data are within 7% except for the ^{209}Bi(n, 10n)^{200}Bi reaction. That of the ^{209}Bi(n, 10n)^{200}Bi reaction is about ±11 to ±48% because of weak radioactivity due to its short half-life. Since the observed reactions cover the threshold energy from 23 to 70.5 MeV, it is possible to obtain rather fine energy spectrum below 70.5 MeV using the present data by the unfolding procedure.

It is noted that the production of ^{201}Bi through the ^{209}Bi(n, 9n) reaction has been also confirmed in the γ-ray measurement. However, the exact branching ratio to the electron capture process is unknown at present. Thus, the results of the ^{209}Bi(n, 9n)^{201}Bi reaction rate are excluded from this paper.

3.5 The ^{59}Co(n,xn) Reactions

The reaction rates have been obtained for the following reactions at incident proton energies of 1.6, 12 and 24 GeV : ^{59}Co(n, γ)^{60}Co, ^{59}Co(n, p)^{59}Fe, ^{59}Co(n, x)^{56}Mn, ^{59}Co(n, 2n)^{58}Co, ^{59}Co(n, 3n)^{57}Co, ^{59}Co(n, 4n)^{56}Co and ^{59}Co(n, 5n)^{55}Co. The results are summarized in Tables 5.11.1 to 5.11.3, 5.12.1 to 5.12.3, 5.13.1 to 5.13.3, 5.14.1 to 5.14.3, 5.15.1 to 5.15.3, 5.16.1 to 5.16.3 and 5.17.1 to 5.17.3, respectively. They are plotted in Figs. 5.14 to 5.20. The ^{59}Co(n, γ)^{60}Co reaction rate shows rather flat distribution in comparison with the other threshold reactions at each incident energy. This is because the (n,γ) reaction is induced even at the positions near the bottom end of the target by not only the neutrons leaked from the target surface but also those reflected by the structure such as secondary target container and the wall of the block house. The other reactions show the similar distribution each other although the absolute values are different depending upon each reaction cross section. This is consistent with the other threshold

reactions mentioned above. The measured reaction rates have the statistical errors from ±4 to ± 5%. The measured reactions cover the threshold energies from 0.8 to 41 MeV so that the energy spectra of the leakage neutrons could be determined in a wide energy range.

3.6 The ^{169}Tm (n,xn) Reactions

As for the ^{169}Tm(n, xn) reactions, the reaction rates have been obtained for four reactions at incident proton energies of 1.6, 12 and 24 GeV : ^{169}Tm(n, 2n)^{168}Tm, ^{169}Tm(n, 3n)^{167}Tm, ^{169}Tm(n, 4n)^{166}Tm and ^{169}Tm(n, 5n)^{165}Tm. The results are summarized in Tables 5.18.1 to 5.18.3, 5.19.1 to 5.19.3, 5.20.1 to 5.20.3 and 5.21.1 to 5.21.3, respectively. They are also plotted in Figs. 5.21 to 5.23. The shape of the reaction rate distributions is almost the same for four reactions at each incident proton energy. Because of the limited conditions on available γ-ray detectors and counting time, the statistical error for the ^{169}Tm(n, 2n) ^{168}Tm reaction with half-life of 93 days is about 10% at the 12-GeV case. It is observed, however, that the ^{169}Tm(n, xn) reaction rates changes smoothly through the foil positions.

It is noted that the systematic error of the reaction rates of the ^{169}Tm(n, 3n)^{167}Tm reaction is exceptionally larger than that of the other reactions. This is mainly due to the uncertainty of the γ-ray emission rate of ^{167}Tm. As shown in Table 2, the emission rate of 207.8 keV γ-ray from ^{167}Tm is 41%. However, it contains the uncertainty of relative error of 19.5% by itself.

3.7 The ^{89}Y(n,xn) Reactions

The reaction rates have been obtained for the following reactions at incident proton energies of 1.6, 12 and 24 GeV : ^{89}Y(n, 2n)^{88}Y, ^{89}Y(n, 3n)$^{87m+g}$Y, ^{89}Y(n, 4n)$^{86m+g}$Y and ^{89}Y(n, 5n)^{85g}Y. The results are summarized in Tables 5.22.1 to 5.22.3, 5.23.1 to 5.23.3, 5.24.1 to 5.24.3 and 5.25.1 to 5.25.3, respectively. They are also plotted in Figs. 5.24 to 5.27. These reactions show the similar distribution each other along the cylindrical surface at each incident energy. As for the ^{89}Y(n,5n)^{85g}Y reaction, it has the uncertainty of about 10% in the γ-ray emission rate so that its systematic error of 13.3 to 14.2% is larger than that of the other reactions. As far as the statistical errors are concerned, however, they are as good as ±4 to ±5%.

3.8 The ^{nat}Ni(n,x) Reactions

The reaction rates have been obtained for the ^{nat}Ni(n, x)^{58}Co and ^{nat}Ni(n, x)^{57}Co reactions at incident proton energies of 1.6, 12 and 24 GeV. The results are summarized in Tables 5.26.1 to 5.26.3 and 5.27.1 to 5.27.3, respectively. They are also plotted in Figs. 5.28 to 5.29. Smooth change along the cylindrical surface is observed in the reaction rate distributions of both reactions

at each incident proton energy. Slight irregular change appears between 80 and 100 cm from the top of the mercury target in the both reaction rate distributions for the 1.6-GeV proton incidence. The statistical error is as good as ±4 to ±5 % at almost all positions for both reactions.

3.9 The ^{nat}Ti(n,x) Reactions

The reaction rates have been obtained for the following reactions at incident proton energies of 1.6, 12 and 24 GeV : ^{nat}Ti(n, x)^{48}Sc, ^{nat}Ti(n, x)^{47}Sc, ^{nat}Ti(n, x)^{46g}Sc, ^{nat}Ti(n, x)^{44g}Sc and ^{nat}Ti(n, x)^{44m}Sc. The results are summarized in Tables 5.28.1 to 5.28.3, 5.29.1 to 5.29.3, 5.30.1 to 5.30.3, 5.31.1 to 5.31.3 and 5.32.1 to 5.32.3, respectively. They are also plotted in Figs. 5.30 to 5.34. All reactions show the similar distribution along the cylindrical surface at each incident energy. For these reactions, the data have good statistical errors ranging from ±4 to ±5%.

4. Summary

In a framework of the ASTE collaboration, the spallation neutron profile on the mercury target was studied by means of the activation technique at incident proton energies of 1.6, 12 and 24 GeV. The reaction rate data of 32 kinds of activation detectors with threshold energies ranging from 0.34 to 70.5 MeV were obtained on the cylindrical surface of the target. Most of the reaction rates were measured with the statistical error within ±10%.

For the ^{115}In(n, n')^{115m}In reaction which has the lowest threshold energy among the detectors, it is found from the measured data that the position where the number of leakage neutrons becomes maximum moves to deeper position with increase of the incident proton energy. Figures 6.1 and 6.2 show the characteristics of the reaction rate distribution of the ^{115}In(n, n')^{115m}In reaction. The peak position lies on 11.1 cm from the top of hemisphere of the mercury target for the 1.6-GeV proton incidence, while it is located on 16.6 and 19.2 cm for the 12- and 24-GeV cases, respectively. The other reactions qualitatively have the similar characteristics as the ^{115}In(n, n')^{115m}In reaction.

The present experiment has provided the first data on the spallation neutron profile of the mercury target bombarded with protons of 1.6, 12 and 24 GeV for the feasibility study. These data are unique enough to validate various code systems used in neutronics design study of the spallation neutron source facility. Estimation of the energy spectrum in the energy range from 0.34 to 70.5 MeV is planned by using the present data with the unfolding technique.

Acknowledgments

The authors would like to thank the operation team of the AGS accelerator for their kind operation in providing the required proton beam for this experiment. They are also grateful to the staffs of the Chemistry Department of BNL for their helpful cooperation on the γ-ray measurements at the Chemistry Building. They are indebted to the Forschungszentrum Jülich (FZJ) team of the ASTE collaboration for their manufacture of the mercury target for this experiment. They are thankful to the spokespersons of the ASTE collaboration, Drs. Jerome Hastings of Brookhaven National Laboratory, Guenter Bauer of Paul Scherrer Institute, John Haines of Oak Ridge National Laboratory, Dr. Yukio Oyama and Prof. Noboru Watanabe of JAERI for their coordination of the experimental program. The experimental work at BNL was supported by the U. S., Department of Energy under the contract DE-AC02-98-CH10886 with Brookhaven Science Associates.

References

1) Appleton, B. R, :"A Progress Report on the Spallation Neutron Source," Proc. of the 14th Mtg. of the Int. Collaboration on Advanced Neutron Sources, Illinois, 1998, vol. I, ANL-98-33, Argonne National Laboratory (1998).
2) The Joint Project Team of JAERI and KEK, "The Joint Project for High-Intensity Proton Accelerator," JAERI-Tech 99-056, Japan Atomic Energy Research Institute (1999).
3) Nakashima, H., et al.: to be published in JAERI-Data/Code.
4) Nakazawa, M. Kobayashi, K., Iwasaki, S., Iguchi, T., Sakurai, K., Ikeda, Y., Nakagawa, T.: "JENDL Dosimetry File," JAERI-1325, (1992).
5) Fukahori, T. :"ALICE-F Calculation of Nuclear Data up to 1 GeV," Proc. of the Specialists' Mtg. on High Energy Nucl. Data, Oct. 3-4, 1991, JAERI, Tokai, JAERI-M 92-039, pp. 114-122 (1992).
6) Firestone, R. B., Shirley, V. S. (Eds.) : "Table of Isotopes 8th Edition," Willey Interscience Publication, N.Y., (1996).

Table 1. Physical characteristics of the foils employed as activation detectors.

Material	Size	Purity	weight	Impurity
In	20 x 20 x 0.1 mm	99.99 %	0.25 g	
Nb	20 x 20 x 1.0 mm	99.95 %	3.4 g	Fe(20), W(<100), Si(20),Mo(<50), Zr(<100), Ta(900), C(50), O(<100), N(40), H(10), unit in ppm.
Al	20 x 20 x 1.0 mm	99.99 %	1.1 g	Cu(29), Fe(13), Mg(8), Si(<50), unit in ppm.
Bi	15 ϕ x 1.5 mm	99.998 %	2.5 g	Cu(0.004), Ag(0.001), Fe(<0.001), Pb(<0.001), unit in wt%
Co	20 x 20 x 1 mm	99.9 %	3.8 g	C(0.001), Si(<0.001), Fe(0.005), Cu(0.005), Ni(0.06), P (0.002), S (0.001), unit in wt%. Zr(<100), Ta(900), unit in ppm.
Tm	10 x 10 x 1 mm	99.9 %	0.93 g	Dy(<0.01), Er(<0.01) , Yb(<0.01), Fe(<0.01), Ca(<0.03), Mg(<0.01), unit in wt%.
Y	20 x 20 x 1 mm	99.9 %	1.9 g	Gd(<0.01), Tb(<0.01), Dy(<0.01) , Er(<0.01), Fe(<0.02), Ca(<0.02), Mg(<0.01), unit in wt%.
Ni	20 x 20 x 1 mm	99.9 %	3.5 g	Al(<0.05), Fe(0.02), Cu(0.01), Mg(<0.01), Pb(<0.005), Co(<0.001), unit in wt%.
Ti	20 x 20 x 1 mm	99.9 %	1.7 g	Fe(<0.05), Si(<0.03), Mn(<0.001), C(<0.01), Al(<0.005), Cr(<0.005), H(<0.01), O(0.08), N(0.005), unit in wt%.

Table 2 List of the reactions and associated decay data [a)]

Reaction			Q-value (MeV)	Threshold Energy (MeV)	Half-life	γ-ray Energy (keV)	γ-ray emission rate (%)
^{115}In	(n,n')	^{115m}In	-0.34	0.34	4.486 h	336.24	45.9(23)[d)]
^{93}Nb	(n,2n)	^{92m}Nb	-8.97	9.06	10.15 d	934.46	99.07(4)
	(n,4n)	^{90}Nb	-28.76	29.08	14.60 h	1129.00	92.7(5)
^{27}Al	(n,x)	^{24}Na	-3.13 [b)]	3.25	14.959 h	1368.6	100
^{209}Bi	(n,4n)	^{206}Bi	-22.45	22.56	6.243 d	803.1	98.9(1)
	(n,5n)	^{205}Bi	-29.48	29.63	15.31 d	703.4	31.1(1)
	(n,6n)	^{204}Bi	-37.90	38.08	11.22 h	984.02	58.8(4)
	(n,7n)	^{203}Bi	-45.12	45.34	11.76 h	820.3	29.6(15)
	(n,8n)	^{202}Bi	-53.97	54.24	1.72 h	960.67	99.28(2)
	(n,9n)	^{201m}Bi [c)]	-62.21	62.52	59.1 m	846.5	5.2
		^{201g}Bi	-61.63	61.67	108 m	629.1	24(5)
	(n,10n)	^{200m}Bi	-70.71	71.07	31 m	1026.5	91(7)
		^{200g}Bi	-70.51	70.51	36.4 m	1026.5	100
^{59}Co	(n,γ)	^{60}Co	5.07	0.0	5.2714 y	1173.2	99.9736(7)
	(n,p)	^{59}Fe	-0.78	0.80	44.503 d	1099.3	56.5(15)
	(n,x)	^{56}Mn	0.33	0.0	2.5785 h	845.8	98.9(3)
	(n,2n)	^{58}Co	-10.45	10.63	70.82 d	810.8	99.4
	(n,3n)	^{57}Co	-19.03	19.36	271.79 d	122.1	85.6(2)
	(n,4n)	^{56}Co	-30.40	30.95	77.27 d	846.8	99.940(25)
	(n,5n)	^{55}Co	-40.49	41.22	17.53 h	931.3	75(4)
^{169}Tm	(n,2n)	^{168}Tm	-8.03	8.08	93.1 d	198.2	52.4(16)
	(n,3n)	^{167}Tm	-14.90	14.99	9.25 d	207.8	41(8)
	(n,4n)	^{166}Tm	-23.61	23.75	7.70 h	778.8	18.9(11)
	(n,5n)	^{165}Tm	-30.63	30.31	30.36 h	242.9	35.5(17)

a) Taken from Table of Isotopes, 8th Edition.

b) for the ^{27}Al(n,α)^{24}Na reaction.

c) The branching ratios to EC(β^+)-decay are unknown.

d) The uncertainty of the last numerical values is shown in the parentheses.

Table 2. List of the reactions and associated decay data [a] (continued).

Reaction	Q-value (MeV)	Threshold Energy (MeV)	Half-life	γ-ray Energy (keV)	γ-ray emission rate (%)
^{89}Y (n,2n)^{88}Y	-11.48	11.61	106.65 d	898.0	93.7(3)
(n,3n)$^{87m+g}$Y	-20.83	21.07	79.8 h	388.5	82.1(5)
(n,4n)$^{86m+g}$Y	-32.86	33.24	14.74 h	1076.6	82.5(4)
(n,5n)^{85g}Y	-42.17	42.66	2.68 h	231.7	84(8)
^{nat}Ni (n,x) ^{58}Co	0.40 [b]	0.0	70.82 d	810.8	99.4
(n,x) ^{57}Co	-8.17 [c]	8.31	271.79 d	122.1	85.6(2)
^{nat}Ti (n,x) ^{48}Sc	-3.21 [d]	3.28	43.67 h	983.5	100(6)
(n,x) ^{47}Sc	-11.45 [e]	11.68	3.3492 d	159.4	68.3(4)
(n,x) ^{46g}Sc	-22.09 [f]	22.55	83.79 d	889.3	100
(n,x) ^{44m}Sc	-42.45 [g]	43.33	58.6 d	271.1	86.7
^{44g}Sc	-42.17 [h]	43.05	3.927 h	1157.0	99.9

a) Taken from Table of Isotopes, 8th Edition.

b) for the ^{58}Ni(n,p)^{58}Co reaction.

c) for the ^{58}Ni(n,np)^{57}Co reaction.

d) for the ^{48}Ti(n,p)^{48}Sc reaction.

e) for the ^{48}Ti(n,np)^{47}Sc reaction.

f) for the ^{48}Ti(n,2np)^{46g}Sc reaction.

g) for the ^{48}Ti(n,4np)^{44m}Sc reaction.

h) for the ^{48}Ti(n,4np)^{44g}Sc reaction.

i) The uncertainty of the last numerical values is shown in the parentheses.

Table 3. Sources of errors in the reaction rate measurements.

Source	Error (%)	Correlation [a]
Gamma ray counting statistics	1-200	
Sample weight	0.1	
Number of protons	9	sys
Detector efficiency	3	sys
Decay Data		
Half-life	0-6	sys
Gamma ray Intensity	0-21	sys

a) Systematic errors are indicated as "sys".

Table 4. Format of Tables listing the experimental results in numerical form.

Distance [a] (cm)	Position on [b] the bar	Reaction Rate [c] (/target nucleus/proton)	d_{sta} [d]	d_{tot} [e]	δ_{sys}= 10.0% [f]
0	upward	2.36E-27	10	11	
.	.	.	.	.	
.	.	.	.	.	
.	.	.	.	.	
.	.	.	.	.	
.	.	.	.	.	

a) Distance from the front-end of the mercury target.

b) The positions of the indium samples on the acrylic-bar are indicated as "upward" or "attached" to the surface of the bar.

c) Read as 2.36×10^{-27}.

d) Statistical errors

e) Total errors including statistical and systematic errors

f) Systematic error

Table 5.1.1 Reaction rates of the $^{115}In(n,n')^{115m}In$ reaction on the main bar for 1.6-GeV proton bombardment.

Distance (cm)	Position on the bar	Reaction Rate (/target nucleus/proton)	δ_{sta}	δ_{tot}	δ_{sys}=10.0%
-1	attached	2.04E-27	1.2%	10.1%	
2	attached	2.23E-27	3.7%	10.7%	
2	upward	2.63E-27	2.9%	10.4%	
5	attached	2.68E-27	3.0%	10.4%	
5	upward	3.02E-27	2.7%	10.4%	
9	attached	2.82E-27	3.2%	10.5%	
9	upward	3.33E-27	2.5%	10.3%	
13	attached	3.04E-27	2.8%	10.4%	
17	attached	2.53E-27	3.2%	10.5%	
17	upward	2.93E-27	2.7%	10.4%	
21	attached	2.22E-27	3.7%	10.7%	
25	attached	1.71E-27	4.1%	10.8%	
25	upward	2.01E-27	3.0%	10.4%	
29	attached	1.34E-27	4.5%	11.0%	
33	attached	1.16E-27	4.9%	11.2%	
37	attached	7.76E-28	5.6%	11.4%	
41	attached	6.89E-28	5.6%	11.5%	
45	attached	5.32E-28	6.8%	12.1%	
50	attached	3.58E-28	6.7%	12.1%	
50	upward	4.05E-28	5.0%	11.2%	
55	attached	2.31E-28	4.8%	11.1%	
65	attached	1.10E-28	7.4%	12.5%	
75	attached	4.65E-29	1.9%	10.2%	
80	attached	3.01E-29	15.2%	18.2%	
80	upward	3.42E-29	9.9%	14.1%	
85	attached	2.24E-29	19.3%	21.7%	
95	attached	1.52E-29	18.6%	21.1%	
100	attached	1.82E-29	15.6%	18.5%	
100	upward	1.56E-29	13.3%	16.7%	

Table 5.1.2 Reaction rates of the $^{115}In(n,n')^{115m}In$ reaction on the sub-1 bar for 1.6-GeV proton bombardment.

Distance (cm)	Position on the bar	Reaction Rate (/target nucleus/proton)	δ_{sta}	δ_{tot}	δ_{sys}=10.0%
-1	attached	1.71E-27	3.5%	10.6%	
5	attached	2.00E-27	3.0%	10.4%	
9	attached	2.49E-27	2.8%	10.4%	
17	attached	2.02E-27	3.3%	10.5%	
21	attached	1.97E-27	3.1%	10.5%	
25	attached	1.67E-27	3.4%	10.5%	
45	attached	4.72E-28	3.3%	10.5%	
50	attached	3.41E-28	3.4%	10.6%	
75	attached	4.71E-29	8.9%	13.4%	
80	attached	3.87E-29	10.1%	14.2%	
85	attached	2.78E-29	11.8%	5.5%	

Table 5.1.3 Reaction rates of the $^{115}In(n,n')^{115m}In$ reaction on the sub-2 bar for 1.6-GeV proton bombardment.

Distance (cm)	Position on the bar	Reaction Rate (/target nucleus/proton)	δ_{sta}	δ_{tot}	δ_{sys}=10.0%
-1	attached	1.08E-27	3.3%	10.5%	
5	attached	1.32E-27	2.8%	10.4%	
9	attached	1.39E-27	2.6%	10.3%	
17	attached	1.34E-27	3.1%	10.5%	
21	attached	1.28E-27	3.1%	10.5%	
25	attached	1.13E-27	3.3%	10.5%	
45	attached	3.43E-28	2.8%	10.4%	
50	attached	2.61E-28	3.1%	10.5%	
75	attached	4.80E-29	6.5%	11.9%	
80	attached	3.28E-29	9.4%	13.7%	
85	attached	2.47E-29	14.2%	17.4%	

Table 5.1.4 Reaction rates of the $^{115}In(n,n')^{115m}In$ reaction on the sub-3 bar for 1.6-GeV proton bombardment.

Distance (cm)	Position on the bar	Reaction Rate (/target nucleus/proton)	δ_{sta}	δ_{tot}	δ_{sys}=10.0%
-1	attached	1.42E-27	2.9%	10.4%	
5	attached	1.64E-27	2.5%	10.3%	
9	attached	1.81E-27	2.5%	10.3%	
17	attached	1.80E-27	2.4%	10.3%	
21	attached	1.49E-27	2.6%	10.3%	
25	attached	1.27E-27	2.7%	10.3%	
45	attached	4.15E-28	2.2%	10.2%	
50	attached	2.90E-28	2.9%	10.4%	
75	attached	5.16E-29	6.3%	11.8%	
80	attached	2.33E-29	10.6%	14.6%	
100	attached	5.41E-30	28.0%	29.8%	

Table 5.1.5 Reaction rates of the $^{115}In(n,n')^{115m}In$ reaction on the main bar for 12-GeV proton bombardment.

Distance (cm)	Position on the bar	Reaction Rate (/target nucleus/proton)	δ_{sta}	δ_{tot}	δ_{sys}=10.0%
-1	attached	3.80E-27	2.5%	10.4%	
2	attached	3.97E-27	2.4%	10.4%	
2	upward	4.48E-27	1.5%	10.2%	
5	attached	4.97E-27	2.1%	10.3%	
5	upward	5.69E-27	1.9%	10.3%	
9	attached	5.60E-27	2.1%	10.3%	
9	upward	6.93E-27	1.8%	10.3%	
13	attached	6.93E-27	1.8%	10.3%	
17	attached	6.61E-27	1.9%	10.3%	
17	upward	7.98E-27	1.7%	10.2%	
21	attached	6.82E-27	1.8%	10.3%	
25	attached	6.41E-27	1.8%	10.3%	
27	attached	5.61E-27	2.0%	10.3%	
27	upward	6.59E-27	1.4%	10.2%	
29	attached	5.53E-27	2.1%	10.3%	
33	attached	5.17E-27	2.2%	10.3%	
37	attached	4.26E-27	2.3%	10.4%	
41	attached	3.81E-27	2.5%	10.4%	
45	attached	3.16E-27	2.7%	10.5%	
50	attached	2.60E-27	2.9%	10.5%	
55	attached	2.05E-27	2.9%	10.5%	
55	upward	2.24E-27	2.9%	10.5%	
65	attached	1.31E-27	1.8%	10.3%	
75	attached	8.45E-28	3.0%	10.5%	
80	attached	6.01E-28	3.0%	10.5%	
80	upward	6.80E-28	2.2%	10.3%	
85	attached	4.89E-28	3.1%	10.6%	
95	attached	3.04E-28	4.0%	10.9%	
100	attached	2.25E-28	4.4%	11.0%	
100	upward	2.46E-28	4.0%	10.9%	

Table 5.1.6 Reaction rates of the $^{115}In(n,n')^{115m}In$ reaction on the sub-1 bar for 12-GeV proton bombardment.

Distance (cm)	Position on the bar	Reaction Rate (/target nucleus/proton)	δ_{sta}	δ_{tot}	δ_{sys}=10.0%
-1	attached	3.61E-27	2.7%	10.5%	
5	attached	4.72E-27	2.3%	10.4%	
9	attached	5.64E-27	2.1%	10.3%	
17	attached	6.46E-27	1.5%	10.2%	
21	attached	6.62E-27	2.00%	10.3%	
25	attached	6.12E-27	2.1%	10.3%	
29	attached	5.56E-27	2.1%	10.3%	
33	attached	4.74E-27	2.3%	10.4%	
45	attached	3.21E-27	2.9%	10.5%	
50	attached	2.79E-27	2.8%	10.5%	
55	attached	2.14E-27	2.2%	10.3%	
75	attached	8.60E-28	3.0%	10.5%	
80	attached	6.37E-28	3.0%	10.5%	
85	attached	5.34E-28	3.0%	10.5%	

Table 5.1.7 Reaction rates of the $^{115}In(n,n')^{115m}In$ reaction on the sub-2 bar for 12-GeV proton bombardment.

Distance (cm)	Position on the bar	Reaction Rate (/target nucleus/proton)	δ_{sta}	δ_{tot}	δ_{sys}=10.0%
-1	attached	5.00E-27	2.2%	10.3%	
5	attached	7.24E-27	1.9%	10.3%	
9	attached	9.18E-27	1.7%	10.2%	
17	attached	1.09E-26	1.6%	10.2%	
21	attached	9.62E-27	1.6%	10.2%	
25	attached	9.20E-27	1.7%	10.2%	
29	attached	7.78E-27	1.9%	10.3%	
33	attached	6.80E-27	2.0%	10.3%	
45	attached	4.28E-27	2.6%	10.4%	
50	attached	3.20E-27	2.1%	10.3%	
55	attached	2.71E-27	2.9%	10.5%	
75	attached	8.83E-28	2.2%	10.3%	
80	attached	7.07E-28	2.8%	10.5%	
85	attached	5.39E-28	2.8%	10.5%	

Table 5.1.8 Reaction rates of the $^{115}In(n,n')^{115m}In$ reaction on the sub-3 bar for 12-GeV proton bombardment.

Distance (cm)	Position on the bar	Reaction Rate (/target nucleus/proton)	δ_{sta}	δ_{tot}	δ_{sys}=10.0%
-1	attached	5.25E-27	2.3%	10.4%	
5	attached	7.62E-27	1.1%	10.2%	
9	attached	8.54E-27	1.8%	10.3%	
17	attached	1.03E-26	1.6%	10.2%	
21	attached	9.68E-27	1.6%	10.2%	
25	attached	8.67E-27	1.8%	10.3%	
29	attached	7.51E-27	2.0%	10.3%	
33	attached	6.78E-27	2.0%	10.3%	
45	attached	3.89E-27	2.9%	10.5%	
50	attached	3.23E-27	2.9%	10.5%	
55	attached	2.39E-27	3.0%	10.5%	
75	attached	9.03E-28	2.8%	10.5%	
80	attached	6.43E-28	2.7%	10.4%	
100	attached	2.43E-28	4.5%	11.1%	

Table 5.1.9 Reaction rates of the $^{115}In(n,n')^{115m}In$ reaction on the main bar for 24-GeV proton bombardment.

Distance (cm)	Position on the bar	Reaction Rate (/target nucleus/proton)	δ_{sta}	δ_{tot}	δ_{sys}=10.1%
-1	attached	5.59E-27	2.4%	10.3%	
2	attached	6.25E-27	2.1%	10.2%	
2	upward	6.76E-27	2.1%	10.2%	
5	attached	7.62E-27	1.9%	10.2%	
5	upward	8.57E-27	1.8%	10.2%	
9	attached	8.80E-27	1.7%	10.1%	
9	upward	9.87E-27	1.6%	10.1%	
13	attached	1.17E-26	1.5%	10.1%	
17	attached	1.20E-26	1.5%	10.1%	
17	upward	1.30E-26	1.4%	10.1%	
21	attached	1.28E-26	1.5%	10.1%	
25	attached	1.20E-26	1.6%	10.1%	
27	attached	1.13E-26	1.5%	10.1%	
27	upward	1.27E-26	1.4%	10.1%	
29	attached	1.10E-26	1.3%	10.1%	
33	attached	1.00E-26	1.7%	10.1%	
37	attached	9.09E-27	1.8%	10.2%	
41	attached	8.02E-27	2.3%	10.3%	
45	attached	6.78E-27	2.2%	10.2%	
50	attached	5.91E-27	2.2%	10.2%	
55	attached	4.50E-27	2.5%	10.3%	
55	upward	5.21E-27	2.3%	10.3%	
65	attached	3.01E-27	1.8%	10.2%	
75	attached	1.41E-27	2.5%	10.3%	
80	upward	1.75E-27	2.9%	10.4%	
85	attached	1.20E-27	2.8%	10.4%	
95	attached	7.66E-28	3.0%	10.4%	
100	attached	5.96E-28	3.6%	10.6%	
100	upward	6.54E-28	3.0%	10.4%	

Table 5.1.10 Reaction rates of the $^{115}In(n,n')^{115m}In$ reaction on the sub-1 bar for 24-GeV proton bombardment.

Distance (cm)	Position on the bar	Reaction Rate (/target nucleus/proton)	δ_{sta}	δ_{tot}	δ_{sys}=10.1%
-1	attached	6.01E-27	2.3%	10.3%	
5	attached	7.99E-27	1.9%	10.2%	
9	attached	1.03E-26	1.7%	10.1%	
17	attached	1.25E-26	1.6%	10.1%	
21	attached	1.28E-26	1.6%	10.1%	
25	attached	1.21E-26	1.6%	10.1%	
29	attached	1.16E-26	1.8%	10.2%	
25	attached	1.10E-26	1.7%	10.1%	
45	attached	7.01E-27	2.0%	10.2%	
50	attached	6.02E-27	2.3%	10.3%	
55	attached	4.99E-27	2.5%	10.3%	
75	attached	2.04E-27	2.8%	10.4%	
80	attached	1.61E-27	2.8%	10.4%	
85	attached	1.26E-27	3.3%	10.5%	

Table 5.1.11 Reaction rates of the $^{115}In(n,n')^{115m}In$ reaction on the sub-2 bar for 24-GeV proton bombardment.

Distance (cm)	Position on the bar	Reaction Rate (/target nucleus/proton)	δ_{sta}	δ_{tot}	δ_{sys}=10.1%
-1	attached	7.11E-27	2.2%	10.2%	
5	attached	1.13E-26	1.7%	10.1%	
9	attached	1.38E-26	1.5%	10.1%	
17	attached	1.70E-26	1.4%	10.1%	
21	attached	1.78E-26	1.4%	10.1%	
25	attached	1.68E-26	1.3%	10.1%	
29	attached	1.53E-26	1.5%	10.1%	
33	attached	1.36E-26	1.5%	10.1%	
45	attached	8.68E-27	2.0%	10.2%	
50	attached	7.50E-27	2.1%	10.2%	
55	attached	5.80E-27	1.4%	10.1%	
75	attached	2.26E-27	2.7%	10.4%	
80	attached	1.77E-27	2.8%	10.4%	
85	attached	1.45E-27	3.1%	10.5%	

Table 5.1.12 Reaction rates of the $^{115}In(n,n')^{115m}In$ reaction on the sub-3 bar for 24-GeV proton bombardment.

Distance (cm)	Position on the bar	Reaction Rate (/target nucleus/proton)	δ_{sta}	δ_{tot}	δ_{sys}=10.1%
-1	attached	7.34E-27	1.5%	10.1%	
5	attached	1.05E-26	1.8%	10.2%	
9	attached	1.31E-26	1.6%	10.1%	
17	attached	1.67E-26	1.4%	10.1%	
21	attached	1.69E-26	1.4%	10.1%	
25	attached	1.56E-26	1.5%	10.1%	
29	attached	1.45E-26	1.5%	10.1%	
33	attached	1.31E-26	1.6%	10.1%	
45	attached	8.70E-27	2.1%	10.2%	
50	attached	7.69E-27	2.1%	10.2%	
55	attached	5.80E-27	2.4%	10.3%	
75	attached	2.10E-27	2.5%	10.3%	
80	attached	1.60E-27	2.9%	10.4%	
100	attached	6.72E-28	3.6%	10.6%	

Table 5.2.1 Reaction rates of the ^{93}Nb(n,2n)^{92m}Nb reaction on the main bar for 1.6-GeV proton bombardment.

Distance (cm)	Reaction Rate (/target nucleus/proton)	δ_{sta}	δ_{tot}	δ_{sys}=8.6%
1	3.54E-28	4.4%	9.7%	
5	3.54E-28	4.5%	9.7%	
9	3.88E-28	5.6%	10.3%	
17	3.57E-28	4.4%	9.7%	
25	2.39E-28	6.0%	10.5%	
50	5.76E-29	9.3%	12.7%	
80	6.73E-30	28.2%	29.5%	
100	4.19E-30	8.9%	12.4%	

Table 5.2.2 Reaction rates of the ^{93}Nb(n,2n)^{92m}Nb reaction on the sub-1 bar for 1.6-GeV proton bombardment.

Distance (cm)	Reaction Rate (/target nucleus/proton)	δ_{sta}	δ_{tot}	δ_{sys}=8.6%
9	3.08E-28	2.2%	8.9%	
17	2.93E-28	2.1%	8.9%	
25	2.07E-28	2.3%	8.9%	
50	4.48E-29	4.1%	9.6%	

Table 5.2.3 Reaction rates of the ^{93}Nb(n,2n)^{92m}Nb reaction on the sub-2 bar for 1.6-GeV proton bombardment.

Distance (cm)	Reaction Rate (/target nucleus/proton)	δ_{sta}	δ_{tot}	δ_{sys}=8.6%
9	1.90E-28	2.1%	8.9%	
17	1.77E-28	1.8%	8.8%	
25	1.34E-28	2.6%	9.0%	
50	3.63E-29	2.9%	9.1%	

Table 5.2.4 Reaction rates of the ^{93}Nb(n,2n)^{92m}Nb reaction on the sub-3 bar for 1.6-GeV proton bombardment.

Distance (cm)	Reaction Rate (/target nucleus/proton)	δ_{sta}	δ_{tot}	δ_{sys}=8.6%
9	2.66E-28	4.6%	9.8%	
17	2.31E-28	4.3%	9.7%	
25	1.93E-28	5.3%	10.1%	
50	3.27E-29	15.3%	17.6%	

Table 5.2.5 Reaction rates of the $^{93}Nb(n,2n)^{92m}Nb$ reaction on the main bar for 12-GeV proton bombardment.

Distance (cm)	Reaction Rate (/target nucleus/proton)	δ_{sta}	δ_{tot}	δ_{sys}=8.8%
1	6.51E-28	2.2%	9.1%	
5	7.78E-28	2.3%	9.1%	
9	8.65E-28	2.0%	9.0%	
17	1.01E-27	1.9%	9.0%	
25	8.91E-28	1.5%	8.9%	
50	3.53E-28	9.0%	12.6%	
80	1.06E-28	10.3%	13.5%	
100	3.41E-29	4.0%	9.7%	

Table 5.2.6 Reaction rates of the $^{93}Nb(n,2n)^{92m}Nb$ reaction on the sub-1 bar for 12-GeV proton bombardment.

Distance (cm)	Reaction Rate (/target nucleus/proton)	δ_{sta}	δ_{tot}	δ_{sys}=8.8%
9	8.50E-28	1.9%	9.0%	
17	9.75E-28	2.2%	9.1%	
25	8.48E-28	2.0%	9.0%	
50	3.40E-28	2.2%	9.1%	

Table 5.2.7 Reaction rates of the $^{93}Nb(n,2n)^{92m}Nb$ reaction on the sub-2 bar for 12-GeV proton bombardment.

Distance (cm)	Reaction Rate (/target nucleus/proton)	δ_{sta}	δ_{tot}	δ_{sys}=8.8%
9	1.43E-27	1.6%	8.9%	
17	1.59E-27	1.6%	8.9%	
25	1.33E-27	1.9%	9.0%	
50	4.57E-28	2.2%	9.1%	

Table 5.2.8 Reaction rates of the $^{93}Nb(n,2n)^{92m}Nb$ reaction on the sub-3 bar for 12-GeV proton bombardment.

Distance (cm)	Reaction Rate (/target nucleus/proton)	δ_{sta}	δ_{tot}	δ_{sys}=8.8%
9	1.41E-27	1.7%	9.0%	
17	1.52E-27	1.7%	9.0%	
25	1.23E-27	2.0%	9.0%	
50	4.09E-28	2.0%	9.0%	

Table 5.2.9 Reaction rates of the ^{93}Nb(n,2n)^{92m}Nb reaction on the main bar for 24-GeV proton bombardment.

Distance (cm)	Reaction Rate (/target nucleus/proton)	δ_{sta}	δ_{tot}	δ_{sys}=10.0%
1	8.67E-28	1.8%	10.1%	
5	1.07E-27	1.8%	10.1%	
9	1.20E-27	1.8%	10.1%	
17	1.62E-27	1.7%	10.1%	
25	1.48E-27	2.0%	10.2%	
50	6.82E-28	2.2%	10.2%	
80	2.07E-28	12.9%	16.3%	
100	8.39E-29	3.5%	10.6%	

Table 5.2.10 Reaction rates of the ^{93}Nb(n,2n)^{92m}Nb reaction on the sub-1 bar for 24-GeV proton bombardment.

Distance (cm)	Reaction Rate (/target nucleus/proton)	δ_{sta}	δ_{tot}	δ_{sys}=10.0%
9	1.38E-27	1.9%	10.1%	
17	1.71E-27	1.8%	10.1%	
25	1.58E-27	1.8%	10.1%	
50	7.62E-28	2.4%	10.2%	

Table 5.2.11 Reaction rates of the ^{93}Nb(n,2n)^{92m}Nb reaction on the sub-2 bar for 24-GeV proton bombardment.

Distance (cm)	Reaction Rate (/target nucleus/proton)	δ_{sta}	δ_{tot}	δ_{sys}=10.0%
9	1.96E-27	1.9%	10.1%	
17	2.42E-27	1.9%	10.1%	
25	2.13E-27	1.5%	10.1%	
50	8.82E-28	1.9%	10.1%	

Table 5.2.12 Reaction rates of the ^{93}Nb(n,2n)^{92m}Nb reaction on the sub-3 bar for 24-GeV proton bombardment.

Distance (cm)	Reaction Rate (/target nucleus/proton)	δ_{sta}	δ_{tot}	δ_{sys}=10.0%
9	1.87E-27	1.9%	10.1%	
17	2.30E-27	1.5%	10.1%	
25	2.09E-27	1.6%	10.1%	
50	8.36E-28	1.4%	10.1%	

Table 5.3.1 Reaction rates of the ^{93}Nb(n,4n)^{90}Nb reaction on the main bar for 1.6-GeV proton bombardment.

Distance (cm)	Reaction Rate (/target nucleus/proton)	δ_{sta}	δ_{tot}	δ_{sys}=8.65%
1	1.25E-28	1.9%	8.9%	
5	1.63E-28	1.9%	8.9%	
9	1.86E-28	1.9%	8.9%	
17	1.74E-28	2.0%	8.9%	
25	1.29E-28	1.9%	8.9%	
50	3.19E-29	3.4%	9.3%	
80	5.47E-30	8.8%	12.3%	
100	2.49E-30	11.6%	14.5%	

Table 5.3.2 Reaction rates of the ^{93}Nb(n,4n)^{90}Nb reaction on the sub-1 bar for 1.6-GeV proton bombardment.

Distance (cm)	Reaction Rate (/target nucleus/proton)	δ_{sta}	δ_{tot}	δ_{sys}=8.65%
9	1.34E-28	2.1%	8.9%	
17	1.42E-28	2.0%	8.9%	
25	1.09E-28	2.1%	8.9%	
50	2.97E-29	3.2%	9.2%	

Table 5.3.3 Reaction rates of the ^{93}Nb(n,4n)^{90}Nb reaction on the sub-2 bar for 1.6-GeV proton bombardment.

Distance (cm)	Reaction Rate (/target nucleus/proton)	δ_{sta}	δ_{tot}	δ_{sys}=8.65%
9	8.50E-29	2.4%	9.0%	
17	8.82E-29	2.1%	8.9%	
25	7.43E-29	2.2%	8.9%	
50	2.17E-29	3.4%	9.3%	

Table 5.3.4 Reaction rates of the ^{93}Nb(n,4n)^{90}Nb reaction on the sub-3 bar for 1.6-GeV proton bombardment.

Distance (cm)	Reaction Rate (/target nucleus/proton)	δ_{sta}	δ_{tot}	δ_{sys}=8.65%
9	1.10E-28	2.1%	8.9%	
17	1.17E-28	1.9%	8.9%	
25	8.90E-29	2.4%	9.0%	
50	2.42E-29	3.4%	9.3%	

Table 5.3.5 Reaction rates of the ^{93}Nb(n,4n)^{90}Nb reaction on the main bar for 12-GeV proton bombardment.

Distance (cm)	Reaction Rate (/target nucleus/proton)	δ_{sta}	δ_{tot}	δ_{sys}=8.8%
1	2.48E-28	2.0%	9.0%	
5	3.15E-28	1.2%	8.9%	
9	3.65E-28	1.2%	8.9%	
17	4.65E-28	1.7%	9.0%	
25	4.34E-28	1.9%	9.0%	
50	1.59E-28	2.4%	9.1%	
80	5.09E-29	3.1%	9.3%	
100	1.86E-29	4.5%	9.9%	

Table 5.3.6 Reaction rates of the ^{93}Nb(n,4n)^{90}Nb reaction on the sub-1 bar for 12-GeV proton bombardment.

Distance (cm)	Reaction Rate (/target nucleus/proton)	δ_{sta}	δ_{tot}	δ_{sys}=8.8%
9	3.57E-28	2.1%	9.0%	
17	4.40E-28	2.2%	9.1%	
25	4.02E-28	1.9%	9.0%	
50	1.73E-28	1.8%	9.0%	

Table 5.3.7 Reaction rates of the ^{93}Nb(n,4n)^{90}Nb reaction on the sub-2 bar for 12-GeV proton bombardment.

Distance (cm)	Reaction Rate (/target nucleus/proton)	δ_{sta}	δ_{tot}	δ_{sys}=8.8%
9	5.87E-28	1.3%	8.9%	
17	7.24E-28	1.7%	9.0%	
25	6.06E-28	1.7%	9.0%	
50	2.24E-28	1.2%	8.9%	

Table 5.3.8 Reaction rates of the ^{93}Nb(n,4n)^{90}Nb reaction on the sub-3 bar for 12-GeV proton bombardment.

Distance (cm)	Reaction Rate (/target nucleus/proton)	δ_{sta}	δ_{tot}	δ_{sys}=8.8%
9	5.91E-28	2.1%	9.0%	
17	6.96E-28	1.4%	8.9%	
25	6.04E-28	2.0%	9.0%	
50	1.97E-28	2.1%	9.0%	

Table 5.3.9 Reaction rates of the ^{93}Nb(n,4n)^{90}Nb reaction on the main bar for 24-GeV proton bombardment.

Distance (cm)	Reaction Rate (/target nucleus/proton)	δ_{sta}	δ_{tot}	δ_{sys}=8.7%
1	3.65E-28	1.3%	8.8%	
5	4.77E-28	1.2%	8.8%	
9	5.84E-28	1.6%	8.8%	
17	7.95E-28	1.3%	8.8%	
25	7.90E-28	1.3%	8.8%	
50	3.63E-28	1.8%	8.9%	
80	1.22E-28	2.2%	9.0%	
100	4.94E-29	1.4%	8.8%	

Table 5.3.10 Reaction rates of the ^{93}Nb(n,4n)^{90}Nb reaction on the sub-1 bar for 24-GeV proton bombardment.

Distance (cm)	Reaction Rate (/target nucleus/proton)	δ_{sta}	δ_{tot}	δ_{sys}=8.7%
9	6.68E-28	1.0%	8.8%	
17	8.49E-28	1.2%	8.8%	
25	8.24E-28	1.2%	8.8%	
50	4.10E-28	1.6%	8.8%	

Table 5.3.11 Reaction rates of the ^{93}Nb(n,4n)^{90}Nb reaction on the sub-2 bar for 24-GeV proton bombardment.

Distance (cm)	Reaction Rate (/target nucleus/proton)	δ_{sta}	δ_{tot}	δ_{sys}=8.7%
9	9.18E-28	1.0%	8.8%	
17	1.18E-27	1.0%	8.8%	
25	1.08E-27	1.0%	8.8%	
50	4.71E-28	1.6%	8.8%	

Table 5.3.12 Reaction rates of the ^{93}Nb(n,4n)^{90}Nb reaction on the sub-3 bar for 24-GeV proton bombardment.

Distance (cm)	Reaction Rate (/target nucleus/proton)	δ_{sta}	δ_{tot}	δ_{sys}=8.7%
9	8.54E-28	1.2%	8.8%	
17	1.14E-27	1.0%	8.8%	
25	1.06E-27	1.1%	8.8%	
50	4.54E-28	0.8%	8.7%	

Table 5.4.1 Reaction rates of the $^{27}Al(n,x)^{24}Na$ reaction on the main bar for 1.6-GeV proton bombardment.

Distance (cm)	Reaction Rate (/target nucleus/proton)	δ_{sta}	δ_{tot}	δ_{sys}=9.0%
1	1.30E-28	4.1%	9.0%	
5	1.51E-28	4.1%	9.0%	
9	1.59E-28	4.1%	9.0%	
17	1.37E-28	4.1%	9.0%	
25	9.66E-29	4.1%	9.0%	
50	2.06E-29	4.1%	9.0%	
80	2.74E-30	4.2%	9.0%	
100	1.49E-30	4.6%	9.0%	

Table 5.4.2 Reaction rates of the $^{27}Al(n,x)^{24}Na$ reaction on the main bar for 12-GeV proton bombardment.

Distance (cm)	Reaction Rate (/target nucleus/proton)	δ_{sta}	δ_{tot}	δ_{sys}=9.2%
1	2.15E-28	4.2%	9.2%	
5	2.56E-28	4.2%	9.2%	
9	2.91E-28	4.2%	9.2%	
17	3.49E-28	4.2%	9.2%	
27	3.09E-28	4.2%	9.2%	
55	1.13E-28	4.2%	9.2%	
80	3.49E-29	4.3%	9.2%	
100	1.12E-29	4.6%	9.2%	

Table 5.4.3 Reaction rates of the $^{27}Al(n,x)^{24}Na$ reaction on the main bar for 24-GeV proton bombardment.

Distance (cm)	Reaction Rate (/target nucleus/proton)	δ_{sta}	δ_{tot}	δ_{sys}=10.3%
1	3.23E-28	4.8%	10.3%	
5	3.97E-28	4.8%	10.3%	
9	4.47E-28	4.8%	10.3%	
17	6.02E-28	4.8%	10.3%	
27	5.88E-28	4.8%	10.3%	
55	2.55E-28	4.8%	10.3%	
80	8.42E-29	4.8%	10.3%	
100	3.26E-29	4.8%	10.3%	

Table 5.5.1 Reaction rates of the $^{209}Bi(n,4n)^{206}Bi$ reaction on the main bar for 1.6-GeV proton bombardment.

Distance (cm)	Reaction Rate (/target nucleus/proton)	δ_{sta}	δ_{tot}	δ_{sys}=8.6%
1	4.49E-28	5.1%	10.1%	
5	6.37E-28	4.7%	9.9%	
9	7.36E-28	4.9%	10.0%	
17	5.90E-28	4.8%	9.9%	
25	4.71E-28	4.2%	9.7%	
50	1.41E-28	8.9%	13.6%*	
80	2.41E-29	15.4%	18.5%*	
100	-	-	-	

* including the error of calibration factor of the detector at 0.5 cm: 5.7%

Table 5.5.2 Reaction rates of the $^{209}Bi(n,4n)^{206}Bi$ reaction on the main bar for 12-GeV proton bombardment.

Distance (cm)	Reaction Rate (/target nucleus/proton)	δ_{sta}	δ_{tot}	δ_{sys}=8.8%
1	8.26E-28	7.4%	11.5%	
5	1.23E-27	5.8%	10.5%	
9	1.29E-27	5.5%	10.4%	
17	1.69E-27	4.4%	9.8%	
27	1.34E-27	5.3%	10.3%	
55	5.40E-28	7.6%	11.6%	
80	1.46E-28	11.5%	14.5%	
100	5.48E-29	16.8%	19.0%	

Table 5.5.3 Reaction rates of the $^{209}Bi(n,4n)^{206}Bi$ reaction on the main bar for 24-GeV proton bombardment.

Distance (cm)	Reaction Rate (/target nucleus/proton)	δ_{sta}	δ_{tot}	δ_{sys}=10.0%
1	1.33E-27	5.1%	11.2%	
5	1.88E-27	4.1%	10.8%	
9	2.11E-27	5.5%	11.4%	
17	2.60E-27	6.2%	11.7%	
27	2.77E-27	4.8%	11.1%	
55	1.29E-27	7.3%	12.3%	
80	3.65E-28	8.8%	13.3%	
100	1.53E-28	15.4%	18.3%	

Table 5.6.1 Reaction rates of the $^{209}Bi(n,5n)^{205}Bi$ reaction on the main bar for 1.6-GeV proton bombardment.

Distance (cm)	Reaction Rate (/target nucleus/proton)	δ_{sta}	δ_{tot}	δ_{sys}=8.7%
1	3.08E-28	4.6%	9.8%	
5	4.33E-28	3.4%	9.3%	
9	4.54E-28	6.3%	10.7%	
17	4.27E-28	2.9%	9.1%	
50	7.72E-29	13.9%	19.9%*	
80	9.71E-30	10.9%	17.9%*	
100	5.19E-30	31.4%	34.5%*	

* : including the error of calibration factor of the detector at 0.5 cm: 11.3%

Table 5.6.2 Reaction rates of the $^{209}Bi(n,5n)^{205}Bi$ reaction on the main bar for 12-GeV proton bombardment.

Distance (cm)	Reaction Rate (/target nucleus/proton)	δ_{sta}	δ_{tot}	δ_{sys}=8.8%
1	5.99E-28	4.9%	10.1%	
5	7.37E-28	4.7%	10.0%	
9	8.51E-28	5.1%	10.2%	
17	1.14E-27	3.5%	9.5%	
27	9.89E-28	4.0%	9.7%	
55	3.80E-28	7.3%	11.4%	
80	1.24E-28	4.7%	10.0%	
100	4.03E-29	10.5%	13.7%	

Table 5.6.3 Reaction rates of the $^{209}Bi(n,5n)^{205}Bi$ reaction on the main bar for 24-GeV proton bombardment.

Distance (cm)	Reaction Rate (/target nucleus/proton)	δ_{sta}	δ_{tot}	δ_{sys}=10.0%
1	9.48E-28	4.8%	11.1%	
5	1.21E-27	2.6%	10.3%	
9	1.58E-27	4.2%	10.8%	
17	1.93E-27	3.2%	10.5%	
27	2.07E-27	3.9%	10.7%	
55	9.30E-28	4.3%	10.9%	
80	2.98E-28	4.0%	10.8%	
100	1.24E-28	7.8%	12.7%	

Table 5.7.1 Reaction rates of the $^{209}Bi(n,6n)^{204}Bi$ reaction on the main bar for 1.6-GeV proton bombardment.

Distance (cm)	Reaction Rate (/target nucleus/proton)	δ_{sta}	δ_{tot}	δ_{sys}=10.5%
1	1.67E-28	2.3%	10.7%	
5	2.43E-28	1.9%	10.7%	
9	2.60E-28	2.3%	10.7%	
17	2.31E-28	2.4%	10.8%	
25	1.87E-28	2.4%	10.8%	
50	6.88E-29	4.7%	12.1%*	
80	9.21E-30	9.8%	14.8%*	
100	-	-	-	

* including the error of calibration factor of the detector at 0.5 cm: 3.6%

Table 5.7.2 Reaction rates of the $^{209}Bi(n,6n)^{204}Bi$ reaction on the main bar for 12-GeV proton bombardment.

Distance (cm)	Reaction Rate (/target nucleus/proton)	δ_{sta}	δ_{tot}	δ_{sys}=10.7%
1	3.34E-28	3.2%	11.2%	
5	4.22E-28	3.2%	11.2%	
9	5.25E-28	2.7%	11.0%	
17	6.45E-28	2.3%	10.9%	
27	5.69E-28	2.4%	11.0%	
55	2.32E-28	3.4%	11.2%	
80	6.44E-29	5.6%	12.1%	
100	2.26E-29	11.0%	15.3%	

Table 5.7.3 Reaction rates of the $^{209}Bi(n,6n)^{204}Bi$ reaction on the main bar for 24-GeV proton bombardment.

Distance (cm)	Reaction Rate (/target nucleus/proton)	δ_{sta}	δ_{tot}	δ_{sys}=11.6%
1	5.52E-28	2.1%	11.8%	
5	7.67E-28	2.1%	11.8%	
9	8.27E-28	3.3%	12.1%	
17	1.19E-27	3.0%	12.0%	
27	1.27E-27	2.2%	11.8%	
55	5.92E-28	3.3%	12.1%	
80	1.95E-28	3.3%	12.1%	
100	7.32E-29	6.0%	13.1%	

Table 5.8.1 Reaction rates of the $^{209}Bi(n,7n)^{203}Bi$ reaction on the main bar for 1.6-GeV proton bombardment.

Distance (cm)	Reaction Rate (/target nucleus/proton)	δ_{sta}	δ_{tot}	δ_{sys}=10.0%
1	1.16E-28	6.2%	11.8%	
5	1.63E-28	5.3%	11.3%	
9	1.72E-28	5.6%	11.5%	
17	1.92E-28	4.7%	11.0%	
25	1.30E-28	5.3%	11.3%	
50	5.07E-29	6.5%	13.6%*	
80	5.98E-30	17.2%	21.0%*	
100	-	-	-	

* including the error of calibration factor of the detector at 0.5 cm: 6.6%

Table 5.8.2 Reaction rates of the $^{209}Bi(n,7n)^{203}Bi$ reaction on the main bar for 12-GeV proton bombardment.

Distance (cm)	Reaction Rate (/target nucleus/proton)	δ_{sta}	δ_{tot}	δ_{sys}=10.2%
1	2.32E-28	6.9%	12.3%	
5	2.67E-28	7.2%	12.5%	
9	3.40E-28	6.4%	12.0%	
17	4.65E-28	4.2%	11.0%	
27	4.21E-28	6.3%	12.0%	
55	1.64E-28	8.7%	13.4%	
80	5.31E-29	11.5%	15.4%	
100	1.76E-29	18.9%	21.5%	

Table 5.8.3 Reaction rates of the $^{209}Bi(n,7n)^{203}Bi$ reaction on the main bar for 24-GeV proton bombardment.

Distance (cm)	Reaction Rate (/target nucleus/proton)	δ_{sta}	δ_{tot}	δ_{sys}=11.2%
1	3.22E-28	7.0%	13.2%	
5	5.73E-28	5.0%	12.3%	
9	6.29E-28	6.2%	12.8%	
17	8.77E-28	7.4%	13.4%	
27	8.86E-28	6.0%	12.7%	
55	4.47E-28	7.3%	13.4%	
80	1.30E-28	9.4%	14.6%	
100	6.16E-29	11.3%	15.9%	

Table 5.9.1 Reaction rates of the $^{209}Bi(n,8n)^{202}Bi$ reaction on the main bar for 1.6-GeV proton bombardment.

Distance (cm)	Reaction Rate (/target nucleus/proton)	δ_{sta}	δ_{tot}	δ_{sys}=8.9%
1	9.06E-29	1.5%	9.0%	
5	1.25E-28	1.7%	9.1%	
9	1.60E-28	1.6%	9.0%	
17	1.57E-28	1.7%	9.1%	
25	1.25E-28	2.1%	9.1%	
50	3.31E-29	4.2%	10.3%*	
80	6.07E-30	7.5%	12.0%*	
100	-	-	-	

* including the error of calibration factor of the detector at 0.5 cm: 3.1%

Table 5.9.2 Reaction rates of the $^{209}Bi(n,8n)^{202}Bi$ reaction on the main bar for 12-GeV proton bombardment.

Distance (cm)	Reaction Rate (/target nucleus/proton)	δ_{sta}	δ_{tot}	δ_{sys}=10.2%
1	1.59E-28	2.0%	10.4%	
5	2.13E-28	1.8%	10.4%	
9	2.62E-28	2.3%	10.5%	
17	3.58E-28	1.9%	10.4%	
27	3.38E-28	2.0%	10.4%	
55	1.35E-28	2.0%	10.4%	
80	4.05E-29	3.4%	10.7%	
100	1.52E-29	5.2%	11.4%	

Table 5.9.3 Reaction rates of the $^{209}Bi(n,8n)^{202}Bi$ reaction on the main bar for 24-GeV proton bombardment.

Distance (cm)	Reaction Rate (/target nucleus/proton)	δ_{sta}	δ_{tot}	δ_{sys}=10.2%
1	2.37E-28	1.5%	10.3%	
5	3.39E-28	1.4%	10.3%	
9	3.76E-28	1.8%	10.4%	
17	6.08E-28	2.5%	10.5%	
27	6.30E-28	2.0%	10.4%	
55	3.16E-28	2.1%	10.4%	
80	1.08E-28	2.3%	10.5%	
100	4.28E-29	4.0%	11.0%	

Table 5.10.1 Reaction rates of the $^{209}Bi(n,10n)^{200m+g}Bi$ reaction on the main bar for 1.6-GeV proton bombardment.

Distance (cm)	Reaction Rate (/target nucleus/proton)	δ_{sta}	δ_{tot}	δ_{sys}=8.7%
1	2.44E-29	16.2%	18.4%	
5	4.35E-29	20.0%	21.8%	
9	3.07E-29	31.0%	32.2%	
17	4.06E-29	38.0%	39.0%	
25	1.16E-29	196.0%	196.2%	

* including the error of calibration factor of the detector at 0.5 cm: 3.1%

Table 5.10.2 Reaction rates of the $^{209}Bi(n,10n)^{200m+g}Bi$ reaction on the main bar for 12-GeV proton bombardment.

Distance (cm)	Reaction Rate (/target nucleus/proton)	δ_{sta}	δ_{tot}	δ_{sys}=8.7%
1	3.67E-29	18.7%	21.2%	
5	6.51E-29	11.1%	14.9%	
9	7.20E-29	28.2%	29.9%	
17	1.04E-28	20.7%	23.0%	
27	6.87E-29	34.3%	35.7%	
55	4.12E-29	15.4%	18.3%	
80	1.15E-29	32.2%	33.7%	
100	5.89E-30	40.1%	41.3%	

Table 5.10.3 Reaction rates of the $^{209}Bi(n,10n)^{200m+g}Bi$ reaction on the main bar for 24-GeV proton bombardment.

Distance (cm)	Reaction Rate (/target nucleus/proton)	δ_{sta}	δ_{tot}	δ_{sys}=10.0%
1	4.83E-29	21.0%	23.2%	
5	7.15E-29	16.4%	19.2%	
9	9.93E-29	20.3%	22.6%	
17	-	-	-	
27	1.99E-28	30.0%	31.6%	
55	8.18E-29	29.3%	30.9%	
80	2.13E-29	48.1%	49.1%	
100	9.66E-30	55.3%	56.2%	

Table 5.11.1 Reaction rates of the $^{59}Co(n,\gamma)^{60}Co$ reaction on the main bar for 1.6-GeV proton bombardment.

Distance (cm)	Reaction Rate (/target nucleus/proton)	δ_{sta}	δ_{tot}	δ_{sys}=9.0%
1	3.55E-27	4.1%	9.9%	
5	3.64E-27	4.1%	9.9%	
9	4.09E-27	4.1%	9.9%	
17	3.89E-27	4.1%	9.9%	
50	1.89E-27	4.2%	10.0%	
80	1.15E-27	4.3%	10.0%	
100	9.30E-28	4.3%	10.0%	

Table 5.11.2 Reaction rates of the $^{59}Co(n,\gamma)^{60}Co$ reaction on the main bar for 12-GeV proton bombardment.

Distance (cm)	Reaction Rate (/target nucleus/proton)	δ_{sta}	δ_{tot}	$\delta_{sys\ s}$=9.2%
1	1.08E-26	4.2%	10.1%	
5	1.00E-26	4.2%	10.1%	
9	1.01E-26	4.2%	10.1%	
17	1.08E-26	4.2%	10.1%	
27	1.04E-26	4.2%	10.1%	
55	6.41E-27	4.2%	10.1%	
80	4.59E-27	4.2%	10.1%	
100	3.82E-27	4.2%	10.1%	

Table 5.11.3 Reaction rates of the $^{59}Co(n,\gamma)^{60}Co$ reaction on the main bar for 24-GeV proton bombardment.

Distance (cm)	Reaction Rate (/target nucleus/proton)	δ_{sta}	δ_{tot}	δ_{sys}=11.4%
1	1.86E-26	4.8%	11.4%	
5	1.74E-26	4.8%	11.4%	
9	1.73E-26	4.8%	11.4%	
17	1.97E-26	4.8%	11.4%	
27	1.89E-26	4.8%	11.4%	
55	1.27E-26	4.8%	11.4%	
80	8.77E-27	4.8%	11.4%	
100	7.15E-27	4.9%	11.4%	

Table 5.12.1 Reaction rates of the $^{59}Co(n,p)^{59}Fe$ reaction on the main bar for 1.6-GeV proton bombardment.

Distance (cm)	Reaction Rate (/target nucleus/proton)	δ_{sta}	δ_{tot}	δ_{sys}=9.4%
1	2.23E-31	4.7%	10.5%	
5	2.41E-31	4.6%	10.5%	
9	2.88E-31	4.6%	10.5%	
17	2.56E-31	4.6%	10.5%	
25	1.59E-31	5.1%	10.7%	
50	3.33E-32	10.6%	14.2%	
80	6.03E-32	10.4%	14.0%	
100	-	-	-	

Table 5.12.2 Reaction rates of the $^{59}Co(n,p)^{59}Fe$ reaction on the main bar for 12-GeV proton bombardment.

Distance (cm)	Reaction Rate (/target nucleus/proton)	δ_{sta}	δ_{tot}	δ_{sys}=9.6%
1	2.99E-31	4.6%	10.6%	
5	3.59E-31	4.5%	10.6%	
9	4.11E-31	4.4%	10.5%	
17	4.75E-31	4.4%	10.5%	
27	4.22E-31	4.4%	10.5%	
55	1.47E-31	5.1%	10.8%	
80	5.35E-32	6.8%	11.8%	
100	-	-	-	

Table 5.12.3 Reaction rates of the $^{59}Co(n,p)^{59}Fe$ reaction on the main bar for 24-GeV proton bombardment.

Distance (cm)	Reaction Rate (/target nucleus/proton)	δ_{sta}	δ_{tot}	δ_{sys}=10.6%
1	4.53E-31	5.0%	11.8%	
5	5.52E-31	5.0%	11.7%	
9	6.40E-31	4.9%	11.7%	
17	8.11E-31	4.9%	11.7%	
27	7.68E-31	4.9%	11.7%	
55	3.29E-31	5.1%	11.8%	
80	1.07E-31	6.3%	12.4%	
100	4.38E-32	9.2%	14.1%	

Table 5.13.1 Reaction rates of the $^{59}Co(n,x)^{56}Mn$ reaction on the main bar for 1.6-GeV proton bombardment.

Distance (cm)	Reaction Rate (/target nucleus/proton)	δ_{sta}	δ_{tot}	δ_{sys}=9.0%
1	3.55E-29	4.1%	9.9%	
5	4.37E-29	4.1%	9.9%	
9	4.66E-29	4.1%	9.9%	
17	4.25E-29	4.1%	9.9%	
25	3.03E-29	4.1%	9.9%	
50	7.04E-30	4.2%	10.0%	
80	9.68E-31	5.2%	10.4%	
100	5.02E-31	6.3%	11.0%	

Table 5.13.2 Reaction rates of the $^{59}Co(n,x)^{56}Mn$ reaction on the main bar for 12-GeV proton bombardment.

Distance (cm)	Reaction Rate (/target nucleus/proton)	δ_{sta}	δ_{tot}	δ_{sys}=9.2%
1	6.34E-29	4.2%	10.1%	
5	7.68E-29	4.2%	10.1%	
9	8.91E-29	4.2%	10.1%	
17	1.08E-28	4.2%	10.1%	
27	9.84E-29	4.2%	10.1%	
55	3.66E-29	4.2%	10.1%	
80	1.13E-29	4.2%	10.1%	
100	3.82E-30	4.3%	10.2%	

Table 5.13.3 Reaction rates of the $^{59}Co(n,x)^{56}Mn$ reaction on the main bar for 24-GeV proton bombardment.

Distance (cm)	Reaction Rate (/target nucleus/proton)	δ_{sta}	δ_{tot}	δ_{sys}=10.3%
1	9.32E-29	4.8%	11.4%	
5	1.19E-28	4.8%	11.4%	
9	1.33E-28	4.8%	11.4%	
17	1.86E-28	4.8%	11.4%	
27	1.85E-28	4.8%	11.4%	
55	8.42E-29	4.8%	11.4%	
80	2.78E-29	4.8%	11.4%	
100	1.05E-29	4.8%	11.4%	

Table 5.14.1 Reaction rates of the $^{59}Co(n,2n)^{58}Co$ reaction on the main bar for 1.6-GeV proton bombardment.

Distance (cm)	Reaction Rate (/target nucleus/proton)	δ_{sta}	δ_{tot}	δ_{sys}=9.0%
1	5.93E-28	4.1%	9.9%	
5	6.93E-28	4.1%	9.9%	
9	7.58E-28	4.1%	9.9%	
17	6.59E-28	4.1%	9.9%	
25	4.59E-28	4.1%	9.9%	
50	9.95E-29	5.1%	10.4%	
80	1.55E-29	19.8%	21.8%	
100	8.44E-30	35.9%	37.0%	

Table 5.14.2 Reaction rates of the $^{59}Co(n,2n)^{58}Co$ reaction on the main bar for 12-GeV proton bombardment.

Distance (cm)	Reaction Rate (/target nucleus/proton)	δ_{sta}	δ_{tot}	δ_{sys}=9.2%
1	1.06E-27	4.2%	10.1%	
5	1.26E-27	4.2%	10.1%	
9	1.45E-27	4.2%	10.1%	
17	1.72E-27	4.2%	10.1%	
27	1.52E-27	4.2%	10.1%	
55	5.51E-28	4.2%	10.1%	
80	1.62E-28	4.3%	10.2%	
100	6.05E-29	4.6%	10.3%	

Table 5.14.3 Reaction rates of the $^{59}Co(n,2n)^{58}Co$ reaction on the main bar for 24-GeV proton bombardment.

Distance (cm)	Reaction Rate (/target nucleus/proton)	δ_{sta}	δ_{tot}	δ_{sys}=10.3%
1	1.59E-27	4.8%	11.4%	
5	1.98E-27	4.8%	11.4%	
9	2.21E-27	4.8%	11.4%	
17	2.96E-27	4.8%	11.4%	
27	2.89E-27	4.8%	11.4%	
55	1.25E-27	4.8%	11.4%	
80	4.23E-28	4.8%	11.4%	
100	1.62E-28	4.9%	11.4%	

Table 5.15.1 Reaction rates of the $^{59}Co(n,3n)^{57}Co$ reaction on the main bar for 1.6-GeV proton bombardment.

Distance (cm)	Reaction Rate (/target nucleus/proton)	δ_{sta}	δ_{tot}	δ_{sys}=9.0%
1	1.38E-28	4.2%	10.0%	
5	1.72E-28	4.2%	10.0%	
9	1.87E-28	4.2%	10.0%	
17	1.78E-28	4.2%	10.0%	
25	1.29E-28	4.3%	10.0%	
50	2.82E-29	5.2%	10.4%	
80	3.70E-30	16.8%	19.1%	
100	3.15E-30	20.1%	22.1%	

Table 5.15.2 Reaction rates of the $^{59}Co(n,3n)^{57}Co$ reaction on the main bar for 12-GeV proton bombardment.

Distance (cm)	Reaction Rate (/target nucleus/proton)	δ_{sta}	δ_{tot}	δ_{sys}=9.2%
1	2.52E-28	4.2%	10.1%	
5	3.18E-28	4.2%	10.1%	
9	3.62E-28	4.2%	10.1%	
17	4.40E-28	4.2%	10.1%	
27	4.10E-28	4.2%	10.1%	
55	1.52E-28	4.3%	10.2%	
80	4.45E-29	4.6%	10.3%	
100	1.75E-29	6.2%	11.1%	

Table 5.15.3 Reaction rates of the $^{59}Co(n,3n)^{57}Co$ reaction on the main bar for 24-GeV proton bombardment.

Distance (cm)	Reaction Rate (/target nucleus/proton)	δ_{sta}	δ_{tot}	δ_{sys}=10.3%
1	3.75E-28	4.8%	11.4%	
5	4.85E-28	4.8%	11.4%	
9	5.48E-28	4.8%	11.4%	
17	7.70E-28	4.8%	11.4%	
27	7.65E-28	4.8%	11.4%	
55	3.45E-28	4.8%	11.4%	
80	1.14E-28	4.9%	11.4%	
100	4.37E-29	5.5%	11.7%	

Table 5.16.1 Reaction rates of the $^{59}Co(n,4n)^{56}Co$ reaction on the main bar for 1.6-GeV proton bombardment.

Distance (cm)	Reaction Rate (/target nucleus/proton)	δ_{sta}	δ_{tot}	δ_{sys}=9.0%
1	1.77E-29	7.7%	11.9%	
5	2.22E-29	6.5%	11.2%	
9	2.51E-29	5.6%	10.6%	
17	2.77E-29	6.0%	10.8%	
25	1.90E-29	7.5%	11.7%	
50	6.87E-30	15.6%	18.0%	
80	3.89E-30	18.7%	20.7%	
100	-	-	-	

Table 5.16.2 Reaction rates of the $^{59}Co(n,4n)^{56}Co$ reaction on the main bar for 12-GeV proton bombardment.

Distance (cm)	Reaction Rate (/target nucleus/proton)	δ_{sta}	δ_{tot}	δ_{sys}=9.2%
1	3.25E-29	5.4%	10.7%	
5	3.96E-29	5.3%	10.6%	
9	5.35E-29	4.7%	10.3%	
17	6.64E-29	4.7%	10.3%	
27	5.91E-29	4.7%	10.3%	
55	2.61E-29	5.6%	10.8%	
80	1.07E-29	9.1%	13.0%	
100	5.73E-30	14.3%	17.0%	

Table 5.16.3 Reaction rates of the $^{59}Co(n,4n)^{56}Co$ reaction on the main bar for 24-GeV proton bombardment.

Distance (cm)	Reaction Rate (/target nucleus/proton)	δ_{sta}	δ_{tot}	δ_{sys}=10.3%
1	4.98E-29	5.8%	11.8%	
5	7.09E-29	5.4%	11.6%	
9	7.02E-29	5.2%	11.6%	
17	1.09E-28	5.1%	11.5%	
27	1.14E-28	5.1%	11.5%	
55	5.43E-29	5.5%	11.7%	
80	1.76E-29	7.3%	12.7%	
100	9.06E-30	12.3%	16.1%	

Table 5.17.1 Reaction rates of the $^{59}Co(n,5n)^{55}Co$ reaction on the main bar for 1.6-GeV proton bombardment.

Distance (cm)	Reaction Rate (/target nucleus/proton)	δ_{sta}	δ_{tot}	δ_{sys}=10.5%
1	1.55E-30	5.5%	11.8%	
5	1.81E-30	5.5%	11.9%	
9	1.80E-30	5.0%	11.6%	
17	1.88E-30	5.0%	11.6%	
25	1.71E-30	5.0%	11.6%	
50	6.45E-31	7.4%	12.9%	
80	-	-	-	
100	2.82E-31	20.7%	23.2%	

Table 5.17.2 Reaction rates of the $^{59}Co(n,5n)^{55}Co$ reaction on the main bar for 12-GeV proton bombardment.

Distance (cm)	Reaction Rate (/target nucleus/proton)	δ_{sta}	δ_{tot}	δ_{sys}=10.6%
1	2.30E-30	7.1%	12.8%	
5	2.94E-30	6.6%	12.5%	
9	3.38E-30	5.7%	12.1%	
17	4.52E-30	5.3%	11.9%	
27	4.56E-30	5.4%	12.0%	
55	1.71E-30	7.4%	12.9%	
80	8.46E-31	10.4%	14.9%	
100	4.04E-31	12.4%	16.4%	

Table 5.17.3 Reaction rates of the $^{59}Co(n,5n)^{55}Co$ reaction on the main bar for 24-GeV proton bombardment.

Distance (cm)	Reaction Rate (/target nucleus/proton)	δ_{sta}	δ_{tot}	δ_{sys}=11.6%
1	3.19E-30	6.8%	13.4%	
5	5.02E-30	5.9%	13.0%	
9	4.83E-30	6.0%	13.1%	
17	8.04E-30	5.6%	12.9%	
27	8.95E-30	5.4%	12.8%	
55	4.12E-30	6.2%	13.2%	
80	1.55E-30	8.6%	14.5%	
100	7.02E-31	12.5%	17.1%	

Table 5.18.1 Reaction rates of the $^{169}Tm(n,2n)^{168}Tm$ reaction on the main bar for 1.6-GeV proton bombardment.

Distance (cm)	Reaction Rate (/target nucleus/proton)	δ_{sta}	δ_{tot}	δ_{sys} =9.2%
3	1.74E-27	6.3%	11.1%	
11	1.91E-27	4.5%	10.2%	
15	1.86E-27	5.6%	10.7%	
27	9.10E-28	11.5%	14.7%	
48	2.99E-28	6.4%	11.2%	
78	2.92E-29	60.0%	60.7%	

Table 5.18.2 Reaction rates of the $^{169}Tm(n,2n)^{168}Tm$ reaction on the main bar for 12-GeV proton bombardment.

Distance (cm)	Reaction Rate (/target nucleus/proton)	δ_{sta}	δ_{tot}	δ_{sys} =9.3%
3	2.86E-27	10.9%	14.4%	
11	3.71E-27	11.0%	14.4%	
15	4.61E-27	8.1%	12.4%	
29	3.29E-27	10.5%	14.1%	
48	1.78E-27	11.7%	15.0%	
78	2.68E-28	23.0%	24.8%	

Table 5.18.3 Reaction rates of the $^{169}Tm(n,2n)^{168}Tm$ reaction on the main bar for 24-GeV proton bombardment.

Distance (cm)	Reaction Rate (/target nucleus/proton)	δ_{sta}	δ_{tot}	δ_{sys}=10.4%
3	4.73E-27	5.8%	11.9%	
11	7.07E-27	6.0%	12.0%	
15	7.57E-27	5.5%	11.8%	
29	6.87E-27	3.6%	11.0%	
48	4.45E-27	7.5%	12.8%	
78	1.05E-27	6.3%	12.2%	

Table 5.19.1 Reaction rates of the $^{169}Tm(n,3n)^{167}Tm$ reaction on the main bar for 1.6-GeV proton bombardment.

Distance (cm)	Reaction Rate (/target nucleus/proton)	δ_{sta}	δ_{tot}	δ_{sys}=20.7%
3	9.44E-28	3.2%	20.9%	
11	1.04E-27	1.6%	20.8%	
15	9.95E-28	2.2%	20.8%	
27	5.61E-28	4.9%	21.3%	
48	1.67E-28	2.5%	20.9%	
78	2.26E-29	26.3%	33.5%	

Table 5.19.2 Reaction rates of the $^{169}Tm(n,3n)^{167}Tm$ reaction on the main bar for 12-GeV proton bombardment.

Distance (cm)	Reaction Rate (/target nucleus/proton)	δ_{sta}	δ_{tot}	δ_{sys}=20.8%
3	1.69E-27	3.9%	21.2%	
11	2.38E-27	3.6%	21.1%	
15	2.54E-27	2.3%	20.9%	
29	2.01E-27	3.8%	21.1%	
48	1.19E-27	4.3%	21.2%	
78	2.88E-28	8.3%	22.4%	

Table 5.19.3 Reaction rates of the $^{169}Tm(n,3n)^{167}Tm$ reaction on the main bar for 24-GeV proton bombardment.

Distance (cm)	Reaction Rate (/target nucleus/proton)	δ_{sta}	δ_{tot}	δ_{sys}=20.8%
3	2.71E-27	2.0%	21.4%	
11	3.74E-27	2.7%	21.5%	
15	4.03E-27	2.5%	21.4%	
29	4.17E-27	1.4%	21.3%	
48	2.63E-27	3.2%	21.5%	
78	7.14E-28	2.4%	21.4%	

Table 5.20.1 Reaction rates of the ^{169}Tm(n,4n)^{166}Tm reaction on the main bar for 1.6-GeV proton bombardment.

Distance (cm)	Reaction Rate (/target nucleus/proton)	δ_{sta}	δ_{tot}	δ_{sys}=10.4%
3	4.16E-28	2.5%	10.7%	
11	5.61E-28	2.4%	10.7%	
15	5.20E-28	2.2%	10.6%	
27	3.25E-28	1.8%	10.6%	
48	9.27E-29	4.7%	11.4%	
78	1.48E-29	13.1%	16.7%	

Table 5.20.2 Reaction rates of the ^{169}Tm(n,4n)^{166}Tm reaction on the main bar for 12-GeV proton bombardment.

Distance (cm)	Reaction Rate (/target nucleus/proton)	δ_{sta}	δ_{tot}	δ_{sys}=10.6%
3	8.04E-28	2.7%	10.9%	
11	1.15E-27	2.6%	10.9%	
15	1.03E-27	2.2%	10.8%	
29	1.12E-27	2.4%	10.8%	
48	5.74E-28	3.7%	11.2%	
78	1.29E-28	6.3%	12.3%	

Table 5.20.3 Reaction rates of the ^{169}Tm(n,4n)^{166}Tm reaction on the main bar for 24-GeV proton bombardment.

Distance (cm)	Reaction Rate (/target nucleus/proton)	δ_{sta}	δ_{tot}	δ_{sys}=11.5%
3	1.16E-27	2.4%	11.7%	
11	1.78E-27	1.7%	11.6%	
15	2.04E-27	1.5%	11.6%	
29	2.01E-27	1.8%	11.6%	
48	1.22E-27	2.5%	11.8%	
78	3.26E-28	3.7%	12.1%	

Table 5.21.1 Reaction rates of the $^{169}Tm(n,5n)^{165}Tm$ reaction on the main bar for 1.6-GeV proton bombardment.

Distance (cm)	Reaction Rate (/target nucleus/proton)	δ_{sta}	δ_{tot}	δ_{sys}=10.3%
3	3.08E-28	2.7%	10.6%	
11	4.01E-28	2.4%	10.6%	
15	3.74E-28	2.5%	10.6%	
27	2.38E-28	2.0%	10.5%	
48	7.30E-29	3.4%	10.8%	
78	1.13E-29	14.9%	18.1%	

Table 5.21.2 Reaction rates of the $^{169}Tm(n,5n)^{165}Tm$ reaction on the main bar for 12-GeV proton bombardment.

Distance (cm)	Reaction Rate (/target nucleus/proton)	δ_{sta}	δ_{tot}	δ_{sys}=10.4%
3	5.38E-28	2.4%	10.7%	
11	8.30E-28	1.9%	10.6%	
15	8.51E-28	1.8%	10.6%	
29	8.33E-28	2.1%	10.6%	
48	4.53E-28	2.4%	10.7%	
78	1.01E-28	4.5%	11.3%	

Table 5.21.3 Reaction rates of the $^{169}Tm(n,5n)^{165}Tm$ reaction on the main bar for 24-GeV proton bombardment.

Distance (cm)	Reaction Rate (/target nucleus/proton)	δ_{sta}	δ_{tot}	δ_{sys}=11.4%
3	8.65E-28	2.4%	11.6%	
11	1.30E-27	2.4%	11.6%	
15	1.54E-27	2.2%	11.6%	
29	1.53E-27	1.1%	11.5%	
48	8.81E-28	3.4%	11.9%	
78	2.58E-28	1.7%	11.5%	

Table 5.22.1 Reaction rates of the $^{89}Y(n,2n)^{88}Y$ reaction on the main bar for 1.6-GeV proton bombardment.

Distance (cm)	Reaction Rate (/target nucleus/proton)	δ_{sta}	δ_{tot}	δ_{sys}=9.0%
3	8.30E-28	4.2%	10.0%	
11	9.69E-28	4.2%	10.0%	
15	8.90E-28	4.2%	10.0%	
27	5.02E-28	4.3%	10.0%	
48	1.46E-28	4.9%	10.3%	
78	1.67E-29	16.4%	18.8%	

Table 5.22.2 Reaction rates of the $^{89}Y(n,2n)^{88}Y$ reaction on the main bar for 12-GeV proton bombardment.

Distance (cm)	Reaction Rate (/target nucleus/proton)	δ_{sta}	δ_{tot}	δ_{sys}=9.2%
3	1.52E-27	4.2%	10.1%	
11	2.10E-27	4.2%	10.1%	
15	2.24E-27	4.2%	10.1%	
29	1.96E-27	4.2%	10.1%	
48	1.02E-27	4.2%	10.1%	
78	2.49E-28	4.4%	10.2%	

Table 5.22.3 Reaction rates of the $^{89}Y(n,2n)^{88}Y$ reaction on the main bar for 24-GeV proton bombardment.

Distance (cm)	Reaction Rate (/target nucleus/proton)	δ_{sta}	δ_{tot}	δ_{sys}=10.3%
3	2.35E-27	4.8%	11.4%	
11	3.46E-27	4.8%	11.4%	
15	3.88E-27	4.8%	11.4%	
29	3.74E-27	4.8%	11.4%	
48	2.22E-27	4.8%	11.4%	
78	6.19E-28	4.8%	11.4%	

Table 5.23.1 Reaction rates of the $^{89}Y(n,3n)^{87m+g}Y$ reaction on the main bar for 1.6-GeV proton bombardment.

Distance (cm)	Reaction Rate (/target nucleus/proton)	δ_{sta}	δ_{tot}	δ_{sys}=9.0%
3	2.52E-28	4.1%	9.9%	
11	3.17E-28	4.1%	9.9%	
15	3.01E-28	4.1%	9.9%	
27	1.85E-28	4.1%	9.9%	
48	5.48E-29	4.1%	9.9%	
78	8.26E-30	4.3%	10.0%	

Table 5.23.2 Reaction rates of the $^{89}Y(n,3n)^{87m+g}Y$ reaction on the main bar for 12-GeV proton bombardment.

Distance (cm)	Reaction Rate (/target nucleus/proton)	δ_{sta}	δ_{tot}	δ_{sys}=9.2%
3	4.60E-28	4.2%	10.1%	
11	6.51E-28	4.2%	10.1%	
15	7.07E-28	4.2%	10.1%	
29	6.41E-28	4.2%	10.1%	
48	3.32E-28	4.2%	10.1%	
78	8.35E-29	4.2%	10.1%	

Table 5.23.3 Reaction rates of the $^{89}Y(n,3n)^{87m+g}Y$ reaction on the main bar for 24-GeV proton bombardment.

Distance (cm)	Reaction Rate (/target nucleus/proton)	δ_{sta}	δ_{tot}	δ_{sys}=10.3%
3	6.95E-28	4.8%	11.4%	
11	1.06E-27	4.8%	11.4%	
15	1.19E-27	4.8%	11.4%	
29	1.19E-27	4.8%	11.4%	
48	7.11E-28	4.8%	11.4%	
78	2.06E-28	4.8%	11.4%	

Table 5.24.1 Reaction rates of the $^{89}Y(n,4n)^{86m+g}Y$ reaction on the main bar for 1.6-GeV proton bombardment.

Distance (cm)	Reaction Rate (/target nucleus/proton)	δ_{sta}	δ_{tot}	δ_{sys}=9.0%
3	1.02E-28	4.1%	9.9%	
11	1.33E-28	4.1%	9.9%	
15	1.33E-28	4.1%	9.9%	
27	8.61E-29	4.1%	9.9%	
48	2.62E-29	4.1%	9.9%	
78	4.08E-30	4.7%	10.2%	

Table 5.24.2 Reaction rates of the $^{89}Y(n,4n)^{86m+g}Y$ reaction on the main bar for 12-GeV proton bombardment.

Distance (cm)	Reaction Rate (/target nucleus/proton)	δ_{sta}	δ_{tot}	δ_{sys}=9.2%
3	1.88E-28	4.2%	10.1%	
11	2.75E-28	4.2%	10.1%	
15	3.06E-28	4.2%	10.1%	
29	2.85E-28	4.2%	10.1%	
48	1.50E-28	4.2%	10.1%	
78	3.75E-29	4.2%	10.2%	

Table 5.24.3 Reaction rates of the $^{89}Y(n,4n)^{86m+g}Y$ reaction on the main bar for 24-GeV proton bombardment.

Distance (cm)	Reaction Rate (/target nucleus/proton)	δ_{sta}	δ_{tot}	δ_{sys}=10.3%
3	2.83E-28	4.8%	11.4%	
11	4.44E-28	4.8%	11.4%	
15	5.07E-28	4.8%	11.4%	
29	5.31E-28	4.8%	11.4%	
48	3.26E-28	4.8%	11.4%	
78	9.51E-29	4.8%	11.4%	

Table 5.25.1 Reaction rates of the $^{89}Y(n,5n)^{85g}Y$ reaction on the main bar for 1.6-GeV proton bombardment.

Distance (cm)	Reaction Rate (/target nucleus/proton)	δ_{sta}	δ_{tot}	δ_{sys} =13.3%
3	1.22E-29	5.3%	14.3%	
11	1.75E-29	5.1%	14.2%	
15	2.24E-29	4.6%	14.1%	
27	1.40E-29	4.9%	14.2%	
48	5.83E-30	5.7%	14.5%	
78	7.94E-31	14.1%	19.4%	

Table 5.25.2 Reaction rates of the $^{89}Y(n,5n)^{85g}Y$ reaction on the main bar for 12-GeV proton bombardment.

Distance (cm)	Reaction Rate (/target nucleus/proton)	δ_{sta}	δ_{tot}	δ_{sys}=13.4%
3	2.76E-29	4.4%	14.1%	
11	3.46E-29	4.3%	14.1%	
15	3.94E-29	4.3%	14.1%	
29	4.74E-29	4.3%	14.1%	
48	2.07E-29	4.3%	14.1%	
78	5.82E-30	4.7%	14.2%	

Table 5.25.3 Reaction rates of the $^{89}Y(n,5n)^{85g}Y$ reaction on the main bar for 24-GeV proton bombardment.

Distance (cm)	Reaction Rate (/target nucleus/proton)	δ_{sta}	δ_{tot}	δ_{sys}=14.2%
3	3.43E-29	5.0%	15.0%	
11	5.69E-29	4.9%	15.0%	
15	6.71E-29	4.8%	15.0%	
29	6.88E-29	4.9%	15.0%	
48	4.39E-29	4.9%	15.0%	
78	1.61E-30	5.0%	15.1%	

Table 5.26.1 Reaction rates of the $^{nat}Ni(n,x)^{58}Co$ reaction on the main bar for 1.6-GeV proton bombardment.

Distance (cm)	Reaction Rate (/target nucleus/proton)	δ_{sta}	δ_{tot}	δ_{sys} =9.0%
1	1.30E-27	4.1%	9.9%	
5	1.47E-27	4.1%	9.9%	
9	1.52E-27	4.1%	9.9%	
17	1.27E-27	4.1%	9.9%	
25	8.93E-28	4.1%	9.9%	
50	1.73E-28	4.5%	10.1%	
80	1.81E-29	18.8%	20.9%	
100	9.25E-30	35.6%	36.7%	

Table 5.26.2 Reaction rates of the $^{nat}Ni(n,x)^{58}Co$ reaction on the main bar for 12-GeV proton bombardment.

Distance (cm)	Reaction Rate (/target nucleus/proton)	δ_{sta}	δ_{tot}	δ_{sys}=9.2%
1	1.99E-27	4.2%	10.1%	
5	2.34E-27	4.2%	10.1%	
9	2.70E-27	4.2%	10.1%	
17	3.13E-27	4.2%	10.1%	
27	2.75E-27	4.2%	10.1%	
55	9.64E-28	4.3%	10.1%	
80	2.83E-28	5.2%	10.6%	
100	1.04E-28	9.6%	13.3%	

Table 5.26.3 Reaction rates of the $^{nat}Ni(n,x)^{58}Co$ reaction on the main bar for 24-GeV proton bombardment.

Distance (cm)	Reaction Rate (/target nucleus/proton)	δ_{sta}	δ_{tot}	δ_{sys}=10.3%
1	3.01E-27	4.8%	11.4%	
5	3.70E-27	4.8%	11.4%	
9	4.16E-27	4.8%	11.4%	
17	5.51E-27	4.8%	11.4%	
27	5.29E-27	4.8%	11.4%	
55	2.19E-27	4.8%	11.4%	
80	7.31E-28	5.0%	11.4%	
100	2.70E-28	6.1%	12.0%	

Table 5.27.1 Reaction rates of the $^{nat}Ni(n,x)^{57}Co$ reaction on the main bar for 1.6-GeV proton bombardment.

Distance (cm)	Reaction Rate (/target nucleus/proton)	δ_{sta}	δ_{tot}	δ_{sys}=9.0%
1	4.75E-28	4.1%	9.9%	
5	5.55E-28	4.1%	9.9%	
9	6.10E-28	4.1%	9.9%	
17	5.35E-28	4.1%	9.9%	
25	3.86E-28	4.1%	9.9%	
50	8.57E-29	4.3%	10.0%	
80	1.12E-29	8.7%	12.5%	
100	7.36E-30	10.8%	14.1%	

Table 5.27.2 Reaction rates of the $^{nat}Ni(n,x)^{57}Co$ reaction on the main bar for 12-GeV proton bombardment.

Distance (cm)	Reaction Rate (/target nucleus/proton)	δ_{sta}	δ_{tot}	δ_{sys}=9.2%
1	8.32E-28	4.2%	10.1%	
5	1.00E-27	4.2%	10.1%	
9	1.16E-27	4.2%	10.1%	
17	1.37E-27	4.2%	10.1%	
27	1.24E-27	4.2%	10.1%	
55	4.55E-28	4.2%	10.1%	
80	1.34E-28	4.9%	10.4%	
100	4.79E-29	8.3%	12.4%	

Table 5.27.3 Reaction rates of the $^{nat}Ni(n,x)^{57}Co$ reaction on the main bar for 24-GeV proton bombardment.

Distance (cm)	Reaction Rate (/target nucleus/proton)	δ_{sta}	δ_{tot}	δ_{sys}=10.3%
1	1.22E-27	4.8%	11.4%	
5	1.56E-27	4.8%	11.4%	
9	1.77E-27	4.8%	11.4%	
17	2.36E-27	4.8%	11.4%	
27	2.35E-27	4.8%	11.4%	
55	1.04E-27	4.8%	11.4%	
80	3.42E-28	4.9%	11.4%	
100	1.31E-28	5.6%	11.7%	

Table 5.28.1 Reaction rates of the $^{nat}Ti(n,x)^{48}Sc$ reaction on the main bar for 1.6-GeV proton bombardment.

Distance (cm)	Reaction Rate (/target nucleus/proton)	δ_{sta}	δ_{tot}	δ_{sys}=9.0%
3	5.28E-29	4.1%	9.9%	
11	6.16E-29	4.1%	9.9%	
15	5.67E-29	4.1%	9.9%	
27	3.35E-29	4.1%	9.9%	
48	9.33E-30	4.8%	10.2%	
78	1.18E-30	12.8%	15.7%	

Table 5.28.2 Reaction rates of the $^{nat}Ti(n,x)^{48}Sc$ reaction on the main bar for 12-GeV proton bombardment.

Distance (cm)	Reaction Rate (/target nucleus/proton)	δ_{sta}	δ_{tot}	δ_{sys}=9.2%
3	9.35E-29	4.2%	10.1%	
11	1.26E-28	4.2%	10.1%	
15	1.34E-28	4.2%	10.1%	
29	1.20E-28	4.2%	10.1%	
48	6.11E-29	4.2%	10.1%	
78	1.51E-29	4.5%	10.3%	

Table 5.28.3 Reaction rates of the $^{nat}Ti(n,x)^{48}Sc$ reaction on the main bar for 24-GeV proton bombardment.

Distance (cm)	Reaction Rate (/target nucleus/proton)	δ_{sta}	δ_{tot}	δ_{sys}=10.3%
3	1.40E-28	4.8%	11.4%	
11	2.05E-28	4.8%	11.4%	
15	2.31E-28	4.8%	11.4%	
29	2.21E-28	4.8%	11.4%	
48	1.29E-28	4.8%	11.4%	
78	3.69E-29	4.9%	11.4%	

Table 5.29.1 Reaction rates of the $^{nat}Ti(n,x)^{47}Sc$ reaction on the main bar for 1.6-GeV proton bombardment.

Distance (cm)	Reaction Rate (/target nucleus/proton)	δ_{sta}	δ_{tot}	δ_{sys}=9.1%
3	1.51E-28	4.1%	9.9%	
11	1.91E-28	4.1%	9.9%	
15	1.83E-28	4.1%	9.9%	
27	1.13E-28	4.1%	9.9%	
48	3.40E-29	4.3%	10.0%	
78	4.82E-30	6.8%	11.3%	

Table 5.29.2 Reaction rates of the $^{nat}Ti(n,x)^{47}Sc$ reaction on the main bar for 12-GeV proton bombardment.

Distance (cm)	Reaction Rate (/target nucleus/proton)	δ_{sta}	δ_{tot}	δ_{sys}=9.2%
3	2.88E-28	4.2%	10.1%	
11	4.01E-28	4.2%	10.1%	
15	4.39E-28	4.2%	10.1%	
29	3.97E-28	4.2%	10.1%	
48	2.11E-28	4.2%	10.1%	
78	5.12E-29	4.3%	10.2%	

Table 5.29.3 Reaction rates of the $^{nat}Ti(n,x)^{47}Sc$ reaction on the main bar for 24-GeV proton bombardment.

Distance (cm)	Reaction Rate (/target nucleus/proton)	δ_{sta}	δ_{tot}	δ_{sys}=10.3%
3	4.28E-28	4.8%	11.4%	
11	6.58E-28	4.8%	11.4%	
15	7.45E-28	4.8%	11.4%	
29	7.37E-28	4.8%	11.4%	
48	4.48E-28	4.8%	11.4%	
78	1.28E-28	4.8%	11.4%	

Table 5.30.1 Reaction rates of the $^{nat}Ti(n,x)^{46g}Sc$ reaction on the main bar for 1.6-GeV proton bombardment.

Distance (cm)	Reaction Rate (/target nucleus/proton)	δ_{sta}	δ_{tot}	δ_{sys}=9.0%
3	9.95E-29	5.3%	10.5%	
11	1.35E-28	4.9%	10.3%	
15	1.32E-28	4.9%	10.3%	
27	6.52E-29	6.3%	11.0%	
48	-	-	-	
78	-	-	-	

Table 5.30.2 Reaction rates of the $^{nat}Ti(n,x)^{46g}Sc$ reaction on the main bar for 12-GeV proton bombardment.

Distance (cm)	Reaction Rate (/target nucleus/proton)	δ_{sta}	δ_{tot}	δ_{sys}=9.2%
3	2.70E-28	4.2%	10.1%	
11	3.76E-28	4.2%	10.1%	
15	4.09E-28	4.2%	10.1%	
29	3.81E-28	4.2%	10.1%	
48	2.00E-28	4.2%	10.1%	
78	4.96E-29	4.7%	10.3%	

Table 5.30.3 Reaction rates of the $^{nat}Ti(n,x)^{46g}Sc$ reaction on the main bar for 24-GeV proton bombardment.

Distance (cm)	Reaction Rate (/target nucleus/proton)	δ_{sta}	δ_{tot}	δ_{sys}=10.3%
3	4.09E-28	4.8%	11.4%	
11	6.18E-28	4.8%	11.4%	
15	6.93E-28	4.8%	11.4%	
29	7.20E-28	4.8%	11.4%	
48	4.32E-28	4.8%	11.4%	
78	1.26E-28	4.9%	11.4%	

Table 5.31.1 Reaction rates of the $^{nat}Ti(n,x)^{44g}Sc$ reaction on the main bar for 1.6-GeV proton bombardment.

Distance (cm)	Reaction Rate (/target nucleus/proton)	δ_{sta}	δ_{tot}	δ_{sys}=9.0%
3	2.81E-29	4.1%	9.9%	
11	3.72E-29	4.2%	10.0%	
15	3.67E-29	4.2%	10.0%	
27	2.40E-29	4.2%	10.0%	
48	9.54E-30	4.4%	10.1%	
78	1.90E-30	5.6%	10.6%	

Table 5.31.2 Reaction rates of the $^{nat}Ti(n,x)^{44g}Sc$ reaction on the main bar for 12-GeV proton bombardment.

Distance (cm)	Reaction Rate (/target nucleus/proton)	δ_{sta}	δ_{tot}	δ_{sys}=9.2%
3	4.68E-29	4.3%	10.2%	
11	7.31E-29	4.2%	10.1%	
15	7.90E-29	4.2%	10.1%	
29	7.93E-29	4.2%	10.1%	
48	4.42E-29	4.2%	10.1%	
78	1.16E-29	4.4%	10.2%	

Table 5.31.3 Reaction rates of the $^{nat}Ti(n,x)^{44g}Sc$ reaction on the main bar for 24-GeV proton bombardment.

Distance (cm)	Reaction Rate (/target nucleus/proton)	δ_{sta}	δ_{tot}	δ_{sys}=10.3%
3	7.25E-29	4.8%	11.4%	
11	1.19E-28	4.8%	11.4%	
15	1.36E-28	4.8%	11.4%	
29	1.49E-28	4.8%	11.4%	
48	9.59E-29	4.8%	11.4%	
78	2.83E-29	4.8%	11.4%	

Table 5.32.1 Reaction rates of the $^{nat}Ti(n,x)^{44m}Sc$ reaction on the main bar for 1.6-GeV proton bombardment.

Distance (cm)	Reaction Rate (/target nucleus/proton)	δ_{sta}	δ_{tot}	δ_{sys}=9.0%
3	1.21E-29	4.2%	10.0%	
11	1.73E-29	4.1%	9.9%	
15	1.71E-29	4.2%	10.0%	
27	1.18E-29	4.3%	10.0%	
48	3.98E-30	5.0%	10.3%	
78	8.08E-31	10.7%	14.0%	

Table 5.32.2 Reaction rates of the $^{nat}Ti(n,x)^{44m}Sc$ reaction on the main bar for 12-GeV proton bombardment.

Distance (cm)	Reaction Rate (/target nucleus/proton)	δ_{sta}	δ_{tot}	δ_{sys}=9.2%
3	2.18E-29	5.3%	10.6%	
11	3.61E-29	4.9%	10.5%	
15	3.81E-29	4.9%	10.4%	
29	3.99E-29	4.6%	10.3%	
48	2.16E-29	5.3%	10.7%	
78	5.89E-30	5.9%	10.9%	

Table 5.32.3 Reaction rates of the $^{nat}Ti(n,x)^{44m}Sc$ reaction on the main bar for 24-GeV proton bombardment.

Distance (cm)	Reaction Rate (/target nucleus/proton)	δ_{sta}	δ_{tot}	δ_{sys}=10.3%
3	3.34E-29	5.2%	11.5%	
11	5.38E-29	5.1%	11.5%	
15	6.51E-29	4.9%	11.4%	
29	6.93E-29	5.0%	11.5%	
48	4.56E-29	5.1%	11.5%	
78	1.19E-29	6.3%	12.1%	

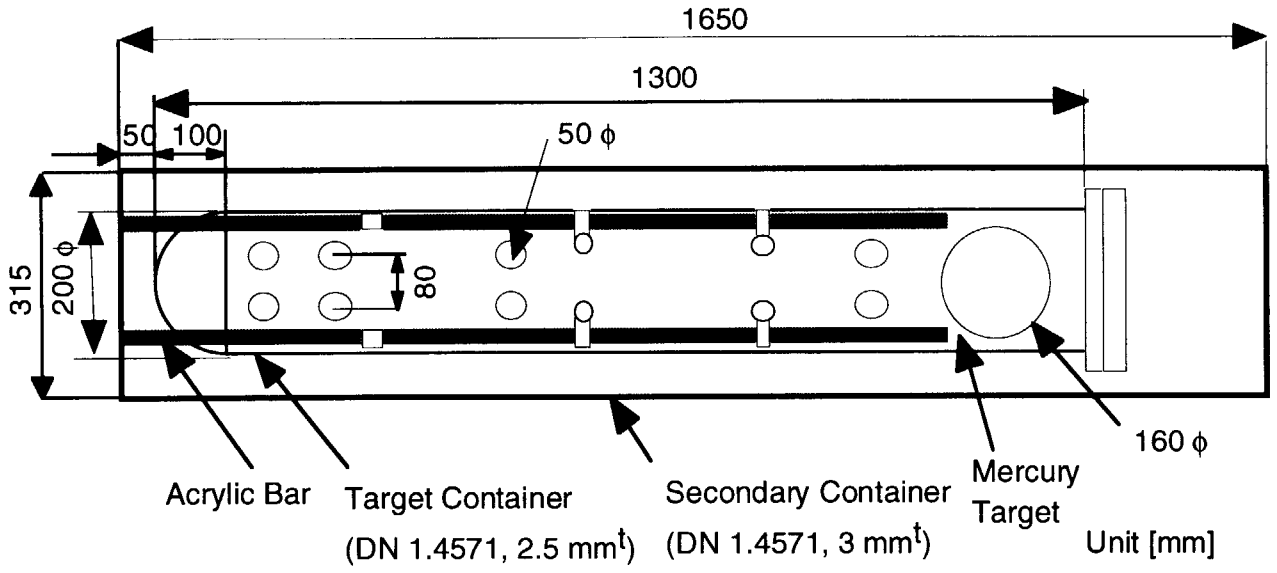

Fig. 1.1 Top view of the mercury target.

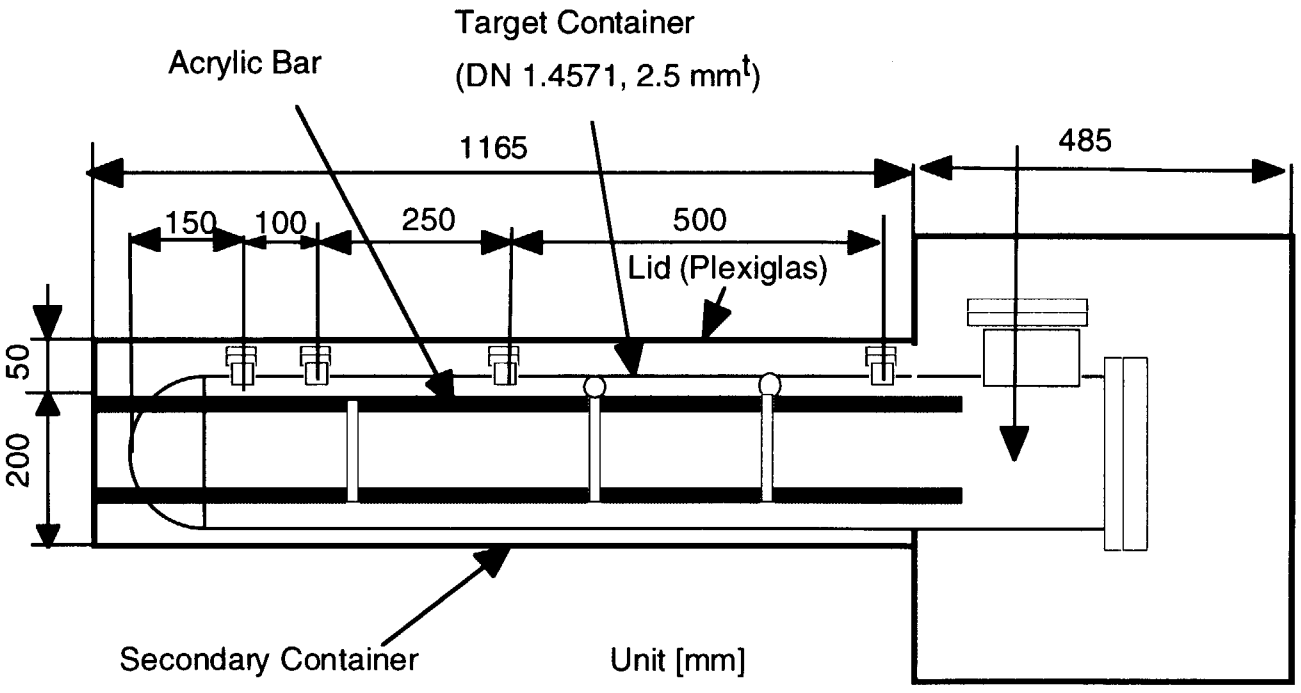

Fig. 1.2 Side view of the mercury target.

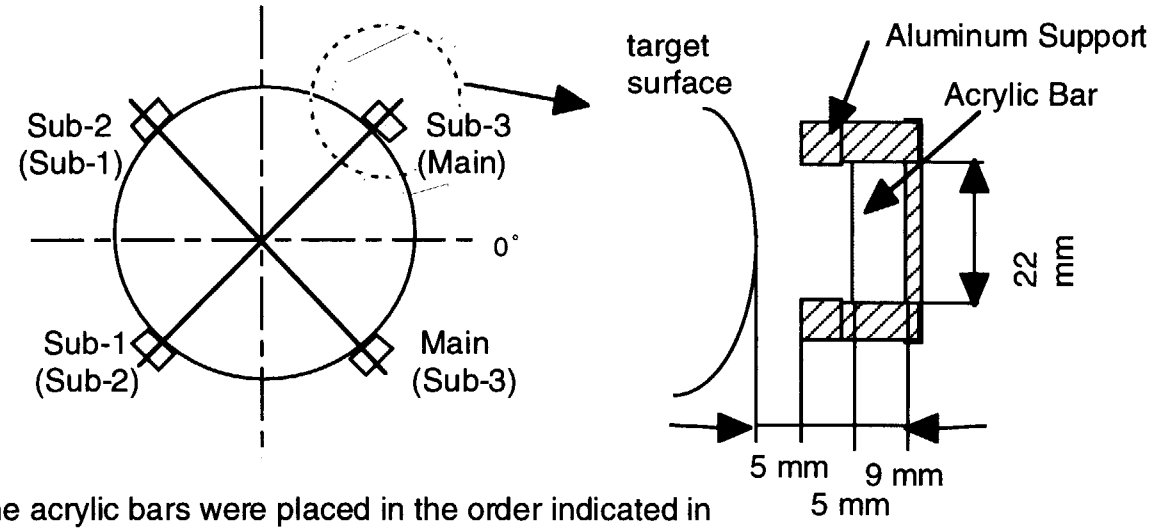

The acrylic bars were placed in the order indicated in the parentheses for 1.6 GeV-proton incidence.

Fig. 1.3 Front view of the mercury target.

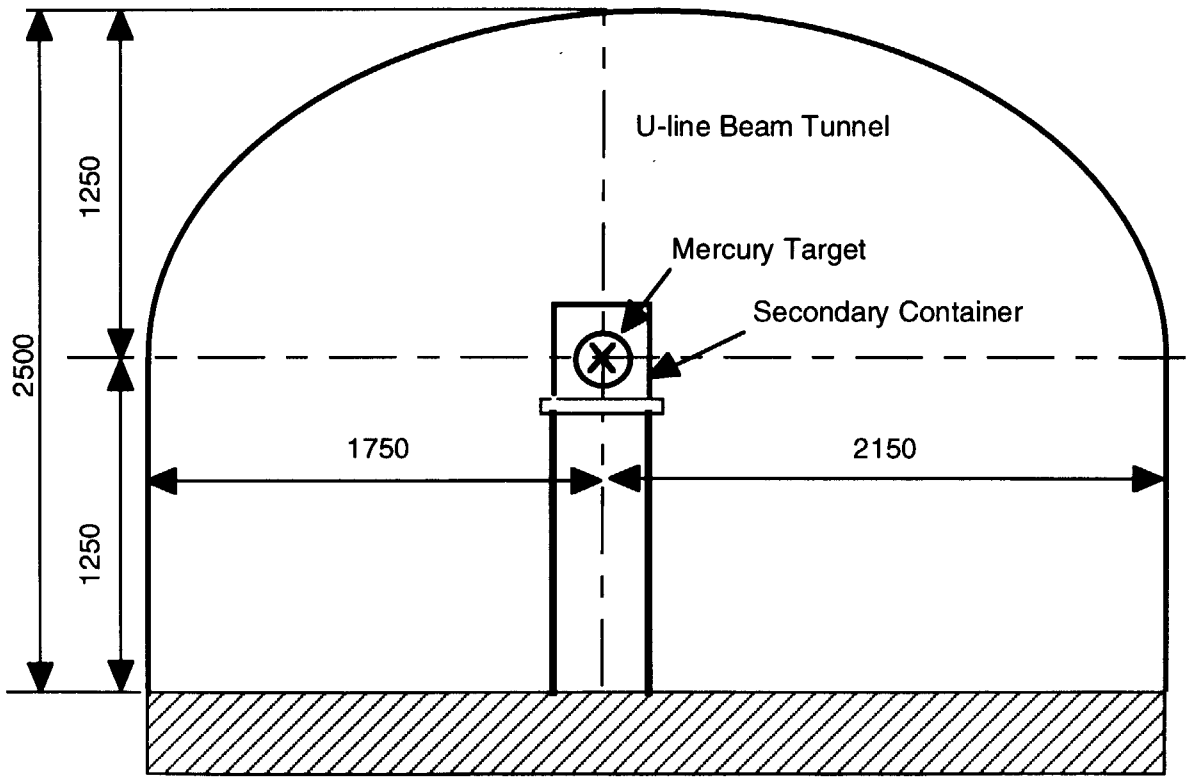

Unit [mm]

Fig. 2 Cross sectional view of the U-line block house in the AGS facility.

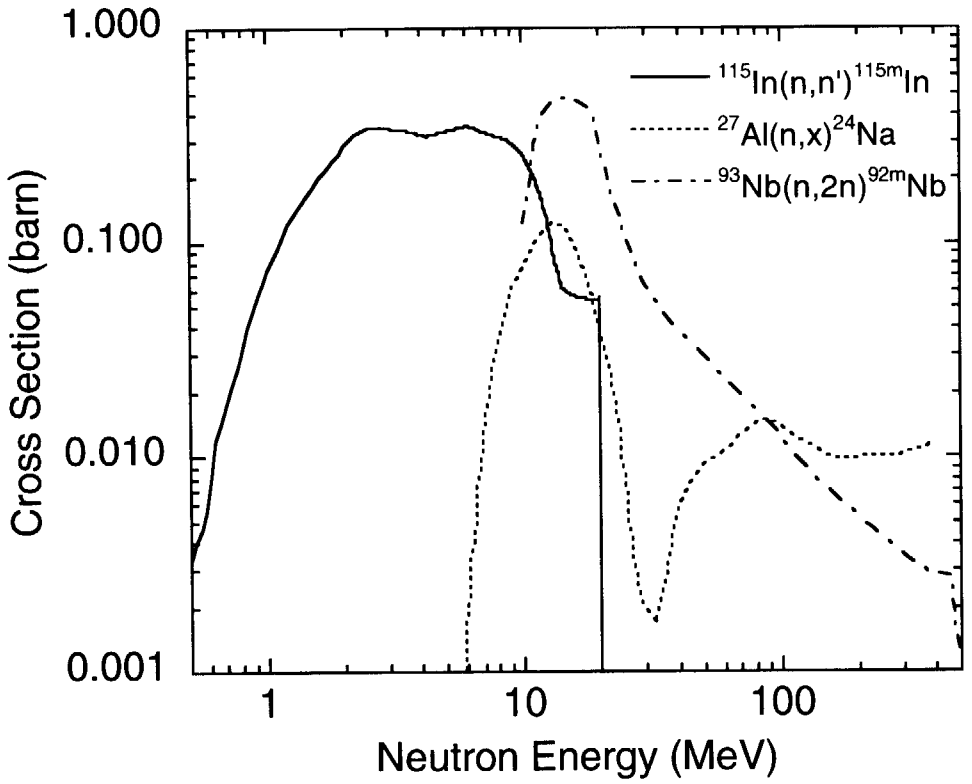

Fig. 3.1 Neutron corss sections of the $^{115}In(n,n')^{115m}In$, $^{27}Al(n,x)^{24}Na$ and $^{93}Nb(n,2n)^{92m}Nb$ reactions.

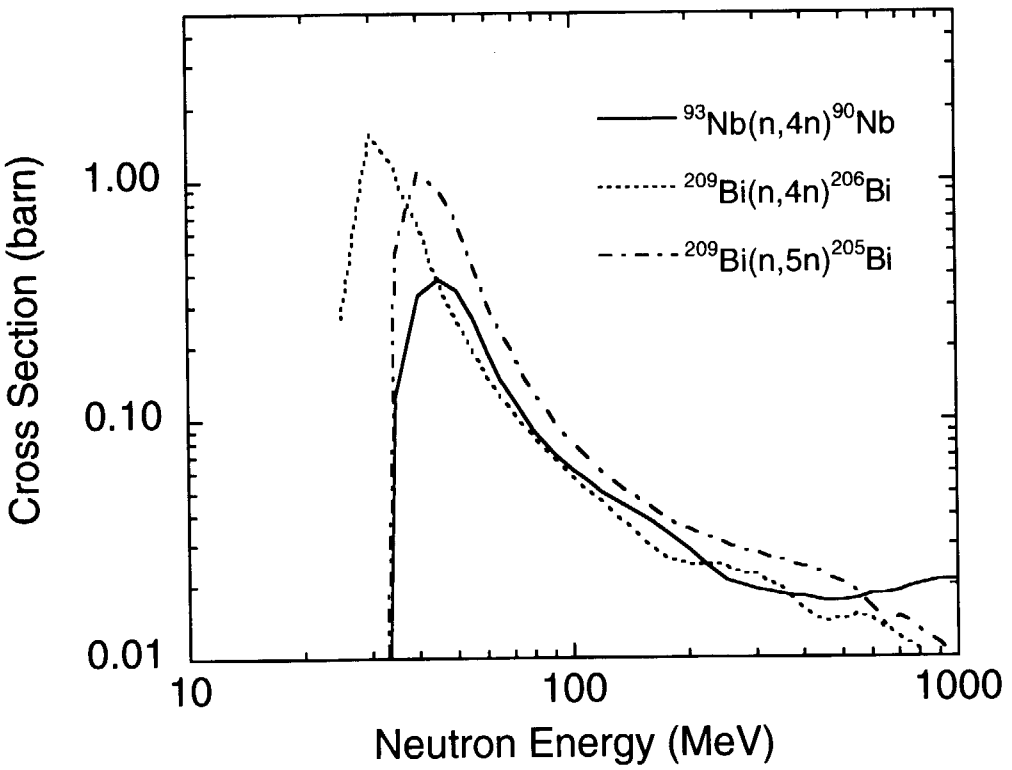

Fig. 3.2 Neutron corss sections of the $^{93}Nb(n,4n)^{90}Nb$, $^{209}Bi(n,4n)^{206}Bi$ and $^{209}Bi(n,5n)^{205}Bi$ reactions.

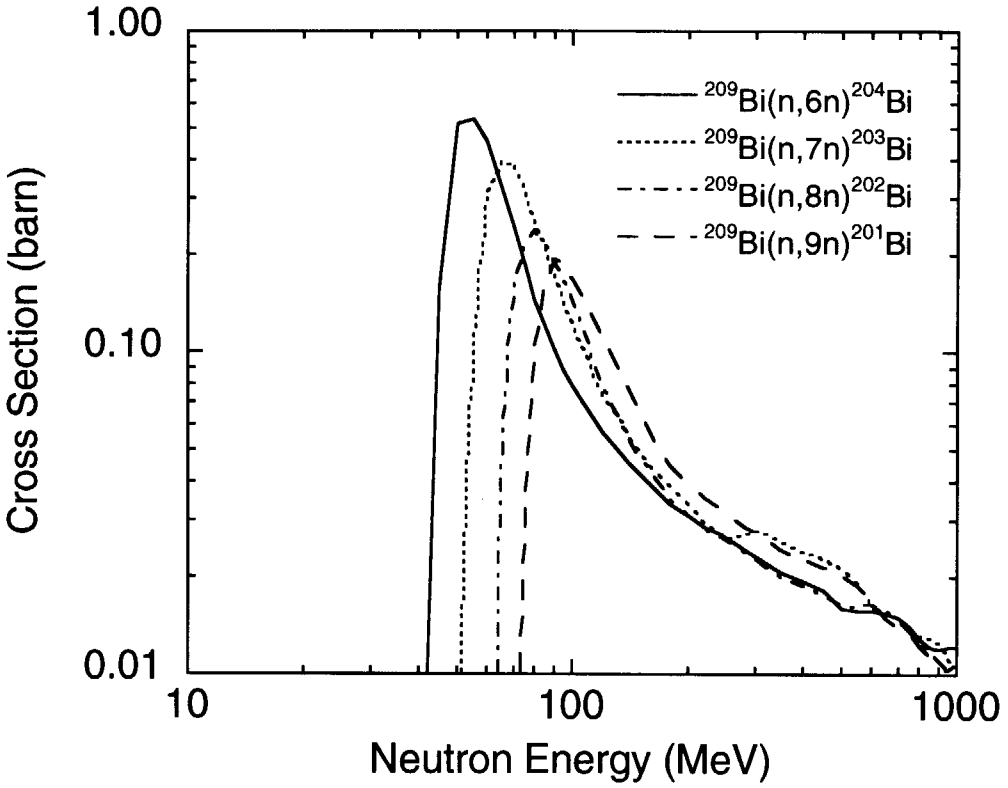

Fig. 3.3 Neutron corss sections of the $^{209}Bi(n,6n)^{204}Bi$, $^{209}Bi(n,7n)^{203}Bi$, $^{209}Bi(n,8n)^{202}Bi$ and $^{209}Bi(n,9n)^{201}Bi$ reactions.

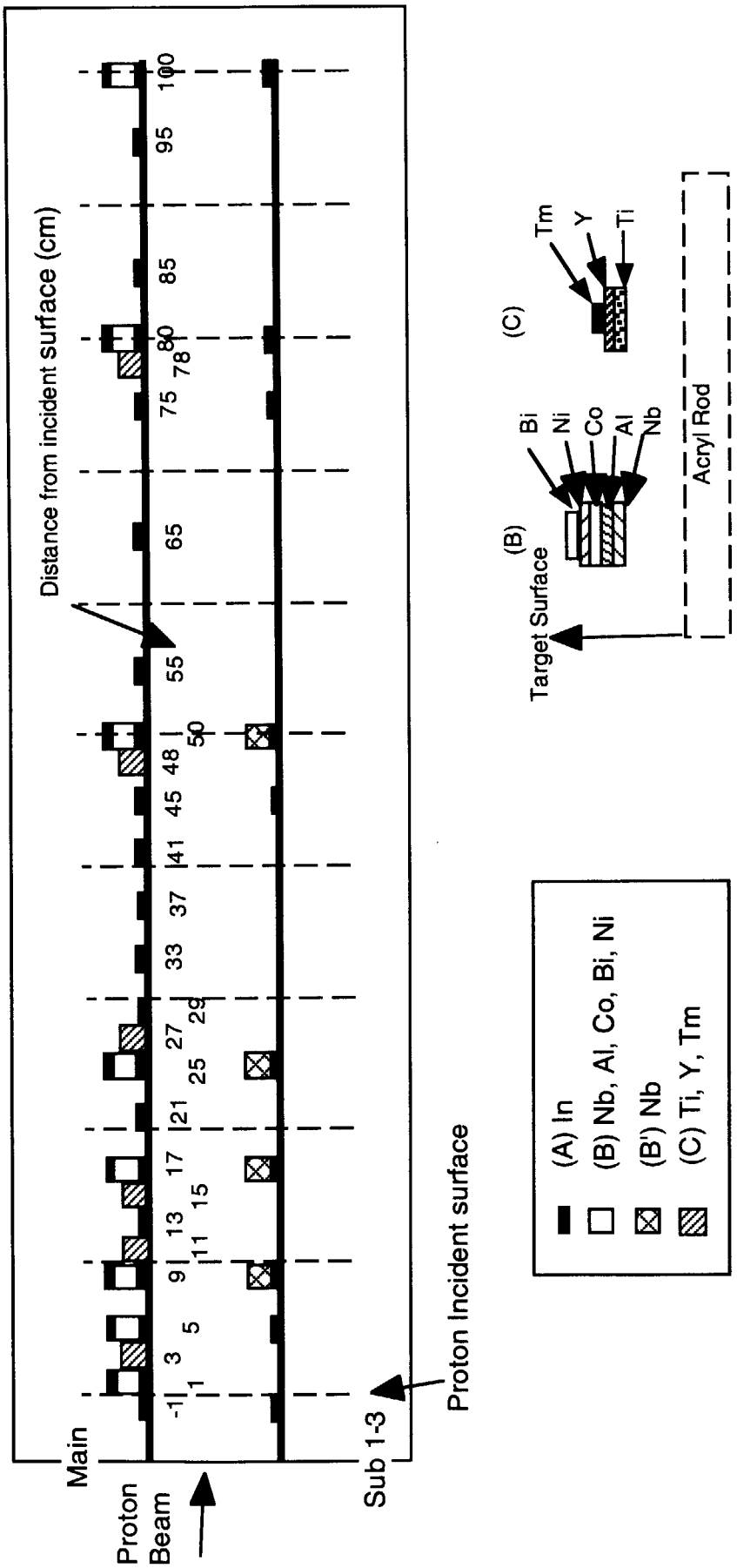

Fig. 4 Sketch of activation foil arrangement on the mercury target for 1.6 GeV proton bombardment.

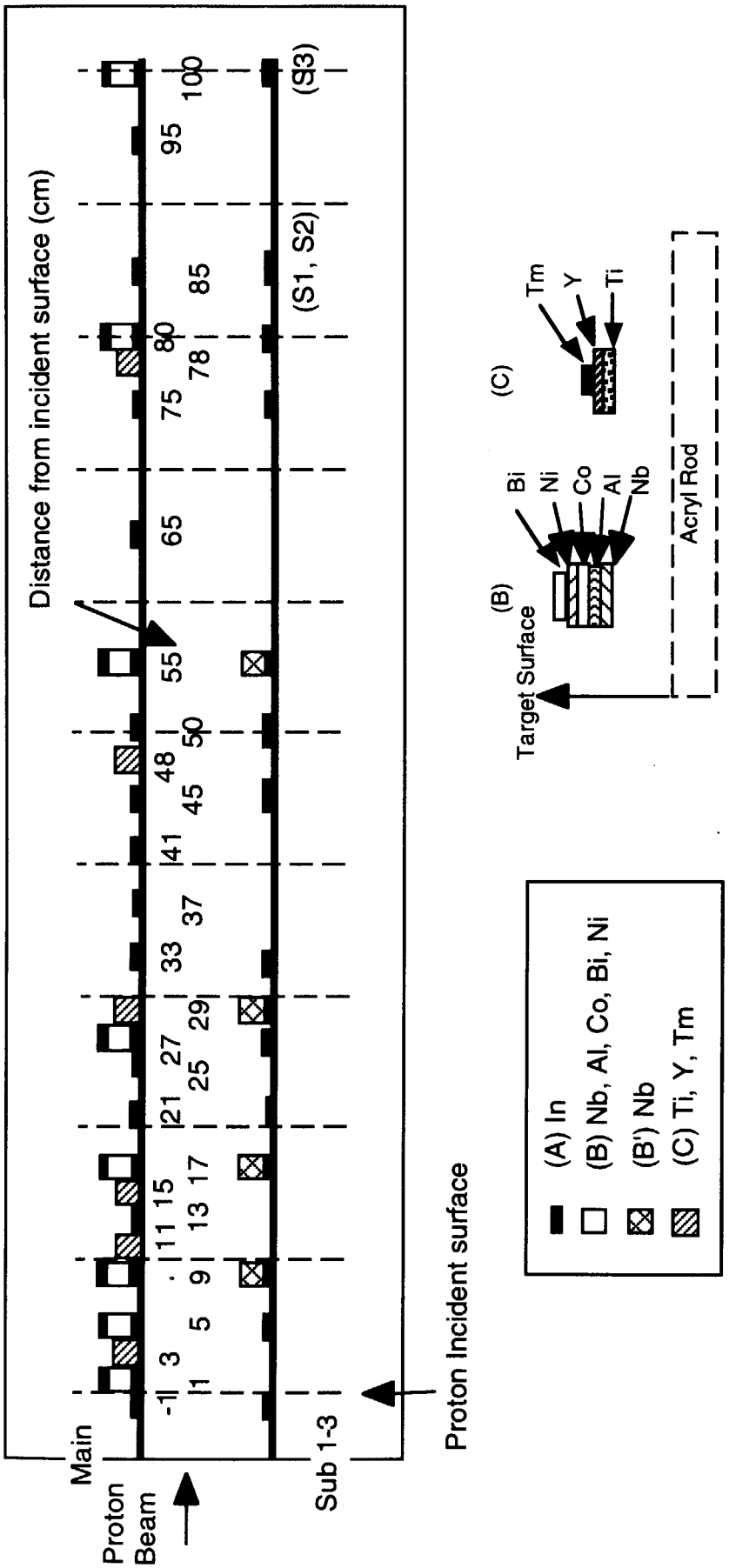

Fig. 5 Sketch of activation foil arrangement on the mercury target for 12 and 24 GeV proton bombardment.

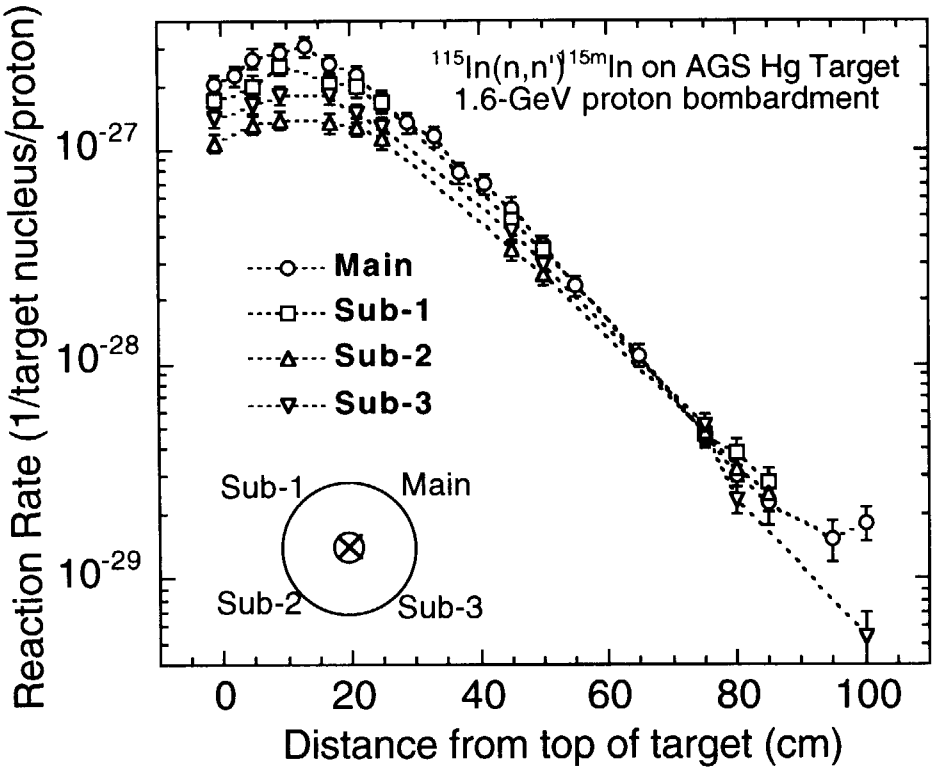

Fig. 5.1 Measured reaction rates of the ^{115}In(n,n')^{115m}In reaction on the cylindrical surface of the mercury target bombarded with 1.6-GeV protons.

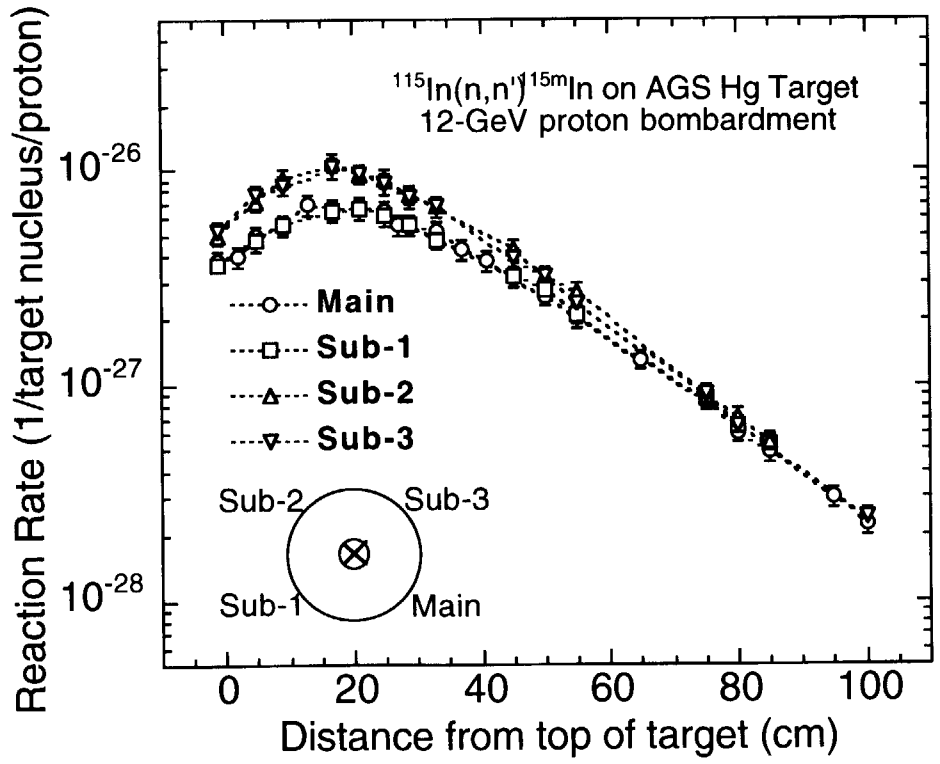

Fig. 5.2 Measured reaction rates of the ^{115}In(n,n')^{115m}In reaction on the cylindrical surface of the mercury target bombarded with 12-GeV protons.

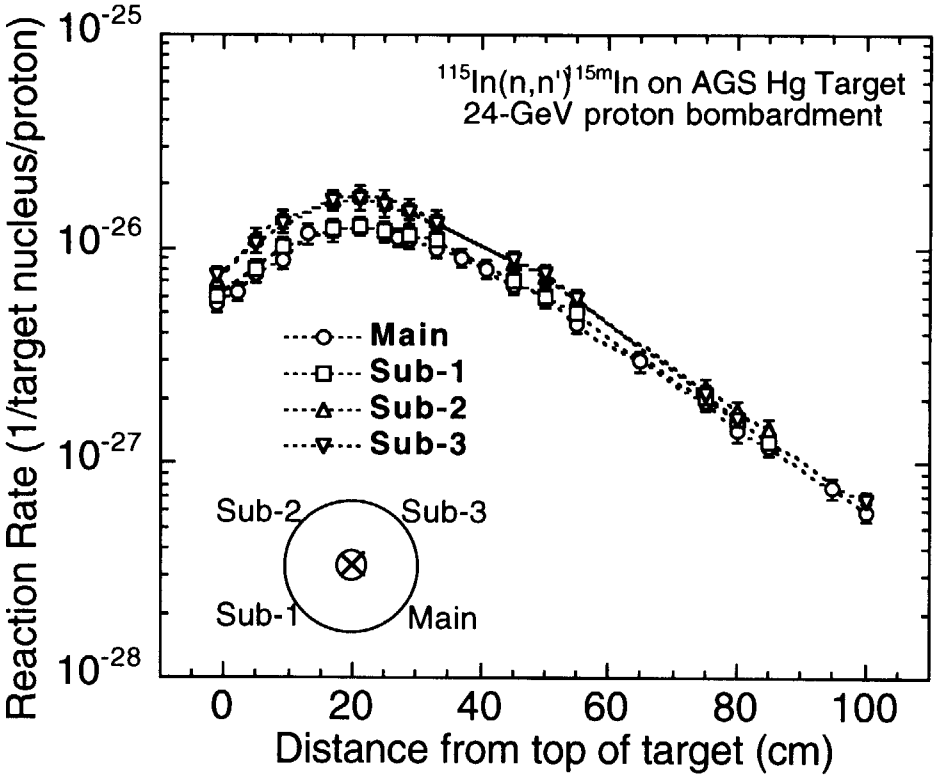

Fig. 5.3 Measured reaction rates of the ^{115}In(n,n')^{115m}In reaction on the cylindrical surface of the mercury target bombarded with 24-GeV protons.

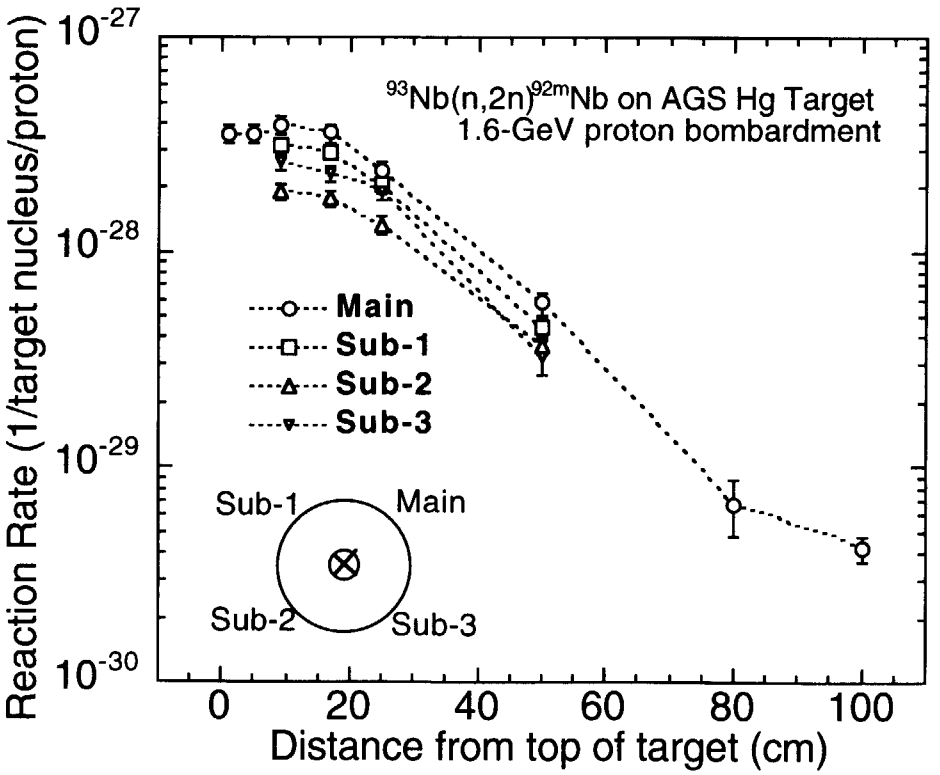

Fig. 5.4 Measured reaction rates of the ^{92}Nb(n,2n)^{92m}Nb reaction on the cylindrical surface of the mercury target bombarded with 1.6-GeV protons.

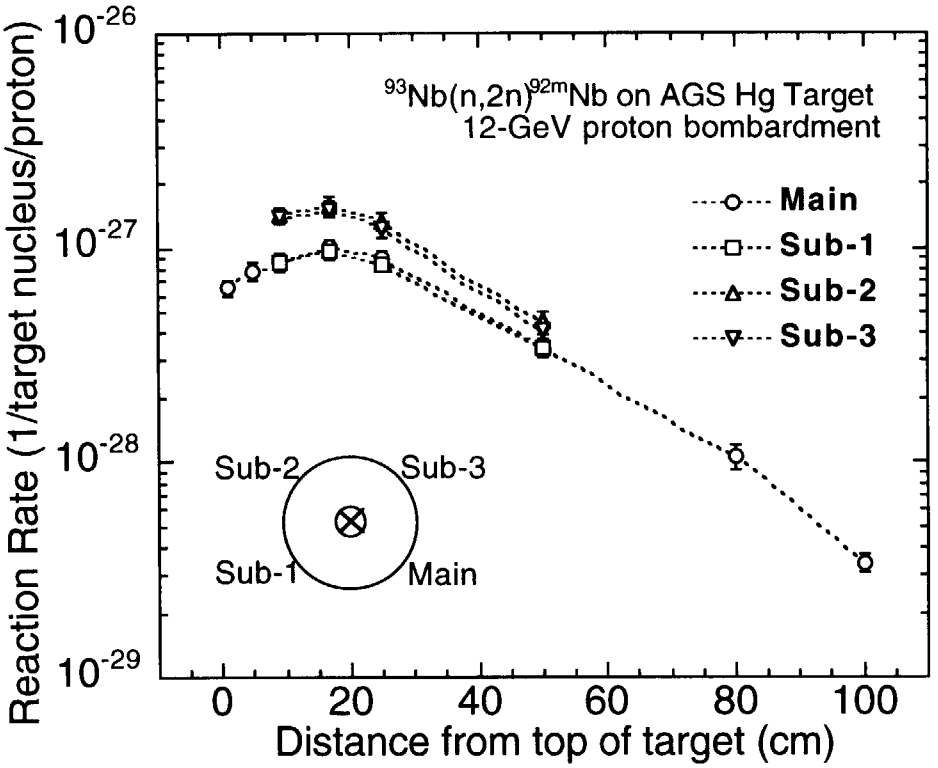

Fig. 5.5 Measured reaction rates of the ^{92}Nb(n,2n)^{92m}Nb reaction on the cylindrical surface of the mercury target bombarded with 12-GeV protons.

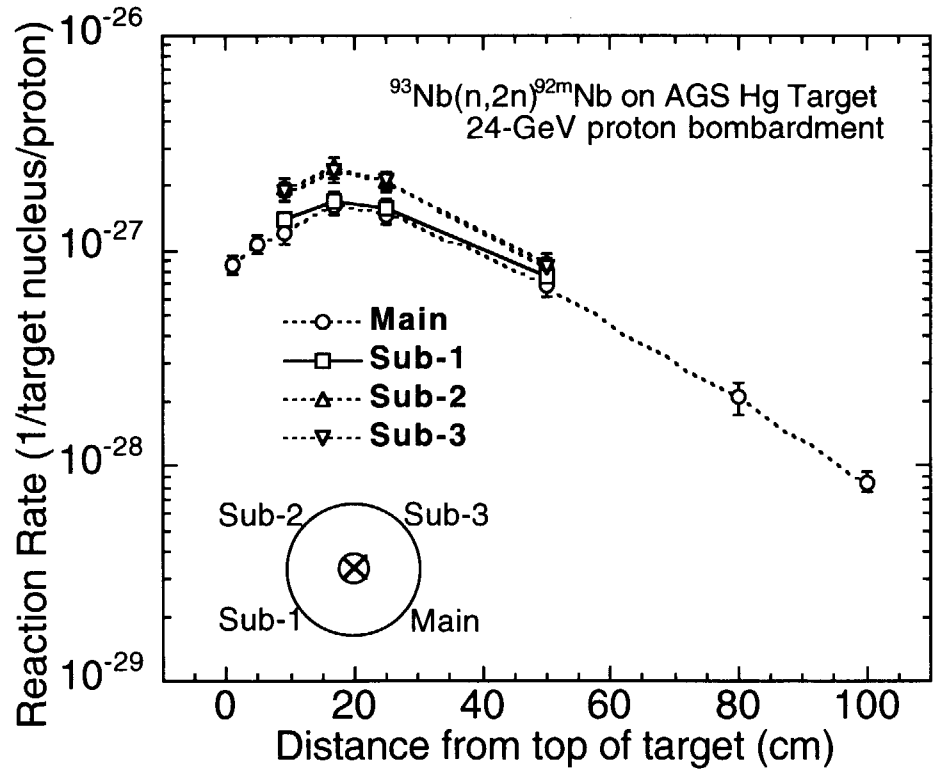

Fig. 5.6 Measured reaction rates of the ^{92}Nb(n,2n)^{92m}Nb reaction on the cylindrical surface of the mercury target bombarded with 24-GeV protons.

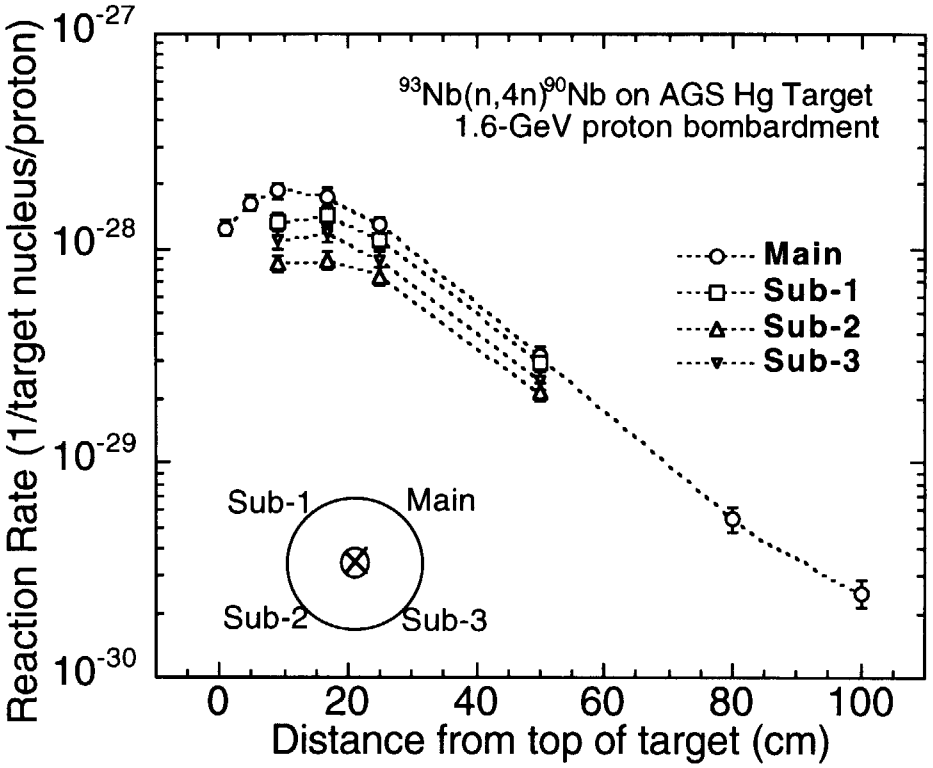

Fig. 5.7 Measured reaction rates of the ^{92}Nb(n,4n)^{90}Nb reaction on the cylindrical surface of the mercury target bombarded with 1.6-GeV protons.

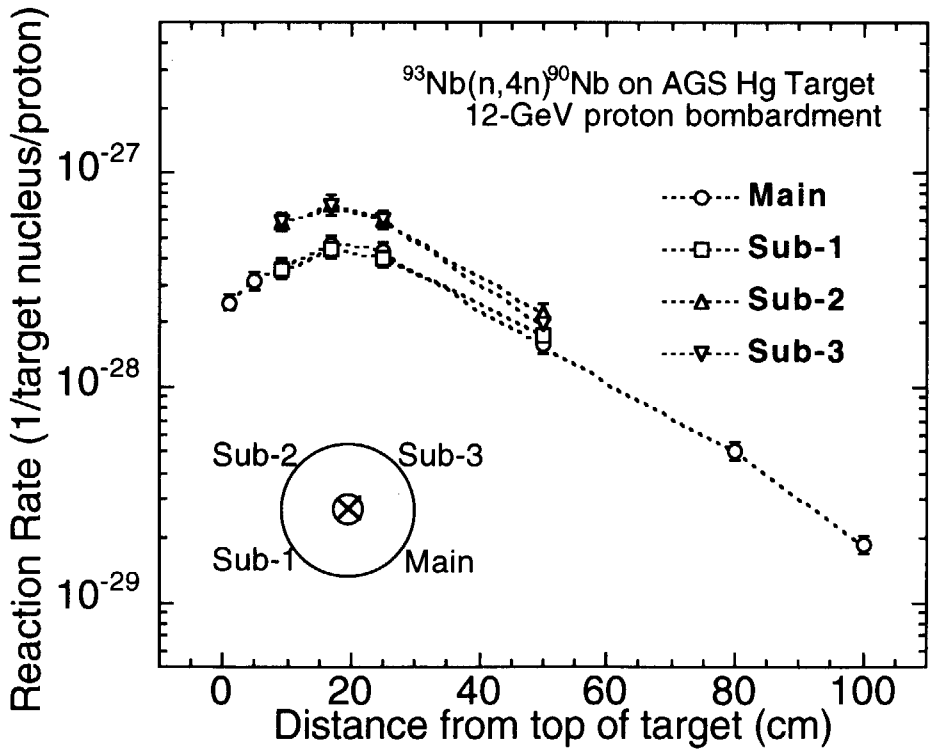

Fig. 5.8 Measured reaction rates of the ^{92}Nb(n,4n)^{90}Nb reaction on the cylindrical surface of the mercury target bombarded with 12-GeV protons.

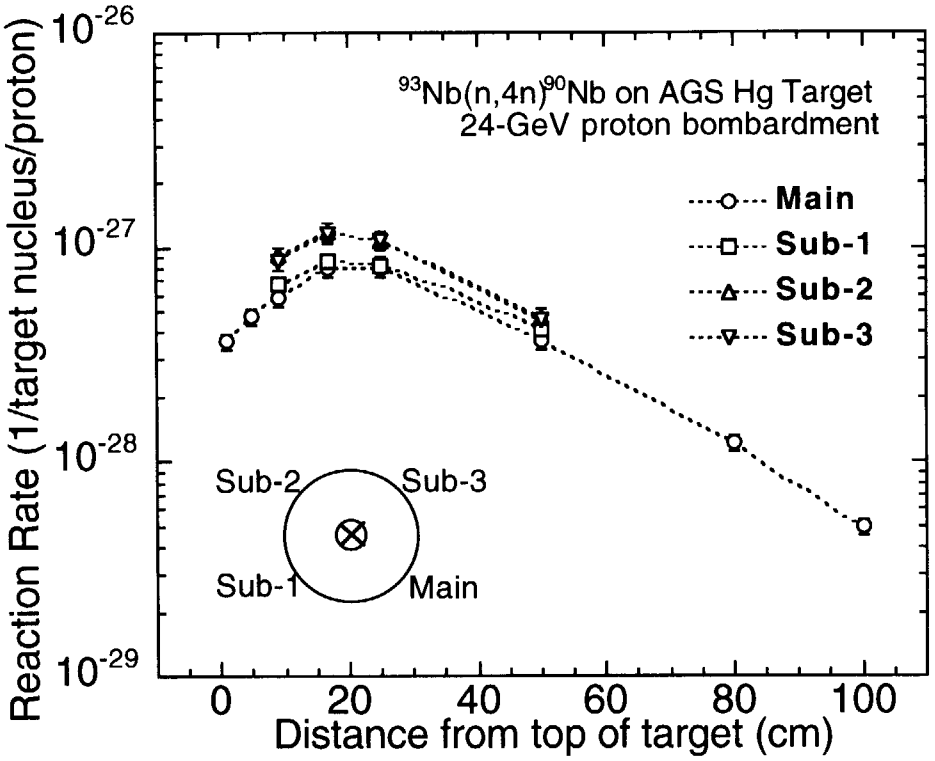

Fig. 5.9 Measured reaction rates of the ^{92}Nb(n,4n)^{90}Nb reaction on the cylindrical surface of the mercury target bombarded with 24-GeV protons.

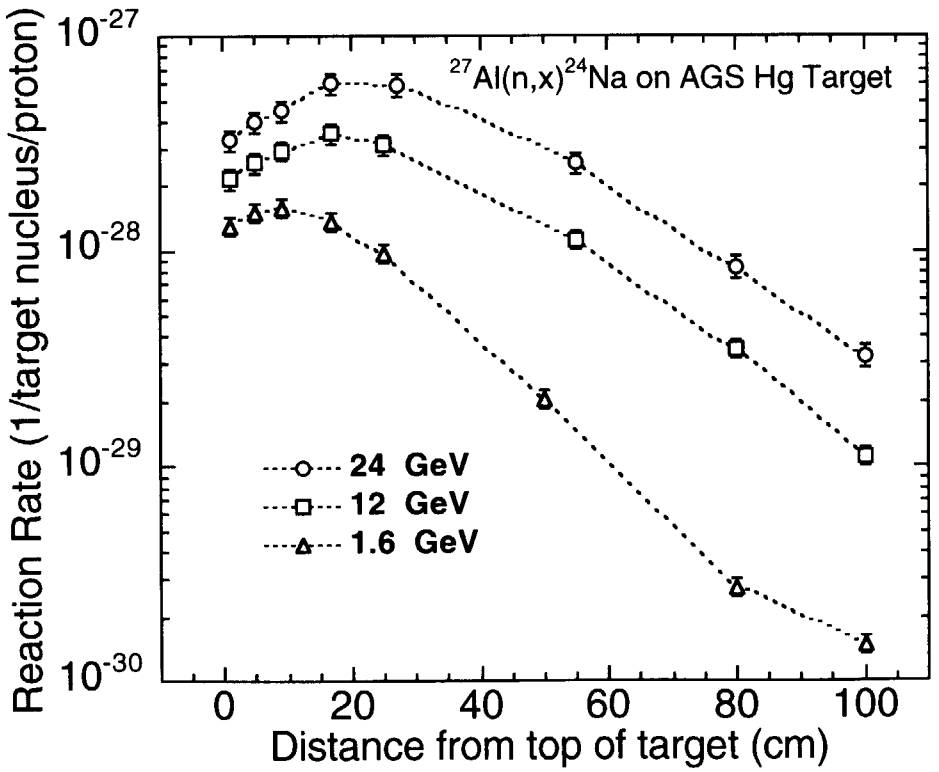

Fig. 5.10 Measured reaction rates of the ^{27}Al(n,x)^{24}Na reaction on the cylindrical surface of the mercury target bombarded with 1.6-, 12- and 24-GeV protons.

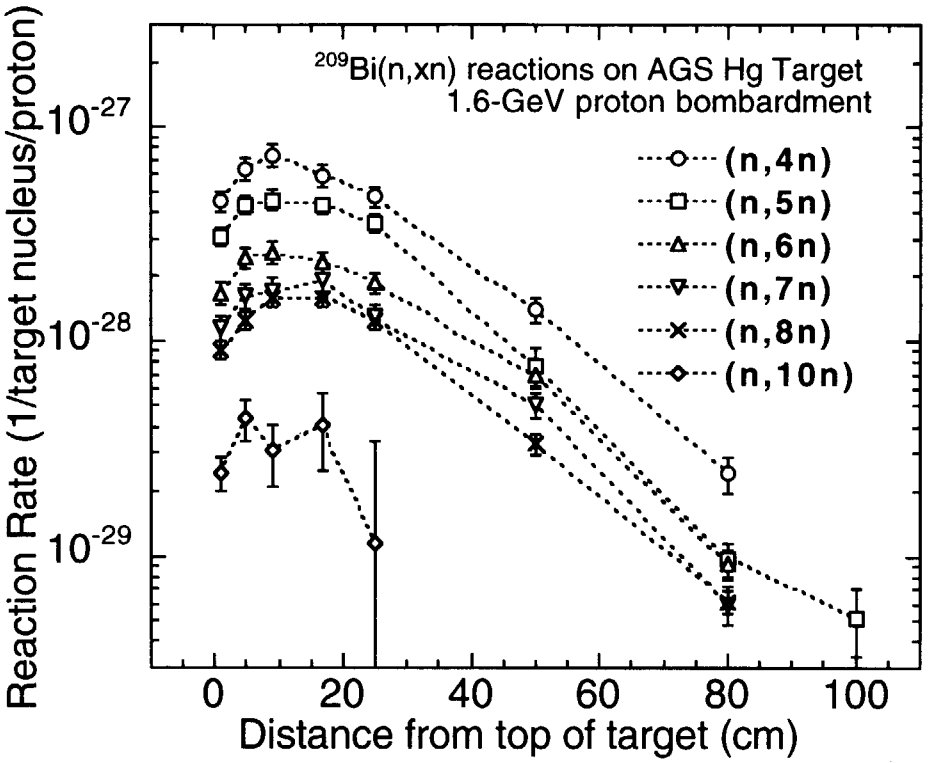

Fig. 5.11 Measured reaction rates of the ^{209}Bi(n,xn) reactions on the cylindrical surface of the mercury target bombarded with 1.6-GeV protons.

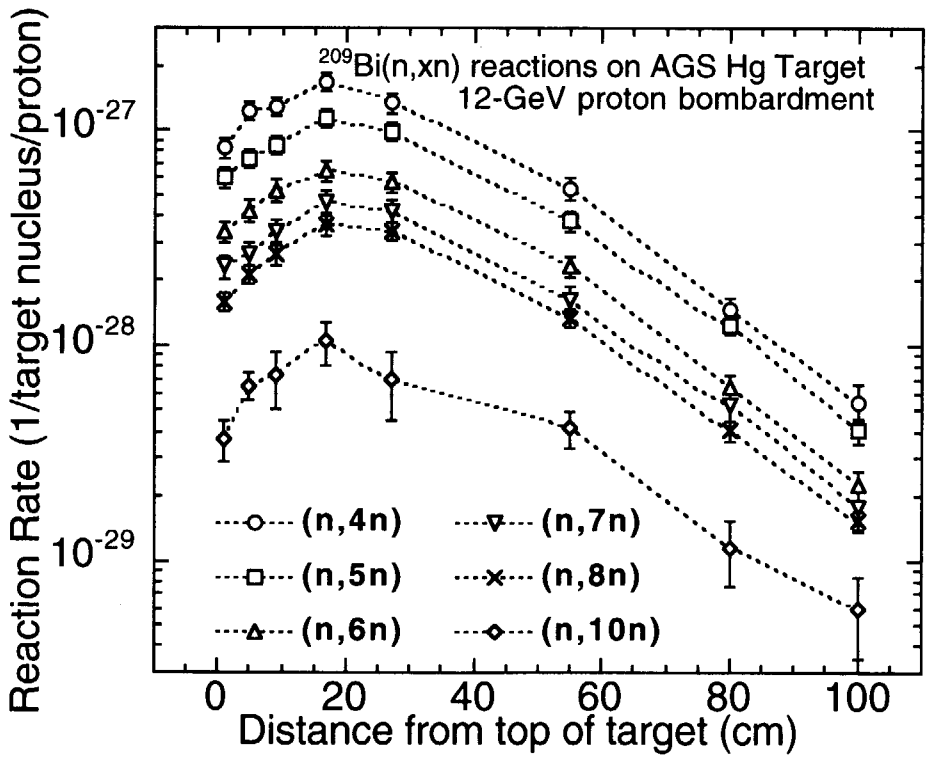

Fig. 5.12 Measured reaction rates of the ^{209}Bi(n,xn) reactions on the cylindrical surface of the mercury target bombarded with 12-GeV protons.

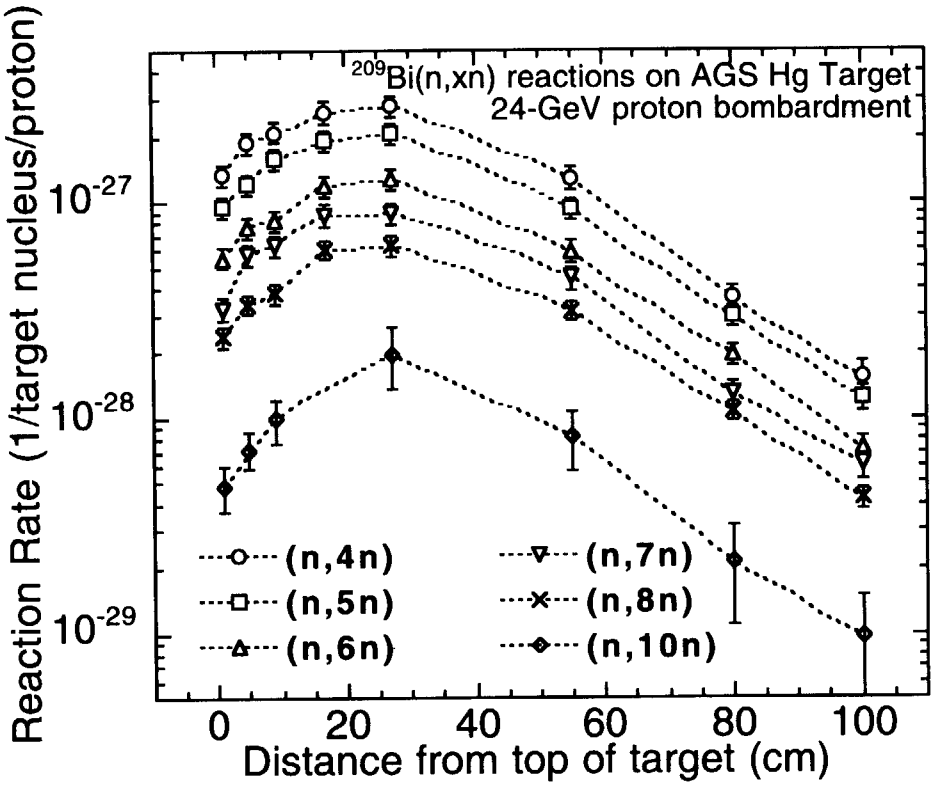

Fig. 5.13 Measured reaction rates of the ^{209}Bi(n,xn) reactions on the cylindrical surface of the mercury target bombarded with 24-GeV protons.

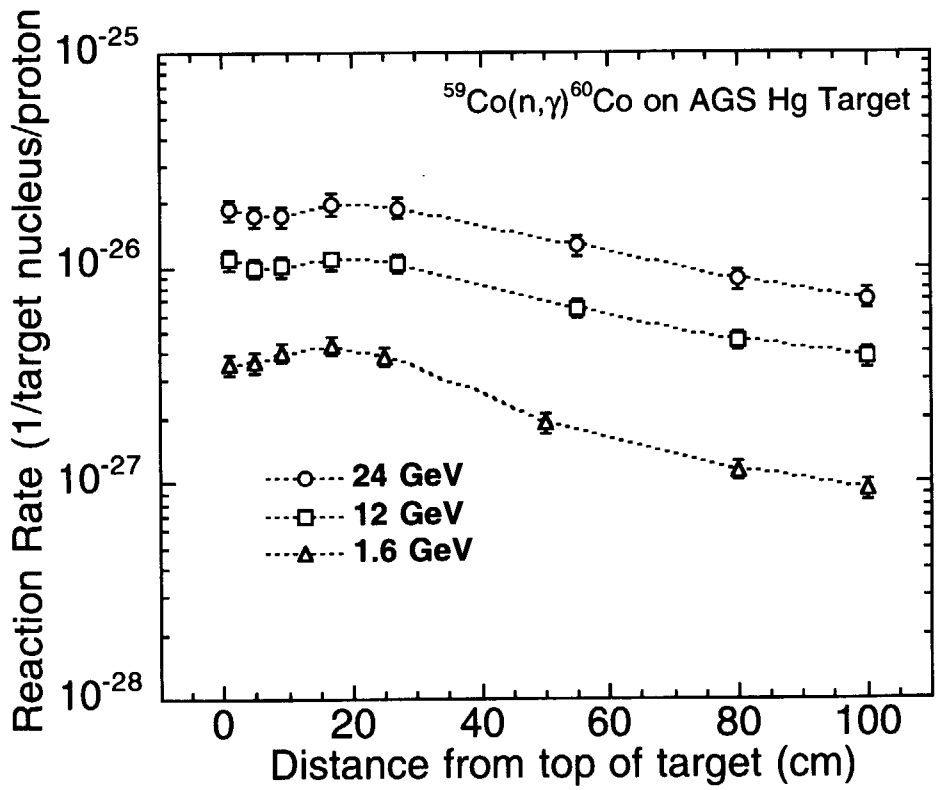

Fig. 5.14 Measured reaction rates of the ^{59}Co(n,γ)^{60}Co reaction on the cylindrical surface of the mercury target bombarded with 1.6-, 12- and 24-GeV protons.

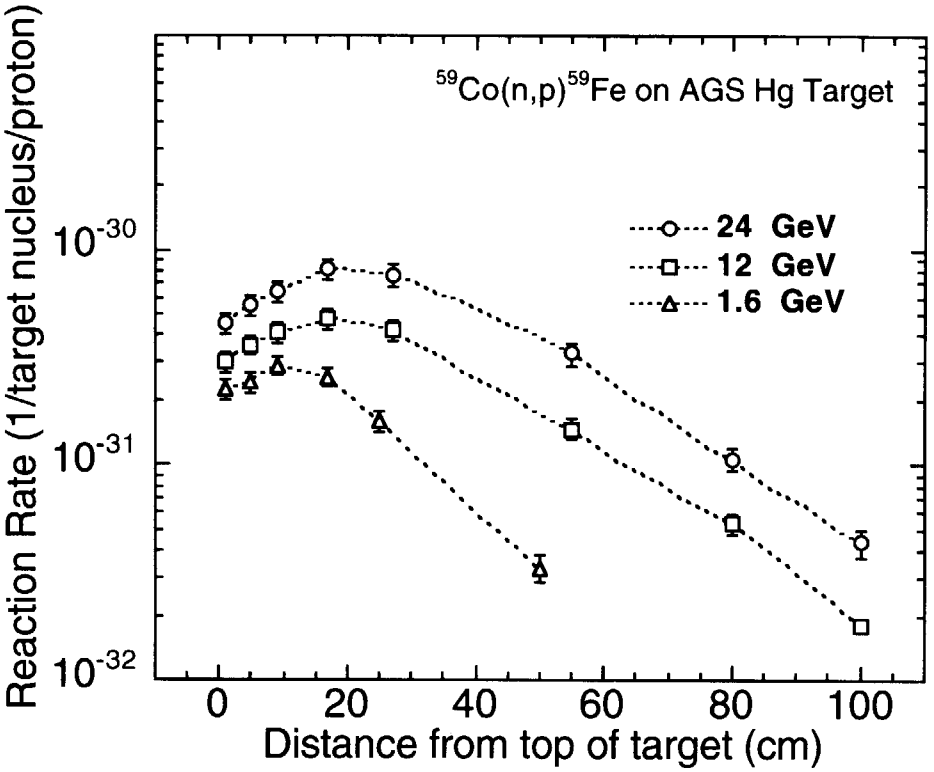

Fig. 5.15 Measured reaction rates of the ^{59}Co(n,p)^{56}Fe reaction on the cylindrical surface of the mercury target bombarded with 1.6-, 12- and 24-GeV protons.

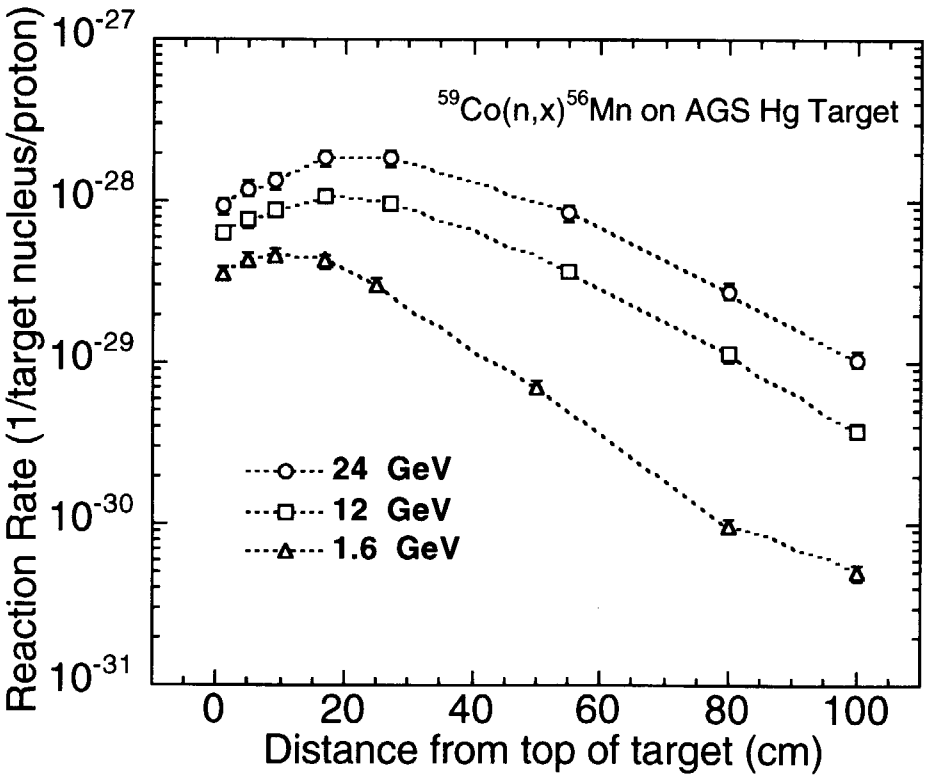

Fig. 5.16 Measured reaction rates of the ^{59}Co(n,x)^{56}Mn reaction on the cylindrical surface of the mercury target bombarded with 1.6-, 12- and 24-GeV protons.

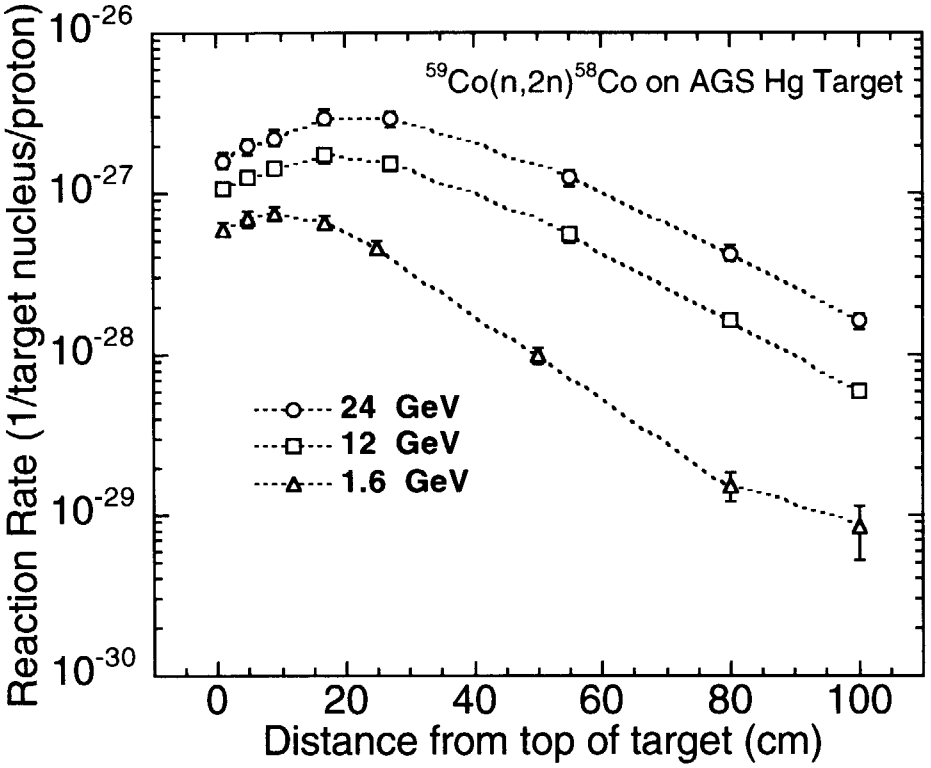

Fig. 5.17 Measured reaction rates of the ^{59}Co(n,2n)^{58}Co reaction on the cylindrical surface of the mercury target bombarded with 1.6-, 12- and 24-GeV protons.

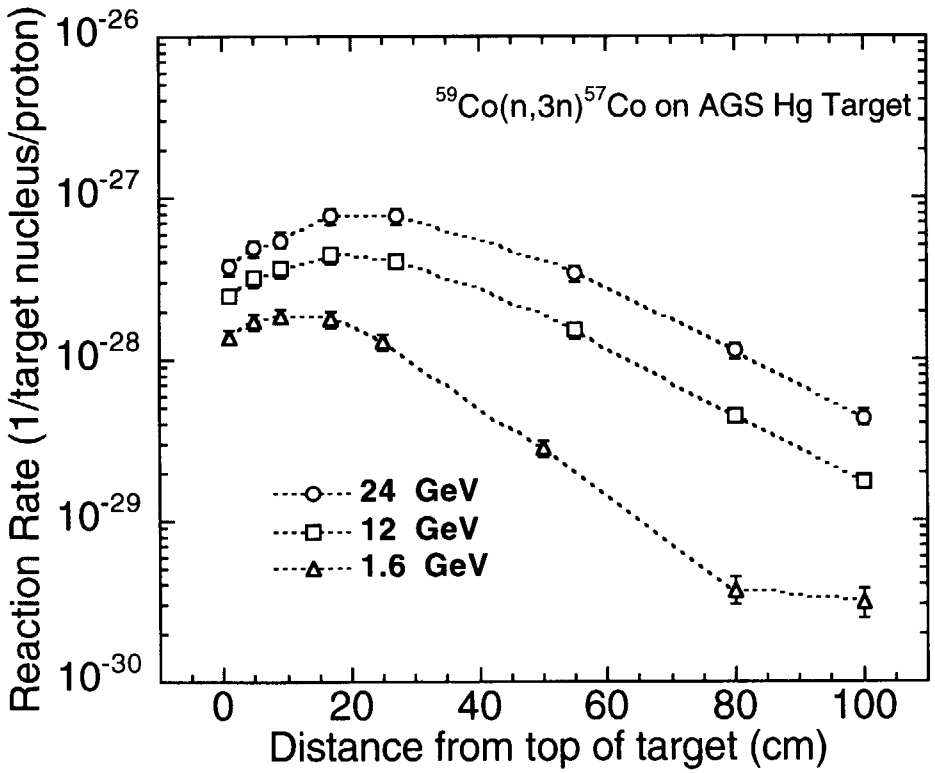

Fig. 5.18 Measured reaction rates of the ^{59}Co(n,3n)^{57}Co reaction on the cylindrical surface of the mercury target bombarded with 1.6-, 12- and 24-GeV protons.

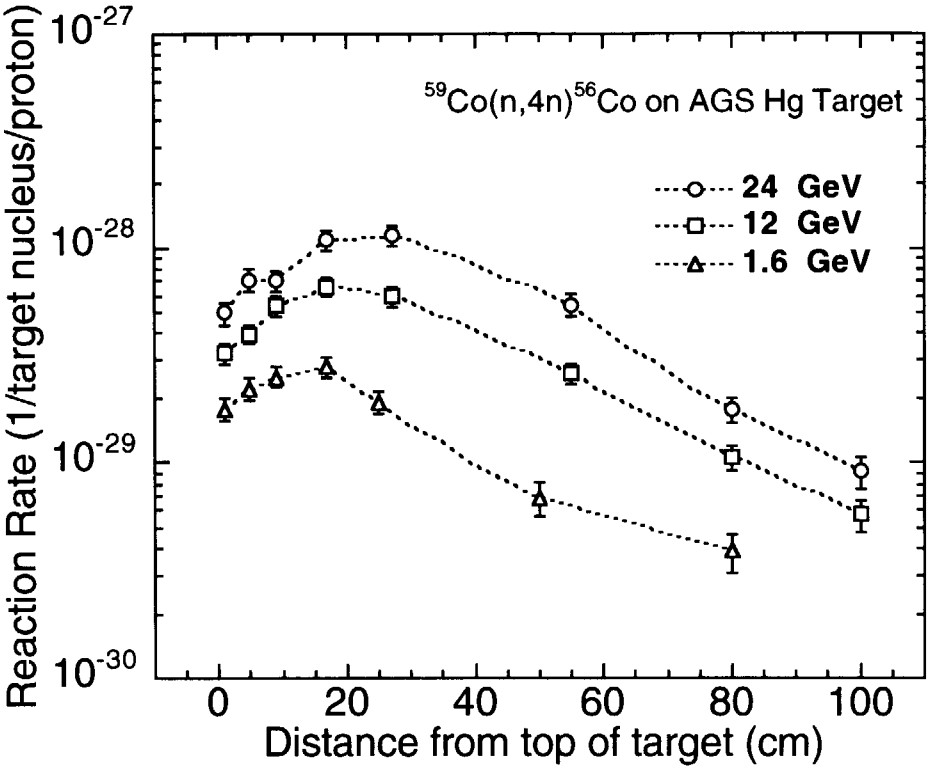

Fig. 5.19 Measured reaction rates of the ^{59}Co(n,4n)^{56}Co reaction on the cylindrical surface of the mercury target bombarded with 1.6-, 12- and 24-GeV protons.

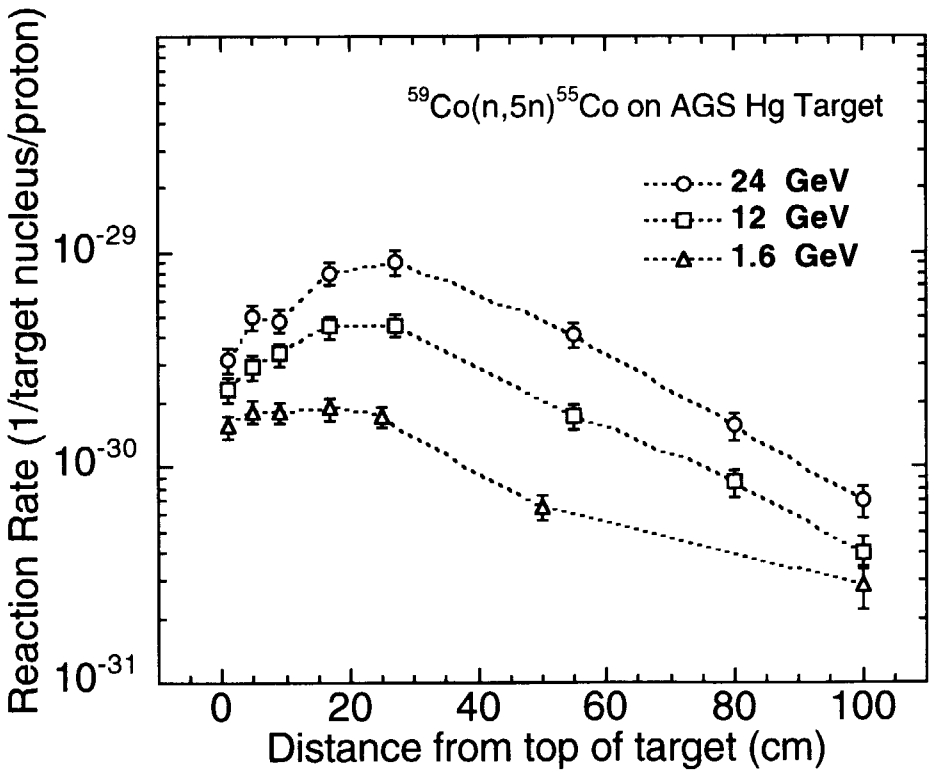

Fig. 5.20 Measured reaction rates of the ^{59}Co(n,5n)^{55}Co reaction on the cylindrical surface of the mercury target bombarded with 1.6-, 12- and 24-GeV protons.

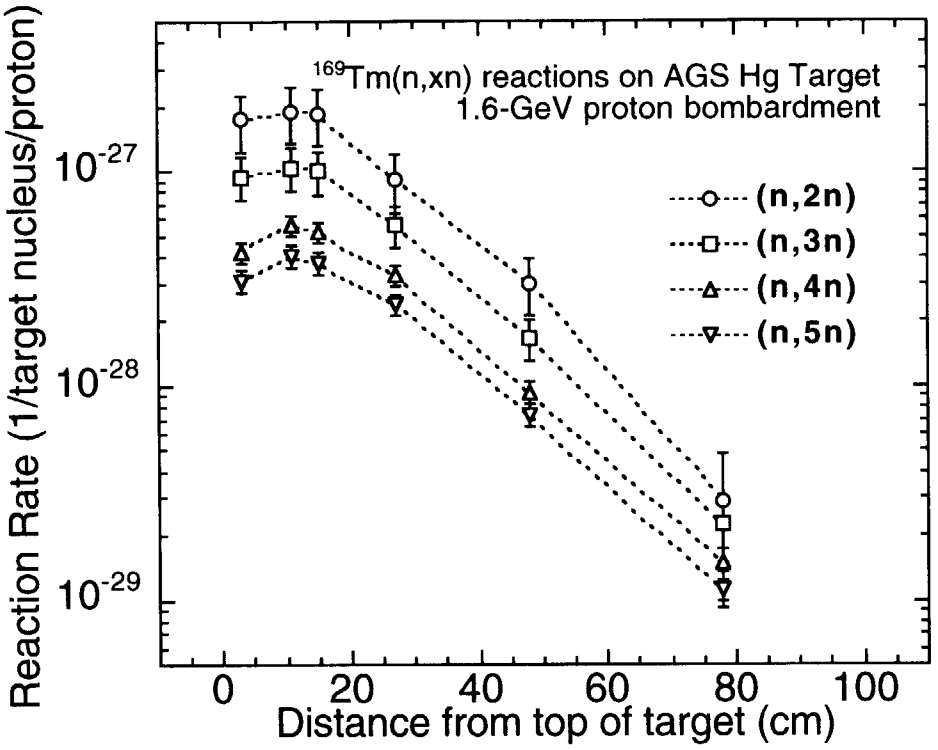

Fig. 5.21 Measured reaction rates of the ^{169}Tm(n,xn) reactions on the cylindrical surface of the mercury target bombarded with 1.6-GeV protons.

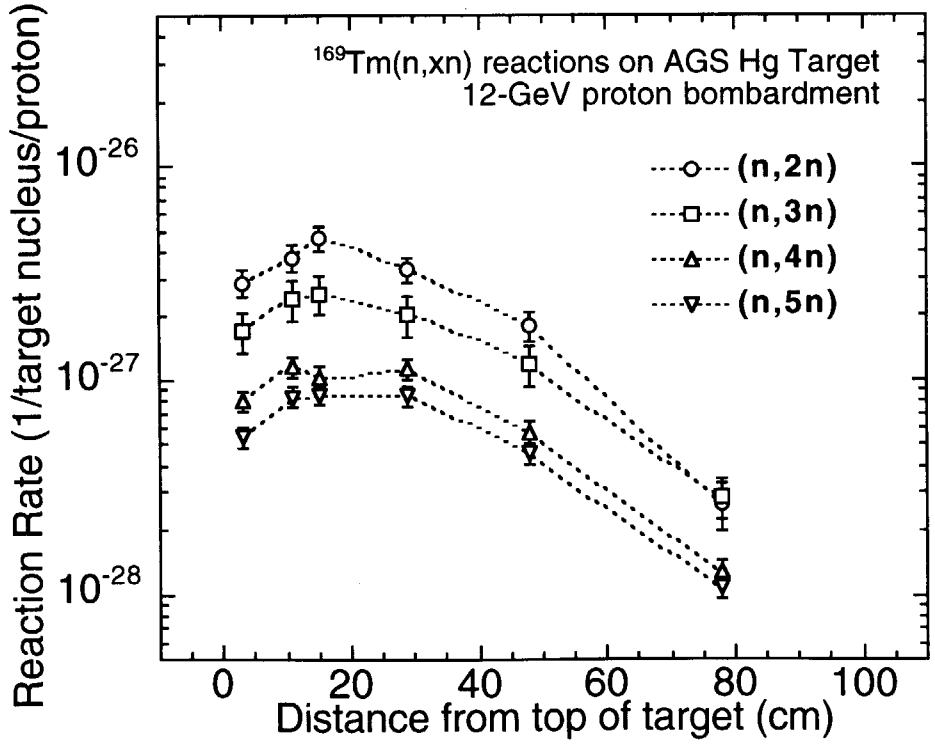

Fig. 5.22 Measured reaction rates of the ^{169}Tm(n,xn) reactions on the cylindrical surface of the mercury target bombarded with 12-GeV protons.

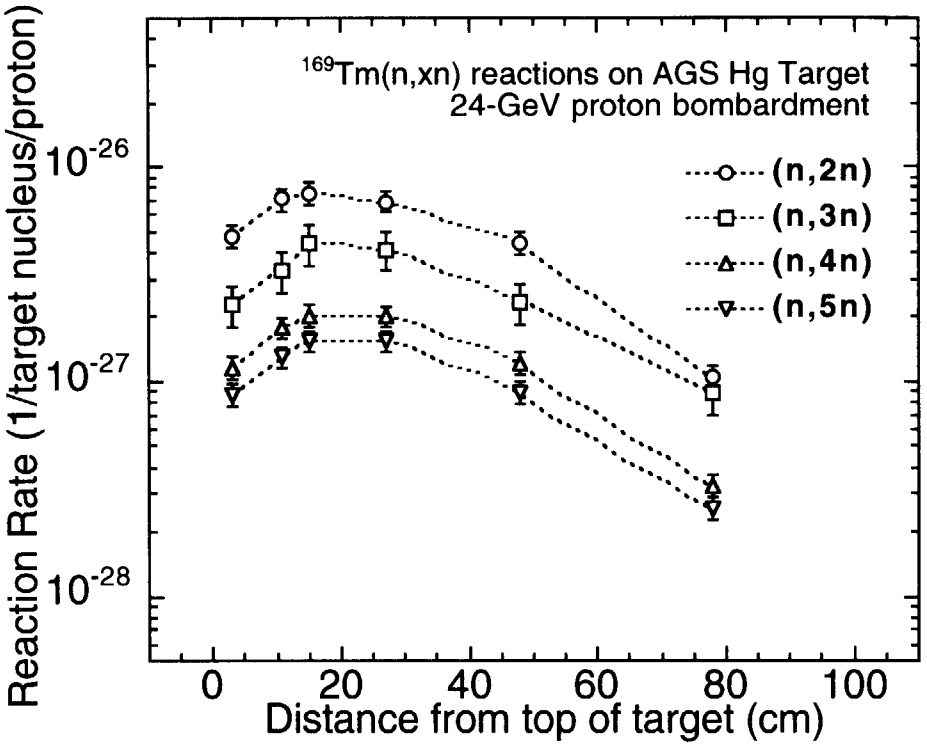

Fig. 5.23 Measured reaction rates of the ^{169}Tm(n,xn) reactions on the cylindrical surface of the mercury target bombarded with 24-GeV protons.

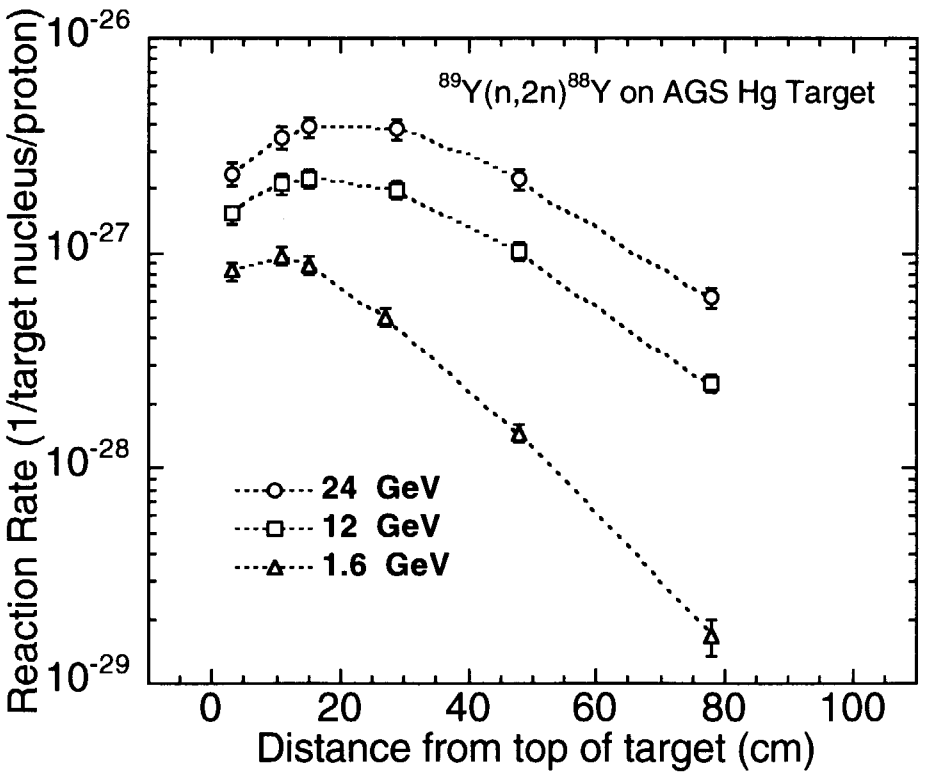

Fig. 5.24 Measured reaction rates of the ^{89}Y(n,2n)^{88}Y reaction on the cylindrical surface of the mercury target bombarded with 1.6-, 12- and 24-GeV protons.

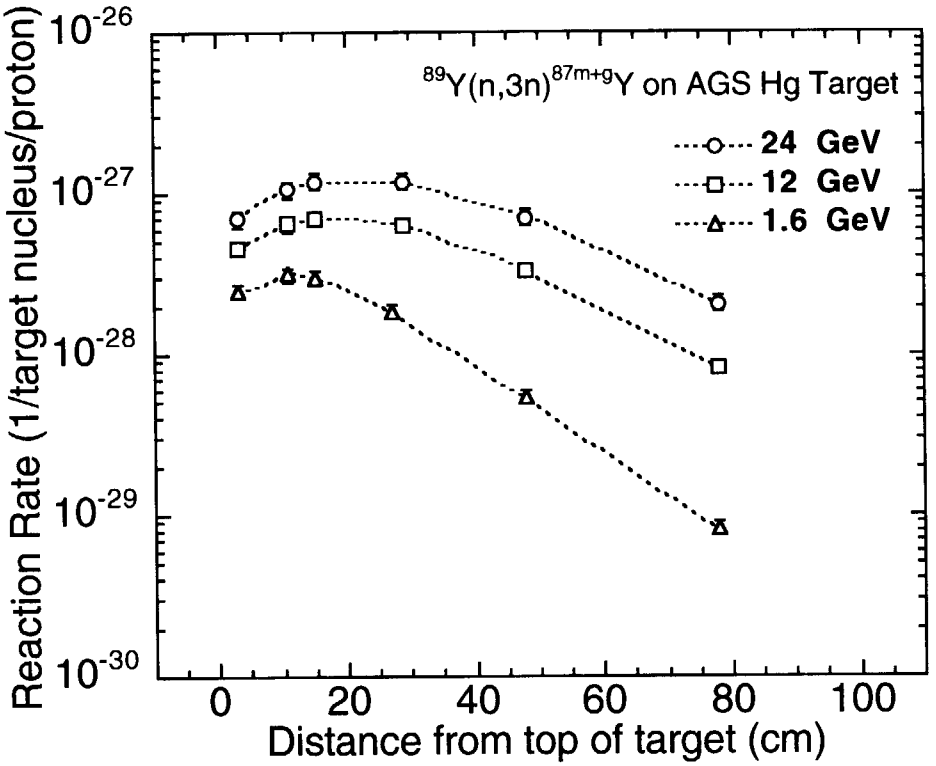

Fig. 5.25 Measured reaction rates of the ^{89}Y(n,3n)$^{87m+g}$Y reaction on the cylindrical surface of the mercury target bombarded with 1.6-, 12- and 24-GeV protons.

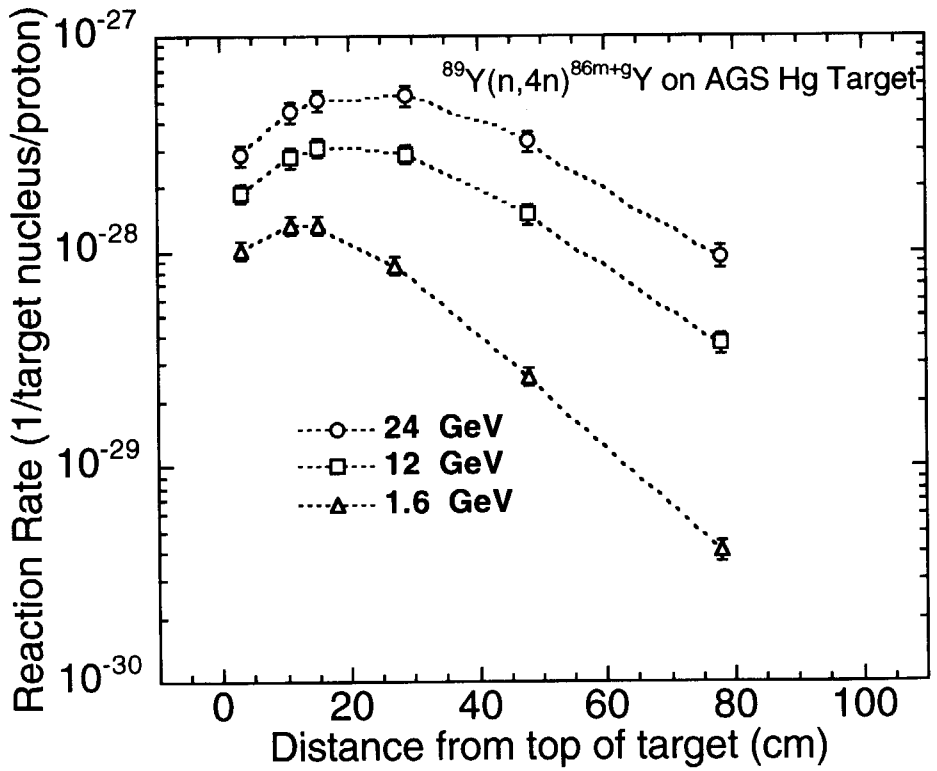

Fig. 5.26 Measured reaction rates of the ^{89}Y(n,4n)$^{86m+g}$Y reaction on the cylindrical surface of the mercury target bombarded with 1.6-, 12- and 24-GeV protons.

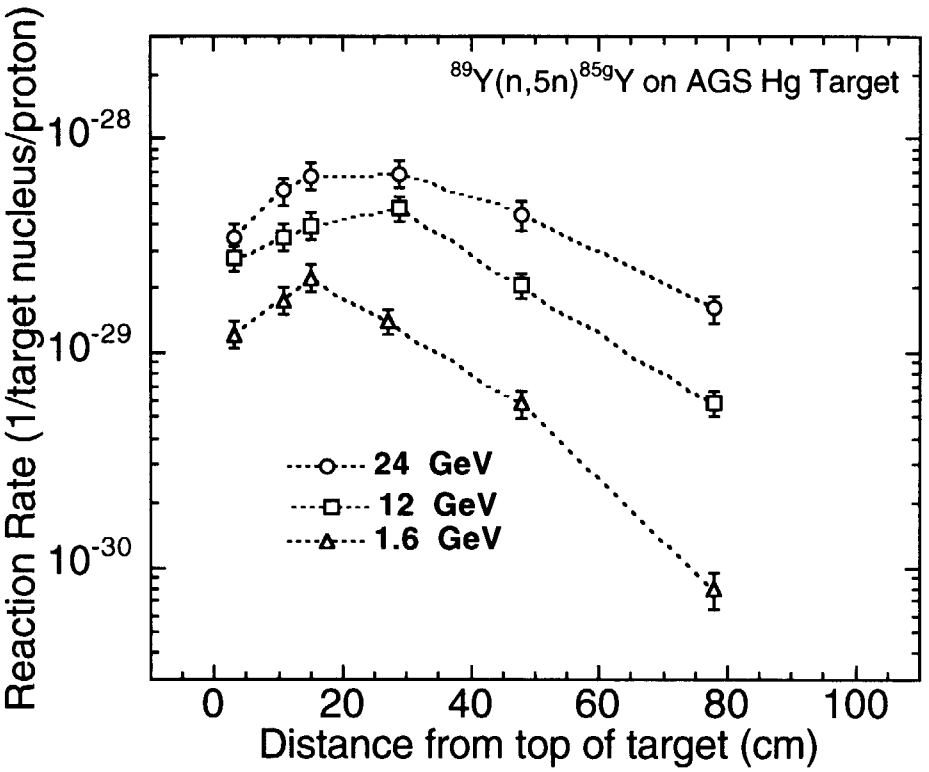

Fig. 5.27 Measured reaction rates of the ^{89}Y(n,5n)^{85g}Y reaction on the cylindrical surface of the mercury target bombarded with 1.6-, 12- and 24-GeV protons.

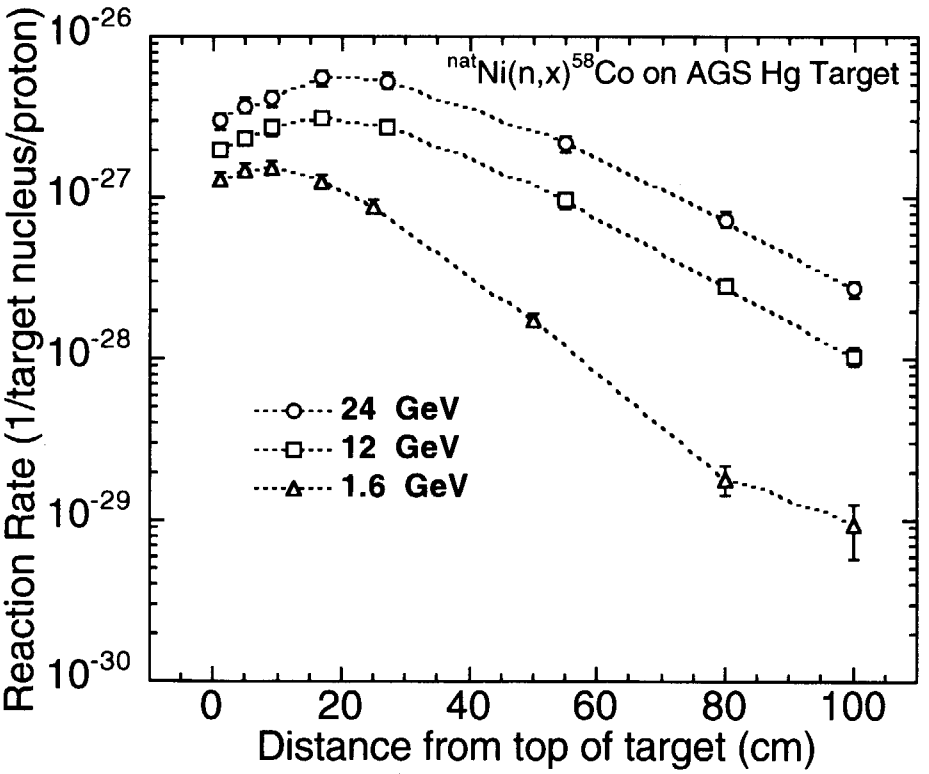

Fig. 5.28 Measured reaction rates of the ^{nat}Ni(n,x)^{58}Co reaction on the cylindrical surface of the mercury target bombarded with 1.6-, 12- and 24- GeV protons.

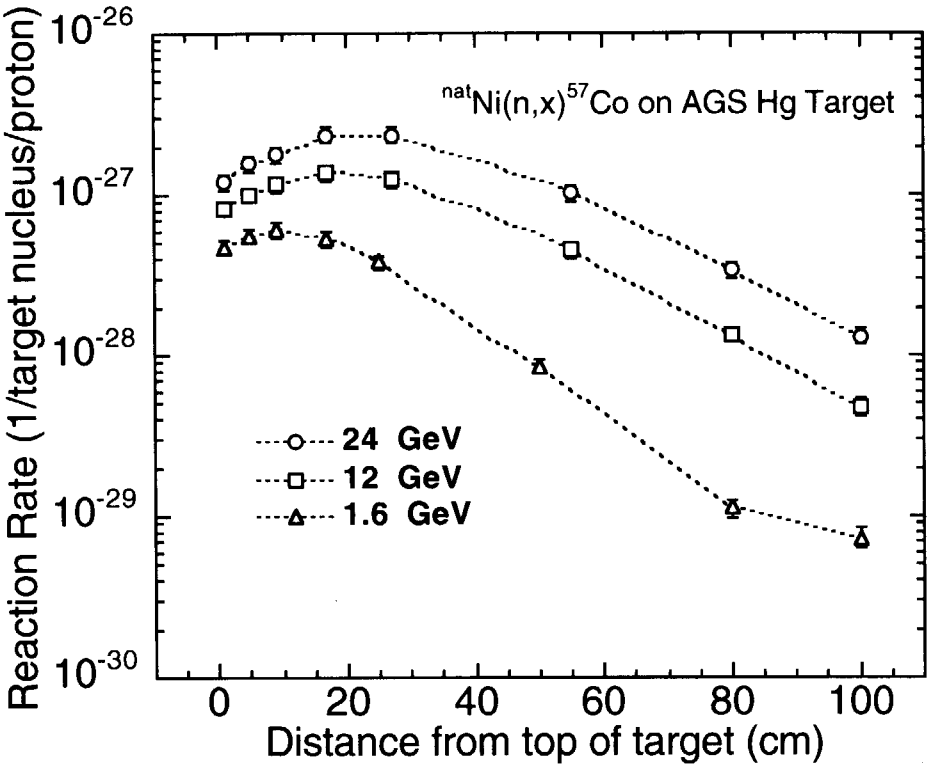

Fig. 5.29 Measured reaction rates of the ^{nat}Ni(n,x)^{57}Co reaction on the cylindrical surface of the mercury target bombarded with 1.6-, 12- and 24- GeV protons.

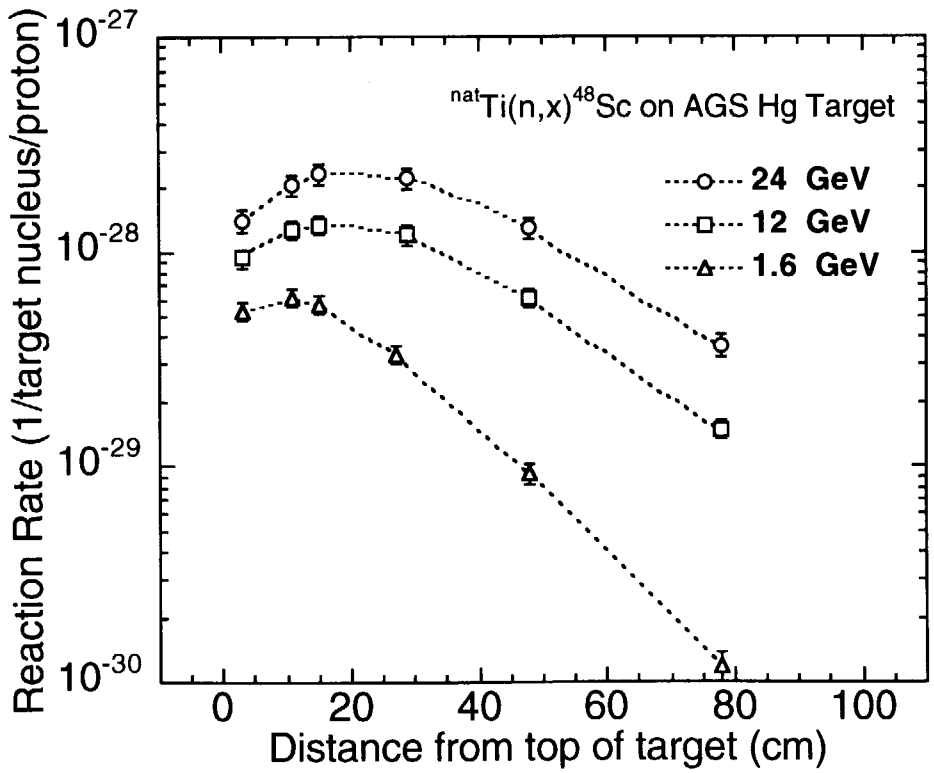

Fig. 5.30 Measured reaction rates of the ^{nat}Ti(n,x)^{48}Sc reaction on the cylindrical surface of the mercury target bombarded with 1.6-, 12- and 24-GeV protons.

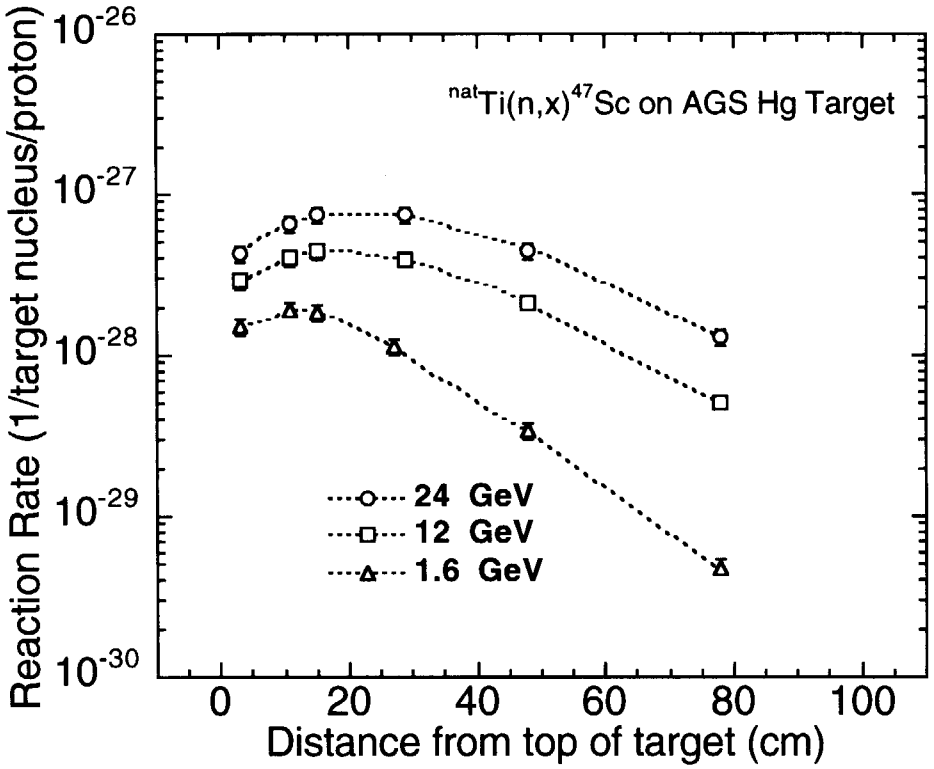

Fig. 5.31 Measured reaction rates of the ^{nat}Ti(n,x)^{47}Sc reaction on the cylindrical surface of the mercury target bombarded with 1.6-, 12- and 24-GeV protons.

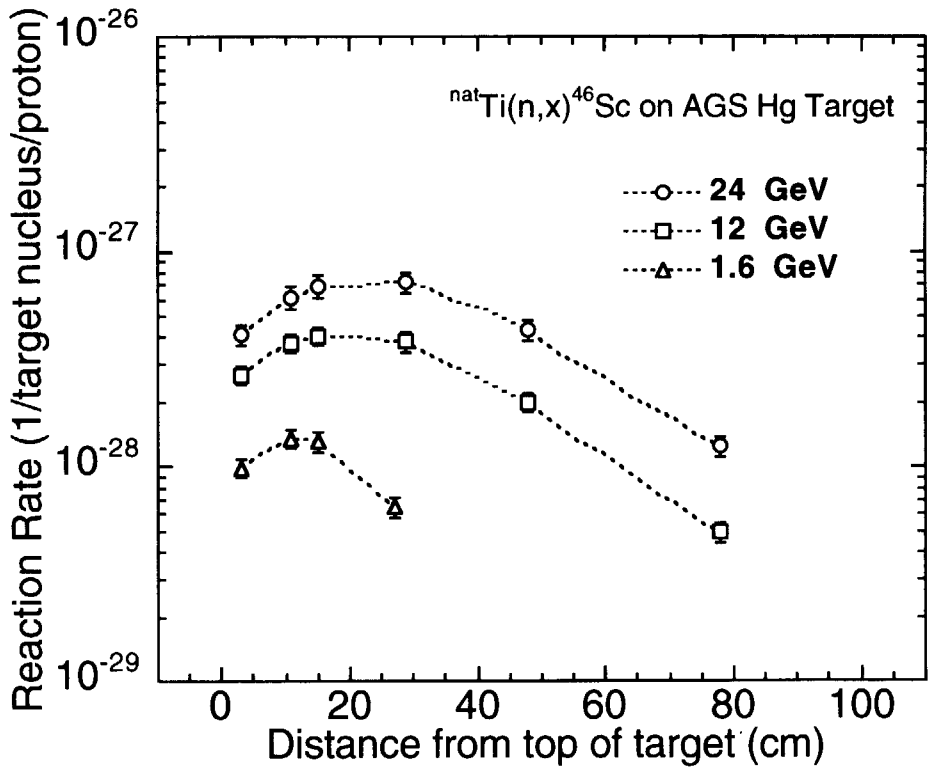

Fig. 5.32 Measured reaction rates of the ^{nat}Ti(n,x)^{46}Sc reaction on the cylindrical surface of the mercury target bombarded with 1.6-, 12- and 24-GeV protons.

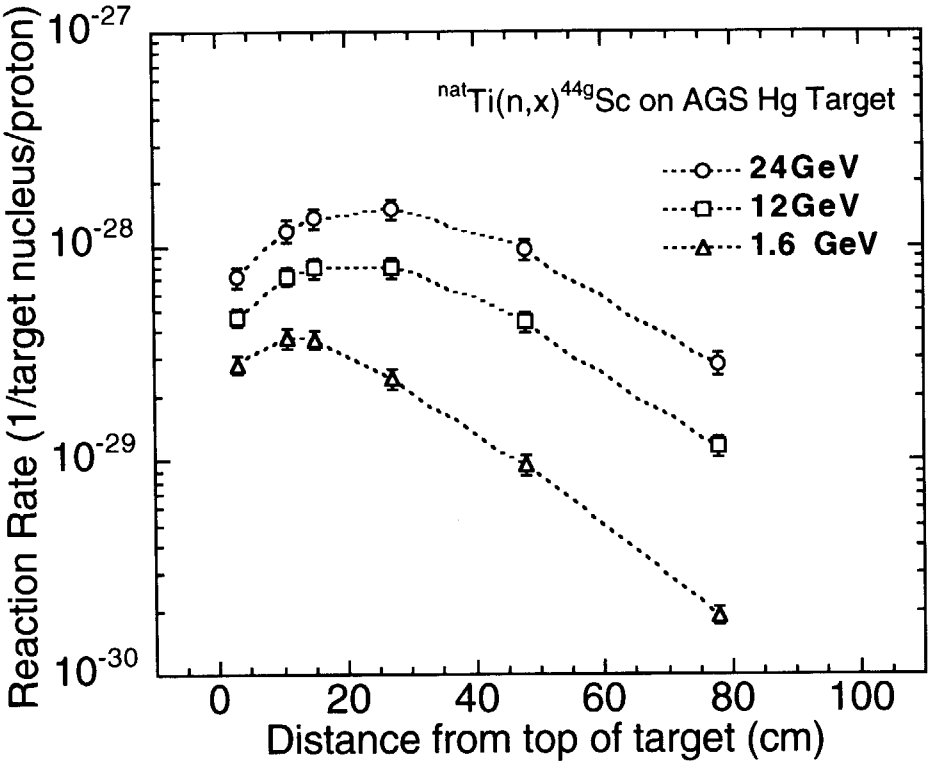

Fig. 5.33 Measured reaction rates of the ^{nat}Ti(n,x)^{44g}Sc reaction on the cylindrical surface of the mercury target bombarded with 1.6-, 12- and 24-GeV protons.

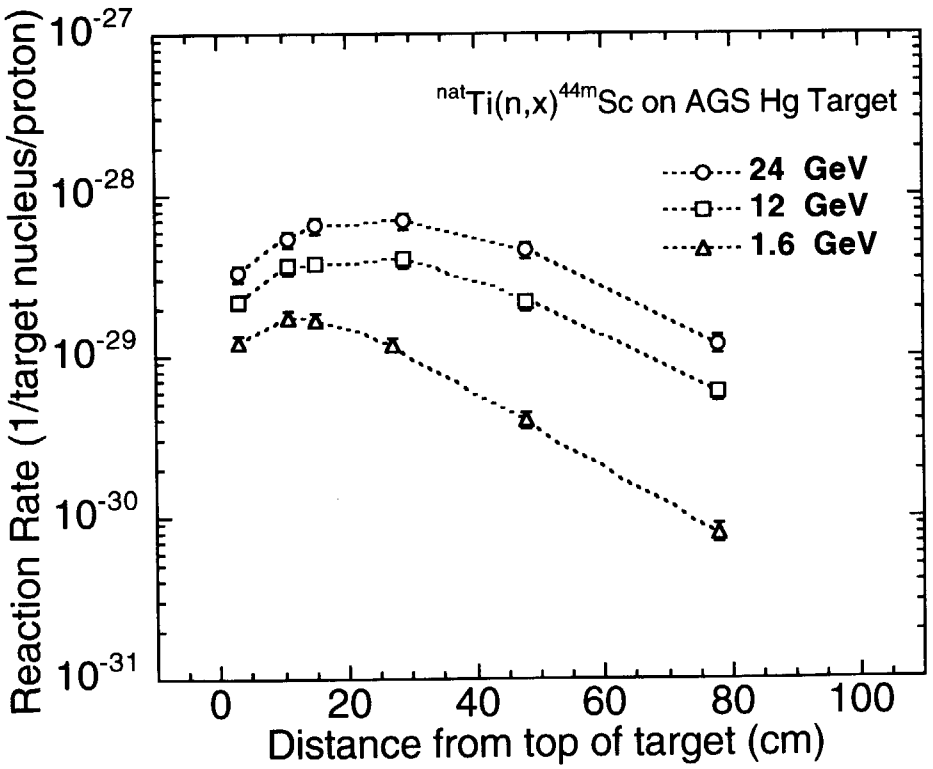

Fig. 5.34 Measured reaction rates of the ^{nat}Ti(n,x)^{44m}Sc reaction on the cylindrical surface of the mercury target bombarded with 1.6-, 12- and 24-GeV protons.

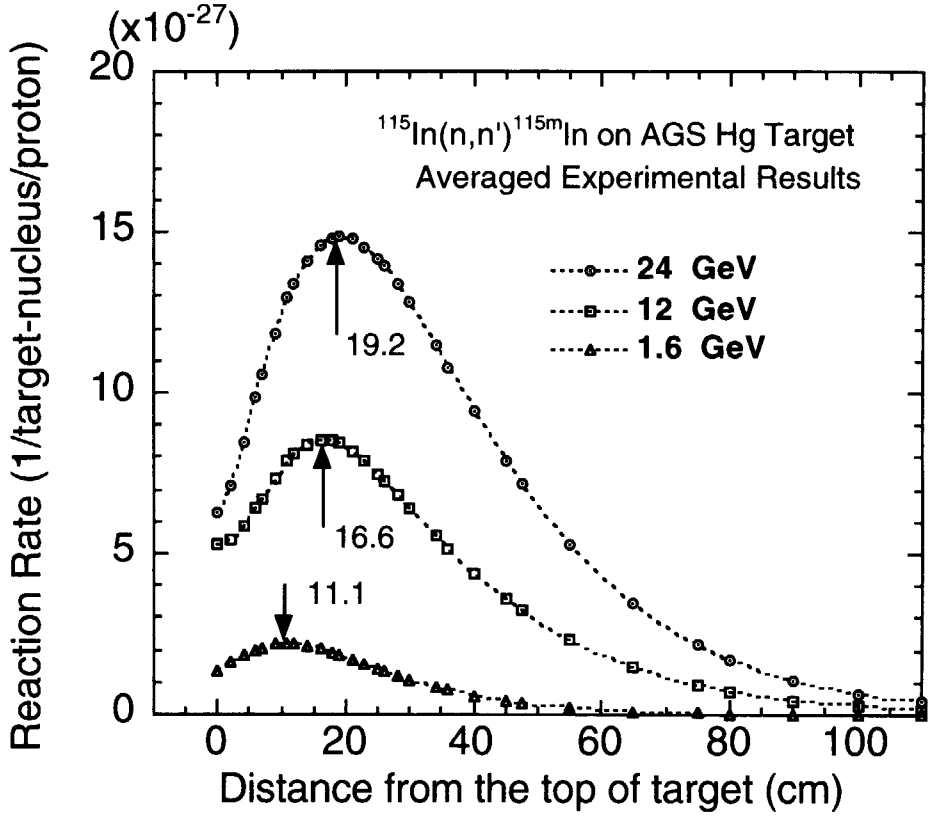

Fig. 6.1 Averaged reaction rates of the $^{115}In(n,n')^{115m}In$ reaction on the cylindrical surface of the mercury target bombarded with 1.6-, 12- and 24-GeV protons.

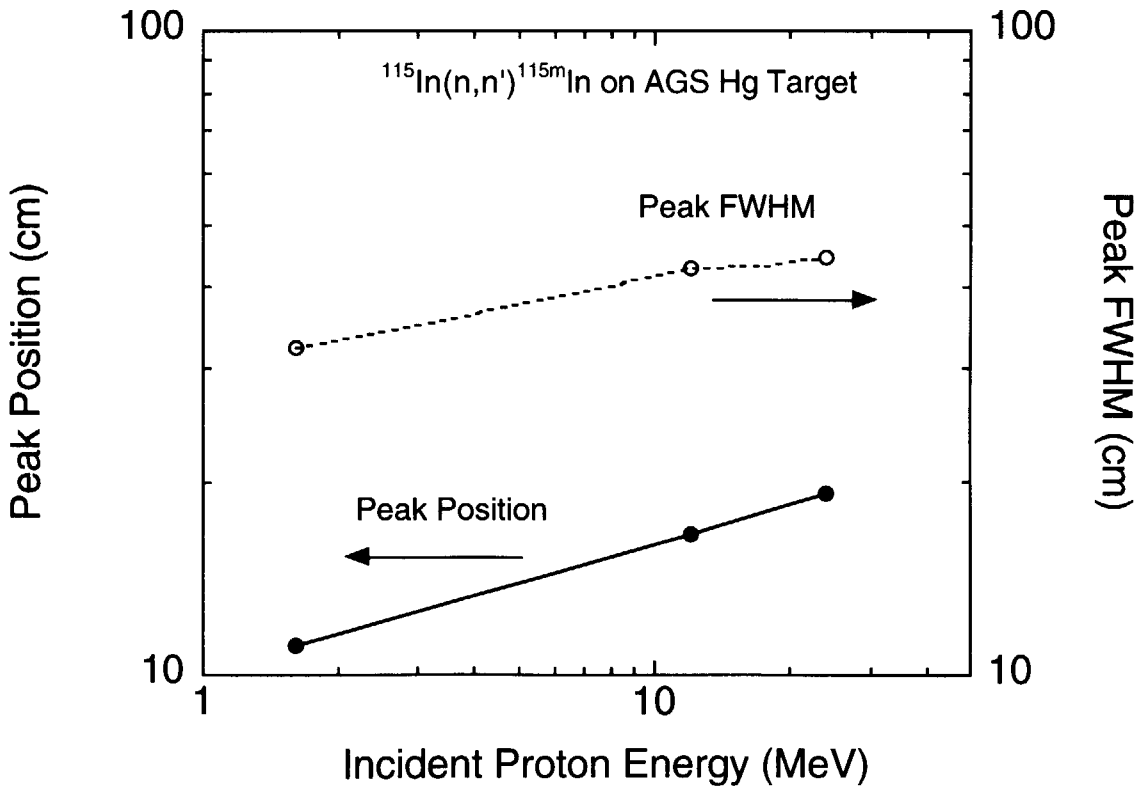

Fig. 6.2 Variation of peak position and peak FWHM of the $^{115}In(n,n')^{115m}In$ reaction rates on the cylindrical surface of the mercury target as a function of incident proton energy.

国際単位系 (SI) と換算表

表 1　SI基本単位および補助単位

量	名称	記号
長さ	メートル	m
質量	キログラム	kg
時間	秒	s
電流	アンペア	A
熱力学温度	ケルビン	K
物質量	モル	mol
光度	カンデラ	cd
平面角	ラジアン	rad
立体角	ステラジアン	sr

表 2　SIと併用される単位

名称	記号
分，時，日	min，h，d
度，分，秒	°，′，″
リットル	l，L
トン	t
電子ボルト	eV
原子質量単位	u

1 eV = 1.60218 × 10^{-19} J

1 u = 1.66054 × 10^{-27} kg

表 5　SI接頭語

倍数	接頭語	記号
10^{18}	エクサ	E
10^{15}	ペタ	P
10^{12}	テラ	T
10^{9}	ギガ	G
10^{6}	メガ	M
10^{3}	キロ	k
10^{2}	ヘクト	h
10^{1}	デカ	da
10^{-1}	デシ	d
10^{-2}	センチ	c
10^{-3}	ミリ	m
10^{-6}	マイクロ	μ
10^{-9}	ナノ	n
10^{-12}	ピコ	p
10^{-15}	フェムト	f
10^{-18}	アト	a

表 3　固有の名称をもつSI組立単位

量	名称	記号	他のSI単位による表現
周波数	ヘルツ	Hz	s^{-1}
力	ニュートン	N	m·kg/s^2
圧力，応力	パスカル	Pa	N/m^2
エネルギー，仕事，熱量	ジュール	J	N·m
工率，放射束	ワット	W	J/s
電気量，電荷	クーロン	C	A·s
電位，電圧，起電力	ボルト	V	W/A
静電容量	ファラド	F	C/V
電気抵抗	オーム	Ω	V/A
コンダクタンス	ジーメンス	S	A/V
磁束	ウェーバ	Wb	V·s
磁束密度	テスラ	T	Wb/m^2
インダクタンス	ヘンリー	H	Wb/A
セルシウス温度	セルシウス度	℃	
光束	ルーメン	lm	cd·sr
照度	ルクス	lx	lm/m^2
放射能	ベクレル	Bq	s^{-1}
吸収線量	グレイ	Gy	J/kg
線量当量	シーベルト	Sv	J/kg

表 4　SIと共に暫定的に維持される単位

名称	記号
オングストローム	Å
バーン	b
バール	bar
ガル	Gal
キュリー	Ci
レントゲン	R
ラド	rad
レム	rem

1 Å = 0.1 nm = 10^{-10} m

1 b = 100 fm^2 = 10^{-28} m^2

1 bar = 0.1 MPa = 10^5 Pa

1 Gal = 1 cm/s^2 = 10^{-2} m/s^2

1 Ci = 3.7 × 10^{10} Bq

1 R = 2.58 × 10^{-4} C/kg

1 rad = 1 cGy = 10^{-2} Gy

1 rem = 1 cSv = 10^{-2} Sv

（注）

1. 表1－5は「国際単位系」第5版，国際度量衡局 1985年刊行による。ただし，1 eVおよび1 uの値はCODATAの1986年推奨値によった。
2. 表4には海里，ノット，アール，ヘクタールも含まれているが日常の単位なのでここでは省略した。
3. barは，JISでは流体の圧力を表わす場合に限り表2のカテゴリーに分類されている。
4. EC閣僚理事会指令ではbar，barnおよび「血圧の単位」mmHgを表2のカテゴリーに入れている。

換算表

力	N(=10^5 dyn)	kgf	lbf
	1	0.101972	0.224809
	9.80665	1	2.20462
	4.44822	0.453592	1

粘度　1 Pa·s(N·s/m^2) = 10 P(ポアズ)(g/(cm·s))

動粘度　1 m^2/s = 10^4 St(ストークス)(cm^2/s)

圧力	MPa(=10 bar)	kgf/cm^2	atm	mmHg(Torr)	lbf/in^2(psi)
	1	10.1972	9.86923	7.50062 × 10^3	145.038
	0.0980665	1	0.967841	735.559	14.2233
	0.101325	1.03323	1	760	14.6959
	1.33322 × 10^{-4}	1.35951 × 10^{-3}	1.31579 × 10^{-3}	1	1.93368 × 10^{-2}
	6.89476 × 10^{-3}	7.03070 × 10^{-2}	6.80460 × 10^{-2}	51.7149	1

エネルギー・仕事・熱量	J(=10^7 erg)	kgf·m	kW·h	cal(計量法)	Btu	ft·lbf	eV
	1	0.101972	2.77778 × 10^{-7}	0.238889	9.47813 × 10^{-4}	0.737562	6.24150 × 10^{18}
	9.80665	1	2.72407 × 10^{-6}	2.34270	9.29487 × 10^{-3}	7.23301	6.12082 × 10^{19}
	3.6 × 10^6	3.67098 × 10^5	1	8.59999 × 10^5	3412.13	2.65522 × 10^6	2.24694 × 10^{25}
	4.18605	0.426858	1.16279 × 10^{-6}	1	3.96759 × 10^{-3}	3.08747	2.61272 × 10^{19}
	1055.06	107.586	2.93072 × 10^{-4}	252.042	1	778.172	6.58515 × 10^{21}
	1.35582	0.138255	3.76616 × 10^{-7}	0.323890	1.28506 × 10^{-3}	1	8.46233 × 10^{18}
	1.60218 × 10^{-19}	1.63377 × 10^{-20}	4.45050 × 10^{-26}	3.82743 × 10^{-20}	1.51857 × 10^{-22}	1.18171 × 10^{-19}	1

1 cal = 4.18605 J (計量法)

= 4.184 J (熱化学)

= 4.1855 J (15 °C)

= 4.1868 J (国際蒸気表)

仕事率　1 PS (仏馬力)

= 75 kgf·m/s

= 735.499 W

放射能	Bq	Ci
	1	2.70270 × 10^{-11}
	3.7 × 10^{10}	1

吸収線量	Gy	rad
	1	100
	0.01	1

照射線量	C/kg	R
	1	3876
	2.58 × 10^{-4}	1

線量当量	Sv	rem
	1	100
	0.01	1

（86年12月26日現在）

MEASUREMENTS OF ACTIVATION REACTION RATE DISTRIBUTIONS ON A MERCURY TARGET BOMBARDED WITH HIGH-ENERGY PROTONS AT AGS